USGS
science for a changing world

Recd
C2)
5/13/03

Analytical and Numerical Simulation of the Steady-State Hydrologic Effects of Mining Aggregate in Hypothetical Sand-and-Gravel and Fractured Crystalline-Rock Aquifers

Water-Resources Investigations Report 02–4267

U.S. Department of the Interior
U.S. Geological Survey

Analytical and Numerical Simulation of the Steady-State Hydrologic Effects of Mining Aggregate in Hypothetical Sand-and-Gravel and Fractured Crystalline-Rock Aquifers

By L.R. Arnold, W.H. Langer, and S.S. Paschke

U.S. GEOLOGICAL SURVEY

Water-Resources Investigations Report 02–4267

Denver, Colorado
2003

U.S. DEPARTMENT OF THE INTERIOR
Gale A. Norton, Secretary

U.S. GEOLOGICAL SURVEY
Charles G. Groat, Director

For additional information write to:

District Chief
U.S. Geological Survey
Box 25046, Mail Stop 415
Denver Federal Center
Denver, CO 80225-0046

Copies of this report can be purchased from:

U.S. Geological Survey
Information Services
Box 25286
Denver Federal Center
Denver, CO 80225

CONTENTS

FIGURES

TABLES

CONVERSION FACTORS AND ABBREVIATIONS

Multiply	By	To obtain
centimeter per year (cm/yr)	0.394	inch per year
cubic meter per day (m^3/d)	0.183	gallon per minute
meter (m)	3.281	foot
meter per day (m/d)	3.281	foot per day

Other abbreviations used in this report:

L	Length
T	Time
L/T	Length per time
L^2/T	Length squared per time

DEFINITION OF TERMS

Alluvium – Unconsolidated gravel, sand, silt, or clay deposited by streams or other moving water.

Anisotropic aquifer – Aquifer in which hydrologic properties vary with direction.

Aquifer – Water-bearing geologic material that will yield significant quantities of water to wells and springs.

Crystalline rock – General term for igneous and metamorphic rocks in contrast to sedimentary rocks.

Confined ground water – Ground water under pressure significantly greater than atmospheric because it is confined by relatively impermeable geologic materials bounding the aquifer.

Heterogeneous aquifer – Aquifer in which hydrologic properties vary by location.

Homogeneous aquifer – Aquifer in which hydrologic properties are identical at all locations.

Hydraulic conductivity – A measure of the ability of a unit area of geologic material to transmit water under a unit hydraulic gradient. It has dimensions of length per time.

Hydraulic conductance – A measure of the ability of a geologic material to transmit water per unit change of hydraulic head. It has dimensions of length squared per time.

Hydraulic head – Height of the free surface of a fluid body above a specified datum. It is a measure of the total mechanical energy per unit weight at a point in the fluid.

Isotropic aquifer – Aquifer in which hydrologic properties are independent of direction.

Saturated thickness – Thickness of that part of an aquifer in which all voids are filled with water under pressure greater than atmospheric.

Steady-state hydrologic conditions – Equilibrium conditions in which hydraulic head and flow do not change with time.

Transient hydrologic conditions – Nonequilibrium conditions in which hydraulic head and flow are time dependent.

Transmissivity – A measure of the ability of a unit width of aquifer to transmit water under a unit hydraulic gradient. It is the product of hydraulic conductivity and saturated thickness of the aquifer and has dimensions of length squared per time.

Unconfined ground water – Ground water in an aquifer with a free water table.

Analytical and Numerical Simulation of the Steady-State Hydrologic Effects of Mining Aggregate in Hypothetical Sand-and-Gravel and Fractured Crystalline-Rock Aquifers

By L.R. Arnold, W.H. Langer, *and* S.S. Paschke

Abstract

Analytical solutions and numerical models were used to predict the extent of steady-state drawdown caused by mining of aggregate below the water table in hypothetical sand-and-gravel and fractured crystalline-rock aquifers representative of hydrogeologic settings in the Front Range area of Colorado. Analytical solutions were used to predict the extent of drawdown under a wide range of hydrologic and mining conditions that assume aquifer homogeneity, isotropy, and infinite extent. Numerical ground-water flow models were used to estimate the extent of drawdown under conditions that consider heterogeneity, anisotropy, and hydrologic boundaries and to simulate complex or unusual conditions not readily simulated using analytical solutions.

Analytical simulations indicated that the drawdown radius (or distance) of influence increased as horizontal hydraulic conductivity of the aquifer, mine penetration of the water table, and mine radius increased; radius of influence decreased as aquifer recharge increased. Sensitivity analysis of analytical simulations under intermediate conditions in sand-and-gravel and fractured crystalline-rock aquifers indicated that the drawdown radius of influence was most sensitive to mine penetration of the water table and least sensitive to mine radius. Radius of influence was equally sensitive to changes in horizontal hydraulic conductivity and recharge.

Numerical simulations of pits in sand-and-gravel aquifers indicated that the area of influence in a vertically anisotropic sand-and-gravel aquifer of medium size was nearly identical to that in an isotropic aquifer of the same size. Simulated area of influence increased as aquifer size increased and aquifer boundaries were farther away from the pit, and simulated drawdown was greater near the pit when aquifer boundaries were close to the pit. Pits simulated as lined with slurry walls caused mounding to occur upgradient from the pits and drawdown to occur downgradient from the pits. Pits simulated as refilled with water and undergoing evaporative losses had little hydrologic effect on the aquifer. Numerical sensitivity analyses for simulations of pits in sand-and-gravel aquifers indicated that simulated head was most sensitive to horizontal hydraulic conductivity and the hydraulic conductance of general-head boundaries in the models. Simulated head was less sensitive to riverbed conductance and recharge and relatively insensitive to vertical hydraulic conductivity.

Numerical simulations of quarries in fractured crystalline-rock aquifers indicated that the area of influence in a horizontally anisotropic aquifer was elongated in the direction of higher horizontal hydraulic conductivity and shortened in the direction of lower horizontal hydraulic conductivity compared to area of influence in a homogeneous, isotropic aquifer. Area of influence was larger in an aquifer with ground-water flow in deep, low-permeability fractures than in a homo-

geneous, isotropic aquifer. Area of influence was larger for a quarry intersected by a hydraulically conductive fault zone and smaller for a quarry intersected by a low-conductivity fault zone. Numerical sensitivity analyses for simulations of quarries in fractured crystalline-rock aquifers indicated simulated head was most sensitive to variations in recharge and horizontal hydraulic conductivity, had little sensitivity to vertical hydraulic conductivity and drain cells used to simulate valleys, and was relatively insensitive to drain cells used to simulate the quarry.

INTRODUCTION

Sand, gravel, and crushed stone are the main sources of natural aggregate. During the year 2000, about 9,900 pits and quarries in the United States produced more than 2.7 billion tons of sand, gravel, and crushed stone (Bolen, 2002; Tepordei, 2002). In many places, natural aggregate lies below the water table, and the effects that mining this material may have on ground-water levels and flow directions are important concerns. The effects of mining aggregate below the water table depend upon the hydrologic properties of the aquifer system and the extent of mining, and predicting the effects of aggregate mining can be difficult because of the potentially complex and unknown nature of the ground-water system in which mining takes place.

The effects of mining can be simulated using analytical solutions or numerical models. Each method has advantages and limitations, and results can vary depending upon how the ground-water system is conceptualized and represented. Because of the uncertainties associated with predicting the hydrologic effects of aggregate mining, conflicts can occur among regulatory agencies, aggregate mining operators, and the public with regard to permitting new mines or predicting the effects of existing mines on nearby wells, wetlands, or streams.

During 2000–01, the U.S. Geological Survey, as part of the Front Range Infrastructure Resources Project (Knepper, 2002), conducted analytical and numerical simulations to study the potential hydrologic effects of mining aggregate below the water table in different hydrogeologic settings. This study seeks to provide information useful in predicting the effects of aggregate mining under various conditions and to assist in planning, managing, and regulating aggregate mine sites.

Purpose and Scope

The purposes of this report are to (1) demonstrate the potential hydrologic effects of mining aggregate below the water table under different hydrogeologic conditions, (2) compare the results of analytical and numerical simulations, and (3) evaluate the sensitivity of simulation results to parameters used in the simulations. A steady-state, one-dimensional analytical solution for ground-water flow to a quarry also is derived.

This report presents analytical and numerical simulations of the steady-state effects of mining aggregate below the water table in two hydrogeologic settings of the Front Range area of Colorado. One set of simulations used hydrogeologic conditions and mining scenarios representative of alluvial sand-and-gravel aquifers in the plains and foothills of the Front Range area. A second set of simulations used hydrogeologic conditions and mining scenarios representative of fractured crystalline-rock aquifers in the mountainous part of the Front Range area. Conceptualizations of each setting were used to provide insight into the magnitude and range of effects that may result from mining aggregate below the water table at real sites having hydrogeologic conditions similar to the conceptualizations. However, because the effects of mining at real sites depend upon site-specific hydrogeologic conditions that may differ from the conceptualizations, the effects of mining at real sites may differ from results presented here.

Analytical simulations were used to predict the extent of drawdown caused by a dewatered pit or quarry as a function of different hydrogeologic conditions (horizontal hydraulic conductivity and recharge) and mining extent (depth and radius/width) within a homogeneous, isotropic aquifer of infinite extent. Numerical simulations were used to predict the extent of drawdown caused by a dewatered pit or quarry under heterogeneous, anisotropic conditions with hydrologic boundaries and to simulate complex or unusual conditions not readily simulated using analytical solutions. Sensitivity analyses show how each parameter in the simulations affected simulation results.

Acknowledgments

Thanks are extended to Curtt Coppage of Aggregate Industries for providing access to mine sites where useful mining information was obtained. Thanks also are extended to Dan Knepper and Roger Melick of the U.S. Geological Survey for their assistance in developing the conceptualizations used in this study. Technical assistance from Ned Banta, Ken Watts, and Alan Burns of the U.S. Geological Survey was very valuable to the completion of the study and is gratefully acknowledged.

HYDROGEOLOGIC SETTINGS

The Colorado Front Range area (fig. 1) straddles the boundary of the Southern Rocky Mountains and the Colorado Piedmont section of the Great Plains in northeastern Colorado (Fenneman, 1946). The Colorado Piedmont separates the Rocky Mountains from the High Plains and contains most of the State's population. The topography of the Colorado Piedmont part of the Front Range area generally has low relief (tens of meters) in comparison to the topography of the mountainous part, which has relief of hundreds of meters.

Because of differences in topography, aspect (sun exposure), and altitude between the Colorado Piedmont and the adjacent Front Range of the Rocky Mountains, the climate of the Colorado Front Range area is varied. The climate of the Colorado Piedmont part of the Front Range area is semiarid temperate continental with average annual precipitation that varied with geographic location and ranged from about 25 to 50 cm/yr during 1961–90 (Western Regional Climate Center, 1997). Average annual pan evaporation for the same area ranged from about 140 to 180 cm/yr during 1946–55 (Robson and Banta, 1995). By contrast, the climate of the Rocky Mountain part of the Front Range area is subhumid (Fenneman, 1946) with average annual precipitation that varied with geographic location and ranged from about 40 to 65 cm/yr during 1991–2000 (Western Regional Climate Center, 1997). Average annual pan evaporation for the Rocky Mountain part of the Front Range area ranged from about 125 to 165 cm/yr during 1946–55 (Robson and Banta, 1995). The Colorado Front Range area is drained primarily by the South Platte River and its tributaries (fig. 1).

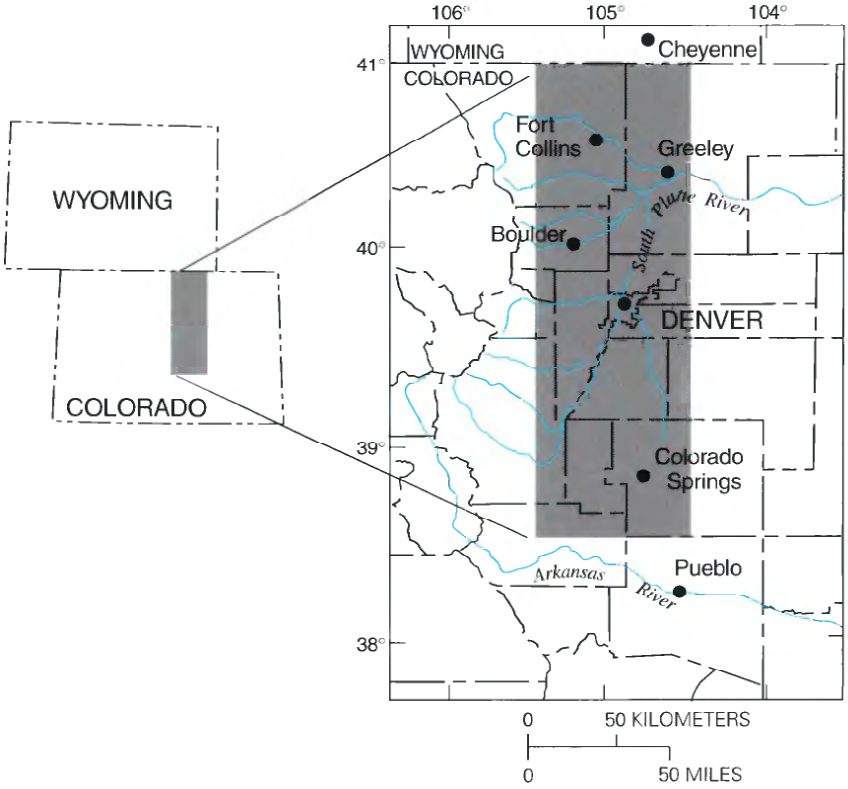

Figure 1. Index map of Colorado Front Range area.

Aggregate mining in the Colorado Front Range area takes place primarily within two distinct hydrogeologic settings: (1) alluvial sand and gravel deposits in the Colorado Piedmont and (2) fractured crystalline rock in the Rocky Mountains. About two-thirds of the aggregate in the Front Range area is sand and gravel from alluvium and about one-third is crushed stone from fractured crystalline rock (Wilburn and Langer, 2000).

Sand-and-Gravel Aquifers

Alluvial deposits in the Colorado Front Range area can be separated into four major landforms (Colton, 1978; Crosby, 1978; Trimble and Machette, 1979) (fig. 2). From highest (oldest) to lowest (youngest), the major alluvial landforms are (1) alluvial fans and pediments, (2) high dissected terraces, (3) high continuous terraces, and (4) flood plain and low terraces. Sand and gravel are mined for aggregate in each of these landforms, but because mining does not commonly penetrate the water table in alluvial fans, pediments, or high dissected terraces, only flood plains, low terraces, and high continuous terraces are represented in this study. Flood-plain, low-terrace, and high-continuous-terrace deposits are composed of clay, silt, sand, gravel, and cobbles; but sediments consist primarily of sand and gravel in areas where aggregate mining occurs. The alluvial sediments commonly are stratified, but stratification is variable.

The sand-and-gravel aquifers of flood plains, low terraces, and high continuous terraces range in width from about 700 to 9,000 m and have a saturated thickness of 0 to more than 30 m (Sheet 4 in Robson, 1996; Robson, Arnold, and Heiny, 2000a and b; Robson, Heiny, and Arnold, 2000a and b). The top of the aquifer is the water table, and the base of the aquifer is bounded by sedimentary bedrock that, on average, is 200–300 times less permeable than the alluvial sediments, which have hydraulic conductivities ranging from about 10 to 1,000 m/d (Robson, 1989; Wilson, 1965). Average water-table gradients in alluvial valleys generally range from 0.002 along

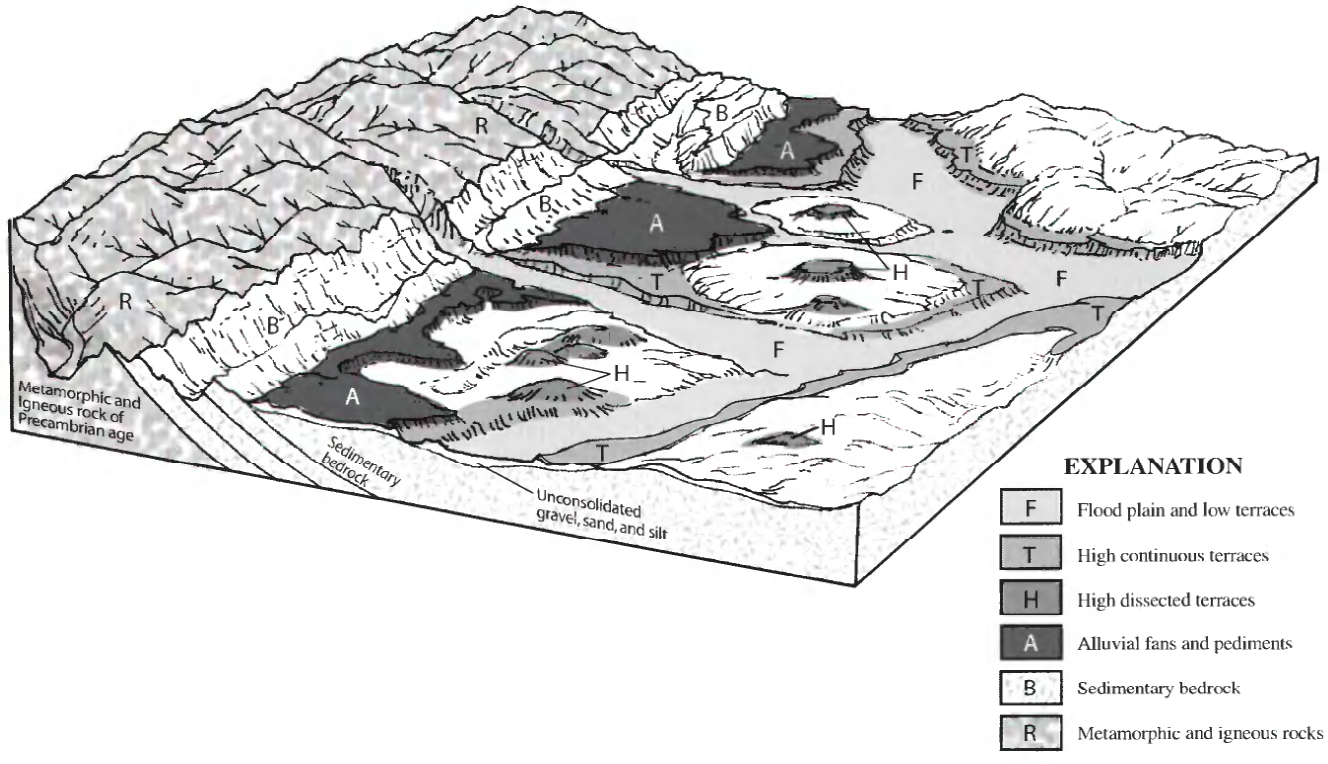

Figure 2. Alluvial and crystalline-rock landforms in the Colorado Front Range area (modified from Crosby, 1978).

downstream reaches of principal rivers to 0.007 along reaches of major tributaries nearer the mountain front (Sheet 3 in Robson, 1996; also Robson, Arnold, and Heiny, 2000a and b and Robson, Heiny, and Arnold, 2000a and b). Water-table gradients generally are steeper along hillslopes between valleys. Groundwater flow in the aquifers generally is down the valley and toward streams. Aquifer recharge is from infiltration of precipitation and irrigation or from inflow of water from adjacent alluvial aquifers or underlying bedrock aquifers (Robson and Banta, 1995). Precipitation recharge to an alluvial aquifer in the Colorado Piedmont near the Front Range has been estimated to be about 5 percent of the total annual precipitation (Buckles and Watts, 1988; Goeke, 1970). Discharge from the alluvial aquifer occurs primarily to the South Platte River and to wells (Robson and Banta, 1995).

Sand and gravel are excavated using both dry and wet mining techniques (Langer, 2001). If the excavation does not penetrate the water table, gravel is mined dry and can be extracted by using conventional earth-moving equipment such as bulldozers, front loaders, and track hoes. If the excavation penetrates the water table and the pit is mined dry, water will be pumped or otherwise removed from the pit. Water removed from the pit lowers the water table in the vicinity of the pit and may affect water levels or flow in nearby wells, wetlands, and streams. In some cases, slurry walls are constructed around the perimeter of a pit to isolate it from the surrounding aquifer. If the excavation penetrates the water table, and the pit cannot be drained, gravel may be mined wet by using draglines, clamshells, bucket and ladder, or hydraulic dredges.

Fractured Crystalline-Rock Aquifers

Precambrian metamorphic rocks (including quartzite, schist, gneiss, and amphibolite; fig. 2) and igneous rocks (including granite, granodiorite, monzonite, diorite, and pegmatite) form the mountains of the Colorado Front Range in the western part of the study area (see summaries in Colton, 1978; Trimble and Machette, 1979). Bedrock in the Front Range is broken by numerous faults that differ greatly in size, orientation, and attitude. Away from fault zones, many metamorphic and igneous rocks are hard and dense, a characteristic that makes both rock types important sources of crushed stone for use in Front Range communities. Within fault zones, the crystalline rocks are extensively fractured and faulted. Faults or fault zones may be more permeable than the surrounding rock and provide a conduit for ground-water flow, or they may be mineralized and constitute barriers to flow.

Ground water in fractured crystalline-rock aquifers is present in discrete fractures and fissures within the rock rather than in continuous, interconnected pore spaces as in sand-and-gravel aquifers. Fractured crystalline-rock aquifers may be discontinuous at a scale of a few meters or tens of meters because fractures are not locally interconnected. However, fractured crystalline-rock aquifers may be continuous at a regional scale because some local fractures may be connected to a regional fracture network. Water levels measured in wells in an area of the Front Range mountains suggest the fractured crystalline-rock aquifer is unconfined and has a high degree of hydraulic connectivity at a regional scale (Lawrence and others, 1991). The permeability and porosity of fractured crystalline-rock aquifers have been shown generally to decrease with depth (Daniel and others, 1997; Davis and Turk, 1964). In the Colorado Front Range, test data indicate the permeability of the fractured crystalline-rock aquifer tends to become exceedingly small at depths 60 to 90 m below land surface, although open fault zones may extend to greater depths (Snow, 1968). Because permeability generally decreases greatly at depth, the effective saturated thickness of the aquifer also may be 60 to 90 m or less.

The permeability of fractured crystalline-rock aquifers depends upon the spacing, aperture, and connectivity of fractures in the rock, and permeability generally is several orders of magnitude less than in unconsolidated sand and gravel deposits. Heath (1983) and Freeze and Cherry (1979) indicate hydraulic conductivity in fractured-rock aquifers generally ranges from about 0.0005 to 15 meters per day (m/d). Folger (1995) reports hydraulic conductivity ranges from about 0.002 to 1 m/d for the fractured crystalline-rock aquifer at a site in the Front Range mountains. Hydraulic conductivity of fractured crystalline-rock aquifers has been estimated to be greater beneath valleys and lesser beneath hilltops than that beneath intermediate topographic terrain, which suggests that fractures may be more numerous beneath valleys and less numerous beneath hilltops (Daniel and others, 1997). Fracture orientation may control anisotropy in fractured crystalline-rock aquifers. Water-table gradients in the fractured crystalline-rock aquifer of the

Front Range mountains generally are steep. Recharge to the fractured crystalline-rock aquifer has been estimated to range from 0 to 21 percent of precipitation with an average of 3.2 percent (Hofstra and Hall, 1975) to 10 percent (Mueller, 1979).

In the Colorado Front Range, rock quarries typically are mined dry (Langer, 2001). Although quarries may penetrate the water table, the discharge rate to quarries commonly is less than the rate of evaporation, and active dewatering measures are not needed. The quarry may drain freely. To produce aggregate, the rock is first drilled and blasted. Blasting commonly breaks the rock into pieces suitable for crushing, and the blasted material is extracted using conventional earth-moving equipment such as bulldozers, front loaders, and track hoes. Material is transported, either by truck or conveyor, from the mining face to the processing plant where it is crushed, washed, and sorted by size.

GROUND-WATER HYDRAULICS AND MATHEMATICAL METHODS

To evaluate the effects of aggregate mining on the surrounding water table, ground-water flow was simulated with analytical and numerical solutions to the ground-water flow equation. A general form of the equation describing transient (time-varying) three-dimensional ground-water flow can be written as (Konikow and Grove, 1977; McDonald and Harbaugh, 1988):

$$\frac{\partial(bK_x\frac{\partial h}{\partial x})}{\partial x}+\frac{\partial(bK_y\frac{\partial h}{\partial y})}{\partial y}+\frac{\partial(bK_z\frac{\partial h}{\partial z})}{\partial z}=S\frac{\partial h}{\partial t}+W(x,y,z,t) \quad (1)$$

where

K_x is aquifer hydraulic conductivity in the x-direction (L^2/T),

K_y is aquifer hydraulic conductivity in the y-direction (L^2/T),

K_z is aquifer hydraulic conductivity in the z-direction (L^2/T),

b is aquifer saturated thickness (L),

h is hydraulic head (L),

S is storage coefficient (dimensionless),

W is volumetric flux per unit area from a hydrologic source or sink as a function of location and time (L/T),

x,y,z are Cartesian coordinates, and

t is time (T).

This equation assumes compressible fluid of constant density is flowing through a heterogeneous anisotropic aquifer according to Darcy's law (Fetter, 1994). It also assumes the principal axes of the hydraulic conductivity tensor are aligned with the x, y, and z coordinate axes, respectively (McDonald and Harbaugh, 1988). Additional details of the ground-water flow equation and its derivation can be found in numerous texts and reports (Freeze and Cherry, 1979; Lohman, 1979; Huyakorn and Pinder, 1983; McDonald and Harbaugh, 1988; Domenico and Schwartz, 1990; Anderson and Woessner, 1992; Fetter, 1994).

The ground-water flow equation can be solved for the dependent variable head (h) by analytical or numerical methods. Analytical solutions use algebraic methods to derive closed-form solutions to the ground-water flow equation, whereas numerical solutions use finite-difference or finite-element numerical methods to solve the ground-water flow equation. Analytical solutions to the ground-water flow equation are most useful for evaluating simplified ground-water systems and often assume a homogeneous and isotropic hydraulic-conductivity distribution, horizontal flow, and infinite horizontal extent or limited boundary conditions. Analytical methods can be useful for estimating mine inflows and drawdowns during initial stages of mine planning when site-specific data may not yet be available (Marinelli and Niccoli, 2000). The applicability of an analytical solution depends on the extent to which the real problem under consideration is consistent with the simplifying assumptions of the analytical solution. Analytical solutions that assume infinite horizontal extent can be useful in predicting drawdown in real aquifers of finite extent when aquifer boundaries lie beyond the cone of depression in the water table (area of influence) caused by the pit. When boundaries lie outside the area of influence, the aquifer within the area of influence responds as though it were

of infinite extent because no boundaries are contacted. Numerical simulations are useful for evaluating more complex flow systems such as heterogeneous or anisotropic hydraulic-conductivity distributions, multiple boundary conditions, and transient conditions. Numerical methods may be required during advanced stages of mine planning when more detailed geologic and hydrologic data are available for a site (Marinelli and Niccoli, 2000). Analytical and numerical methods can be coded into computer programs to facilitate their use.

Both analytical and numerical simulation methods were used in this study to evaluate the steady-state (time-invariant) effects of mining aggregate on water-table conditions. A steady-state two-dimensional analytical solution to the ground-water flow equation by Marinelli and Niccoli (2000) and a steady-state one-dimensional analytical solution derived during this study were used to estimate the extent of drawdown around a mine in a homogeneous, isotropic aquifer of infinite extent. The U.S. Geological Survey modular ground-water model, MODFLOW–2000 (Harbaugh and others, 2000), was used to evaluate steady-state effects of aggregate mining under more complex hydrogeologic conditions.

The steady-state two-dimensional analytical solution of Marinelli and Niccoli (2000) estimates radial ground-water flow toward a circular mine pit. The analytical solution for head in the aquifer adjacent to a circular pit of radius r_p is given as:

$$h = \sqrt{h_p^{\,2} + \frac{W}{K_h}\left[r_i^{\,2}\ln\left(\frac{r}{r_p}\right) - \left(\frac{r^2 - r_p^{\,2}}{2}\right)\right]} \qquad (2)$$

where

h is saturated thickness above the pit base at r (radial distance from pit center) [L],
h_p is saturated thickness above the pit base at r_p (at the mine wall) [L],
W is distributed recharge flux [L/T],
K_h is horizontal hydraulic conductivity of surrounding geologic materials [L/T],
r_i is radius of influence (maximum extent of the cone of depression) [L],
r is radial distance from pit center [L],
r_p is effective pit radius [L] (fig. 3).

Given input values of h_p, W, K_h, r_p, and initial (premining) saturated thickness above the pit base ($h = h_o$), the radius of influence (r_i) can be determined through iteration by setting r equal to r_i. Once r_i is

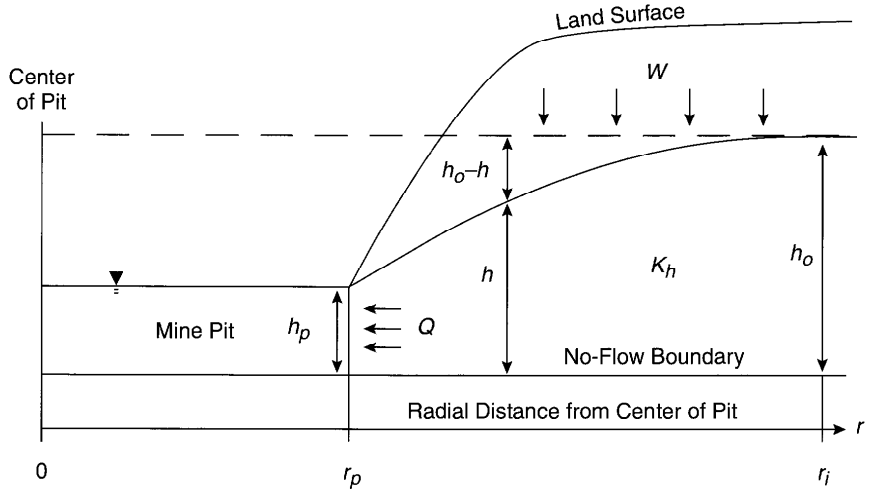

Figure 3. Conceptual diagram of the Marinelli and Niccoli analytical solution (modified from Marinelli and Niccoli, 2000).

determined, h can be calculated for any radial distance from the pit, and drawdown can be calculated as $h_o - h$. In addition, the inflow rate, Q [L^3/T], through the pit wall can be calculated as:

$$Q = W\pi(r_i^2 - r_i^2) \quad (3)$$

The analytical solution of Marinelli and Niccoli (2000) is valid for ground-water flow systems that meet the following assumptions:

- The geologic materials are homogeneous and isotropic;
- Ground-water flow is steady state, unconfined, horizontal, radial, and axially symmetric;
- Recharge is uniformly distributed at the water table and all recharge within the radius of influence is captured by the pit;
- Pit walls are approximated as a right circular cylinder;
- The static premining water table is approximately horizontal; and
- The base of the pit is coincident with the base of the aquifer, and there is no flow through the pit bottom.

Marinelli and Niccoli (2000) also present an analytical solution for upward ground-water flow through the bottom of a pit that partially penetrates an aquifer.

However, inflow to the bottom of a pit is not considered in this report because (1) analytical solutions are used only to calculate hydraulic head at the water table, which is independent of ground-water flow through the mine bottom in the solution, (2) the bottom of aggregate mines in sand-and-gravel aquifers in the Front Range area generally are near the base of the aquifer, and (3) hydraulic conductivity of fractured crystalline-rock aquifers generally becomes exceedingly small with depth, which limits inflow to the mine bottom. For pits that do not meet these conditions, consideration of flow to the mine bottom may be important.

A steady-state, one-dimensional analytical solution is derived for ground-water flow to a mine excavated into a steep hillside such as in the mountainous part of the Front Range area. The derivation of the one-dimensional solution is similar to the Marinelli and Niccoli (2000) solution, but the mine is represented as a straight line along a hillside rather than a circular pit. The mine in this situation intercepts only the upgradient ground water within the hillside. Ground-water flow toward the mine at distance x upgradient from the mine wall can be expressed as:

$$Q = K_h h \frac{dh}{dx} \quad (4)$$

where

Q is flow per unit length of the mine [L^2/T],
K_h is horizontal hydraulic conductivity of surrounding geologic materials [L/T],
h is saturated thickness above the mine base at distance x from the mine wall [L], and
x is distance upgradient from mine wall [L].

If all ground-water flow to the mine is assumed to originate from uniform distributed recharge (W) within the drawdown distance of influence (x_i) of the mine, then flow toward the mine also can be expressed as:

$$Q = W(x_i - x) \quad (5)$$

Substituting equation 5 into equation 4 and integrating from the mine wall to distance x gives:

$$\frac{W}{K_h}\int_0^x (x_i - x)dx = \int_{h_m}^h hdh \quad (6)$$

where

h_m is saturated thickness above the mine base at the mine wall [L].

Carrying out the integration leads to an analytical solution for head in the aquifer adjacent to a linear mine that is given as:

$$h = \sqrt{h_m^2 + \frac{W}{K_h}\left[2x_i x - x^2\right]} \quad (7)$$

Given input values of h_m, W, K_h, and initial (premining) saturated thickness above the base of the mine ($h = h_o$), the distance of influence (x_i) can be calculated directly by setting x equal to x_i and rearranging equation 7. Once x_i is determined, h can be calculated for any distance upgradient from the mine wall, and drawdown can be calculated as $h_o - h$. In addition, the inflow rate per unit length of mine, Q [L^2/T], can be calculated as:

$$Q = Wx_i \qquad (8)$$

The analytical solution for a linear mine wall is valid for ground-water flow systems that meet the following assumptions:

- The geologic materials are homogeneous and isotropic;
- Ground-water flow is steady state, unconfined, horizontal, and perpendicular to the mine wall;
- Recharge is uniformly distributed at the water table, and all recharge within the distance of influence is captured by the mine;
- The uphill mine wall is approximated as a straight line;
- The static premining water table is approximately horizontal; and
- The base of the pit is coincident with the base of the aquifer, and there is no flow through the mine bottom.

MODFLOW-2000 (Harbaugh and others, 2000) was used to estimate the steady-state extent of drawdown near a mine and ground-water inflow to a mine under conditions that consider heterogeneity, anisotropy, and boundaries. MODFLOW–2000 solves the transient ground-water flow equation by using implicit finite-difference methods and is based on a three-dimensional, block-centered, finite-difference grid. Aquifer properties can be heterogeneous and anisotropic provided the principal axes of hydraulic conductivity are aligned with the coordinate directions (Harbaugh and others, 2000; McDonald and Harbaugh, 1988), and aquifer layers can be simulated as confined, unconfined, or a combination of both (Harbaugh and others, 2000). MODFLOW–2000 can simulate several types of hydrologic sources and sinks including aquifer recharge, evapotranspiration, wells, drains, and rivers, and it can simulate either steady-state or transient conditions.

SIMULATION OF THE HYDROLOGIC EFFECTS OF MINING AGGREGATE

Two hydrogeologic settings in the Colorado Front Range area were simulated using analytical and numerical methods. The first set of simulations used conceptualizations of aggregate mining in sand-and-gravel aquifers, and the second set of simulations used conceptualizations of aggregate mining in fractured crystalline-rock aquifers. Analytical and numerical simulations were used to estimate the steady-state hydrologic effects of mining. Under steady-state conditions, discharge to a mine reaches equilibrium with the surrounding ground-water system, and the extent of drawdown caused by dewatering a mine ceases to increase. Therefore, steady-state simulations predict the maximum potential effects of mining over time. To predict short-term effects, transient (time-varying) simulations are necessary. Steady-state simulations of pits in sand-and-gravel aquifers may overpredict the effects of mining if active dewatering of the pit ceases before steady-state conditions are reached. The hydrologic effects of pits in sand-and-gravel aquifers after active dewatering ceases (pits lined with slurry walls or refilled pits undergoing evaporative losses) likely reach steady-state conditions because such pits may be left open indefinitely. The hydrologic effects of quarries in fractured crystalline-rock aquifers also likely reach steady-state conditions because quarries commonly drain without the aid of active dewatering measures (Knepper, 2002) and may be left open indefinitely. Predicting the transient hydrologic effects of mining is beyond the scope of this report.

Simulation of Pits in Sand-and-Gravel Aquifers

Definitions of input parameters for simulations of aggregate mining in sand-and-gravel aquifers were based on data reported in the literature (see "Hydrogeologic Settings"). Definitions of mining extents (area and depth) were defined based on mine

footprints shown by Robson (1996) and Robson, Arnold, and Heiny (2000a and b) and Robson, Heiny, and Arnold (2000a and b) and onsite data. Intermediate parameter values and boundary conditions were used in simulations to represent average hydrogeologic conditions and mining extents. Parameter values and boundary conditions were then varied over a range of values and conditions typical for pits in sand-and-gravel aquifers to determine the potential effects of mining over a wide range of conditions. Intermediate hydraulic conductivity was defined in the simulations as 100 m/d, and intermediate recharge was defined as 0.00005 m/d, which is about 5 percent of the average annual precipitation for the Colorado Piedmont part of the Front Range area. Intermediate pit penetration of the water table was defined as 6 m, and intermediate pit radius was defined as 100 m.

Analytical Simulations and Sensitivities

The analytical solution of Marinelli and Niccoli (2000) was used to solve for the radius of influence (r_i) and saturated thickness (h) above the base of a dewatered pit in a homogeneous, isotropic sand-and-gravel aquifer of infinite extent. Horizontal hydraulic conductivity (K_h), recharge (W), initial saturated thickness above the pit base ($h = h_o$), and pit radius (r_p) were varied independently over a range of values typical for pits in sand-and-gravel aquifers in the Front Range area. By varying the parameters independently, the effects of each parameter on simulation results were evaluated, and sensitivities for parameters were calculated. Because initial saturated thickness is measured relative to the pit base, h_o also is equal to the depth to which the pit penetrates the water table. The water level in the pit was defined at the base of the pit.

Figures 4–7 show drawdown ($h_o - h$) and radius of influence measured from the pit wall ($r_i - r_p$) caused by a dewatered circular pit in a sand-and-gravel aquifer for different values of K_h (10, 100, and 1,000 m/d), W (0.000025, 0.00005, and 0.0001 m/d), h_o (4, 6, and 8 m), and r_p (25, 100, and 500 m). Results indicate radius of influence from the wall of a dewatered pit in a homogeneous, isotropic sand-and-gravel aquifer of infinite extent was 4,544 m under intermediate conditions (K_h = 100 m/d, W = 0.00005 m/d, h_o = 6 m, r_p = 100 m). Radius of influence increased as K_h, h_o, and r_p increased and as W decreased.

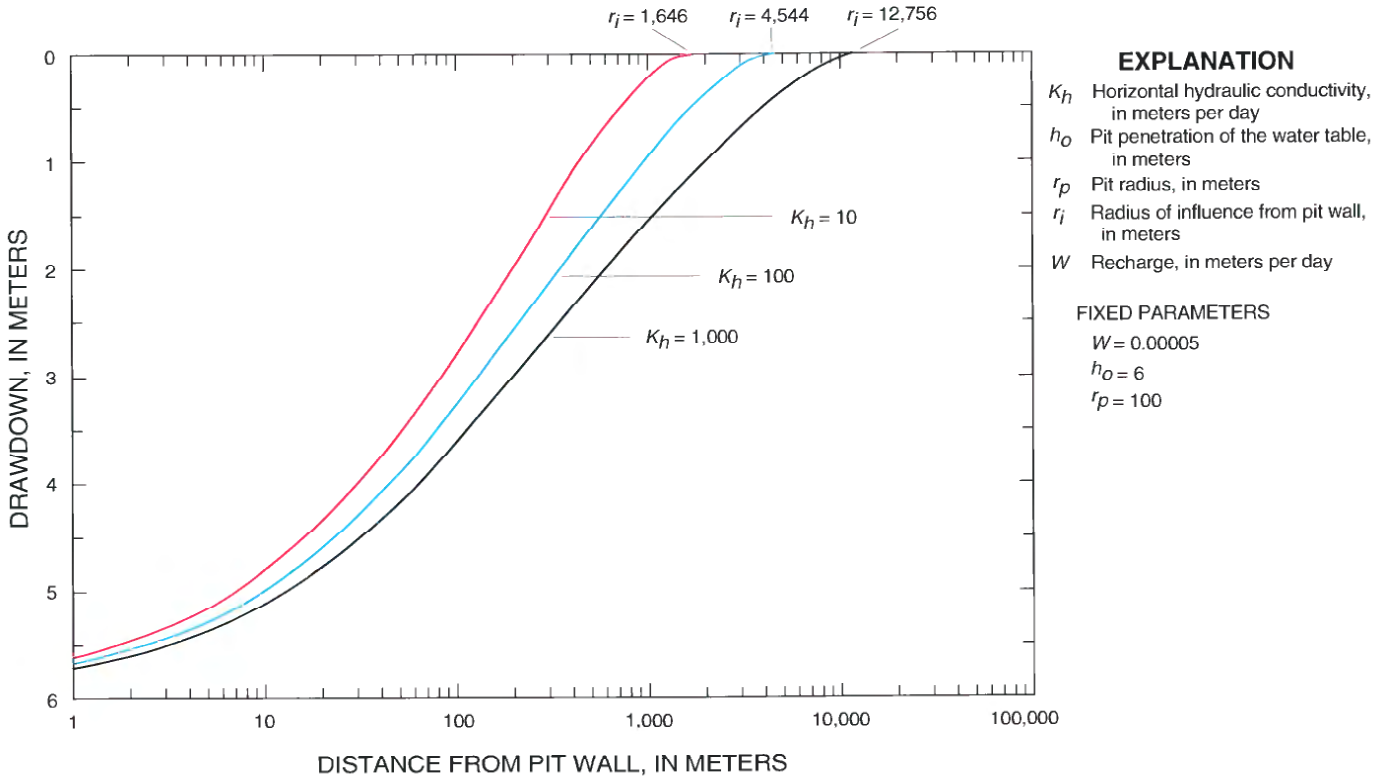

Figure 4. Drawdown relative to distance from a dewatered pit in a sand-and-gravel aquifer for three values of horizontal hydraulic conductivity, simulated by use of the Marinelli and Niccoli (2000) analytical solution.

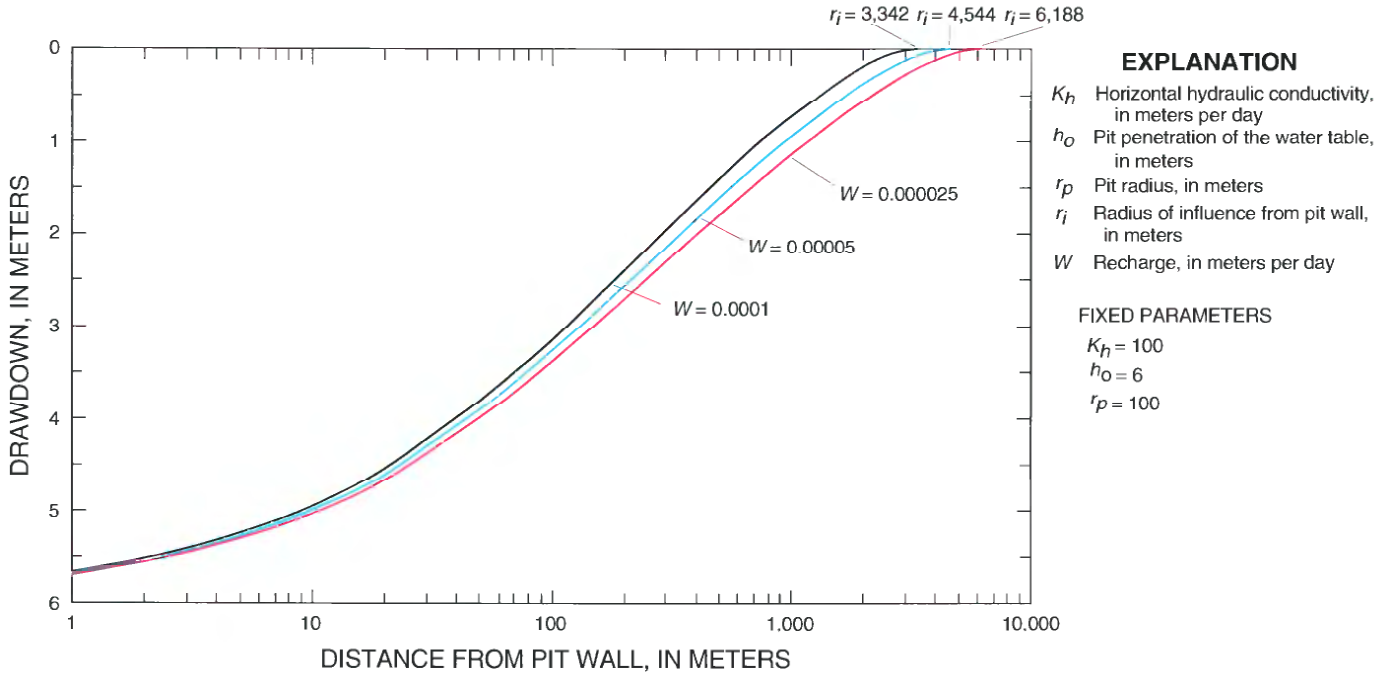

Figure 5. Drawdown relative to distance from a dewatered pit in a sand-and-gravel aquifer for three values of recharge, simulated by use of the Marinelli and Niccoli (2000) analytical solution.

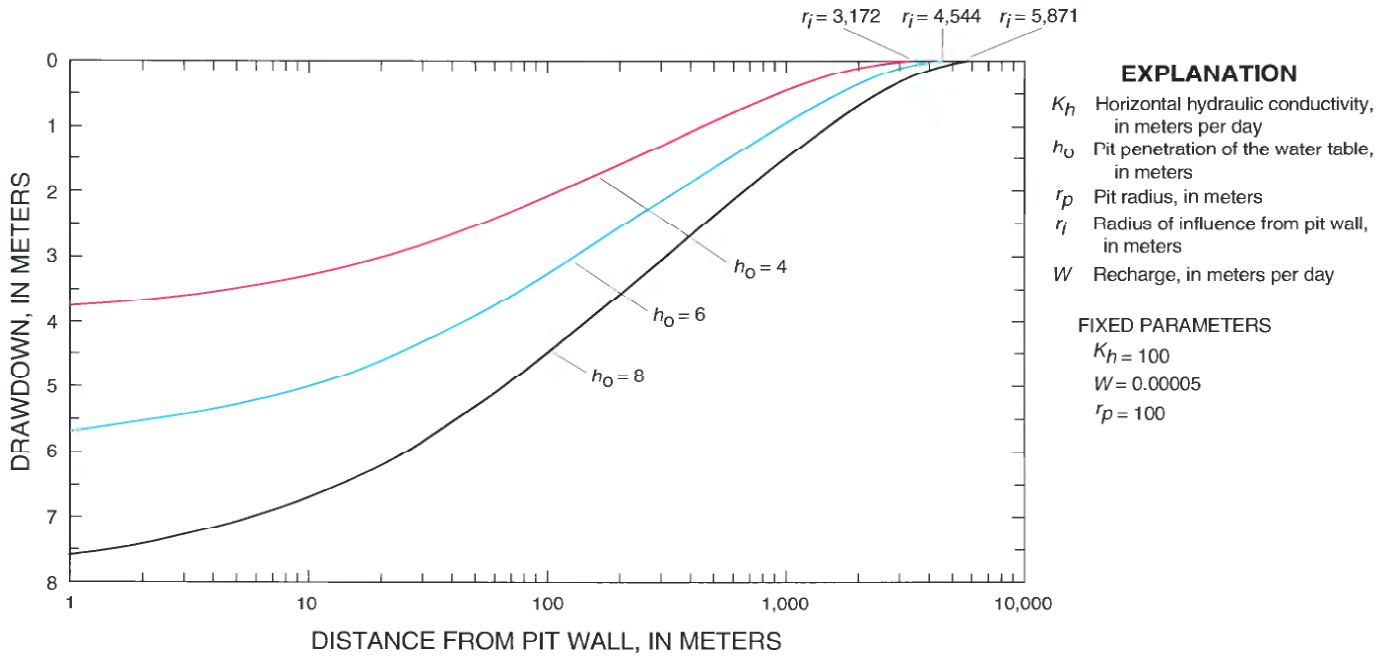

Figure 6. Drawdown relative to distance from a dewatered pit in a sand-and-gravel aquifer for three values of pit peneration of the water table, simulated by use of the Marinelli and Niccoli (2000) analytical solution.

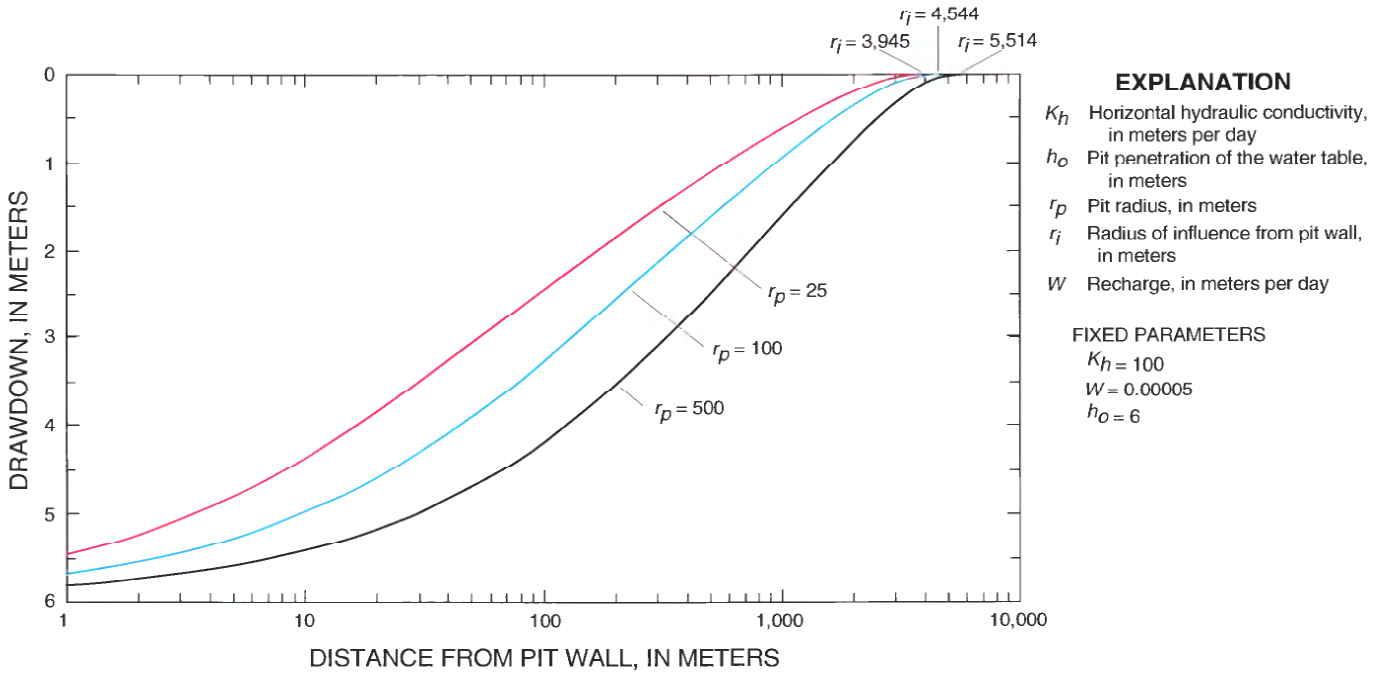

Figure 7. Drawdown relative to distance from a dewatered pit in a sand-and-gravel aquifer for three values of pit radius, simulated by use of the Marinelli and Niccoli (2000) analytical solution.

One-percent scaled sensitivities were calculated for each parameter used in the analytical solution of Marinelli and Niccoli (2000) to determine the effect of each parameter on simulation results under intermediate conditions. One-percent scaled sensitivities, $1ss_{ij}$ are calculated as (Hill, 1998):

$$1ss_{ij} = \frac{\partial y_i'}{\partial b_j}\frac{b_j}{100} \qquad (9)$$

where

y'_i is the simulated value associated with the ith observation;

b_j is the jth estimated parameter;

$\frac{\partial y'}{\partial b_j}$ is the sensitivity of the simulated value associated with the ith observation with respect to the jth parameter and is evaluated at $\underline{b}$; and

$\underline{b}$ is a vector that contains the parameter values at which the sensitivities are evaluated.

In this application, y_i' is the radius of influence, and b_j is the parameter (K_h, W, h_o, or r_p) for which sensitivity is calculated. Resulting sensitivities have units of meters and are the change in radius of influence caused by a 1-percent change in the parameter value. Parameters with high sensitivities affect simulated radius of influence more than parameters with low sensitivities. Therefore, parameters with high sensitivities may be more important to accurately define than parameters with low sensitivities at real sites with conditions similar to those in the analytical simulations. Because one-percent scaled sensitivities depend upon the parameter values at which they are evaluated, sensitivity results will be different for different hydrogeologic conditions and mining extents. Results of analytical sensitivity analysis (fig. 8) under intermediate conditions (K_h = 100 m/d, W = 0.00005 m/d, h_o = 6 m, r_p = 100 m) indicate radius of influence was most sensitive to changes in pit penetration of the water table and least sensitive to changes in pit radius. Radius of influence was equally sensitive to changes in horizontal hydraulic conductivity and recharge; however, the parameters had opposite effects on

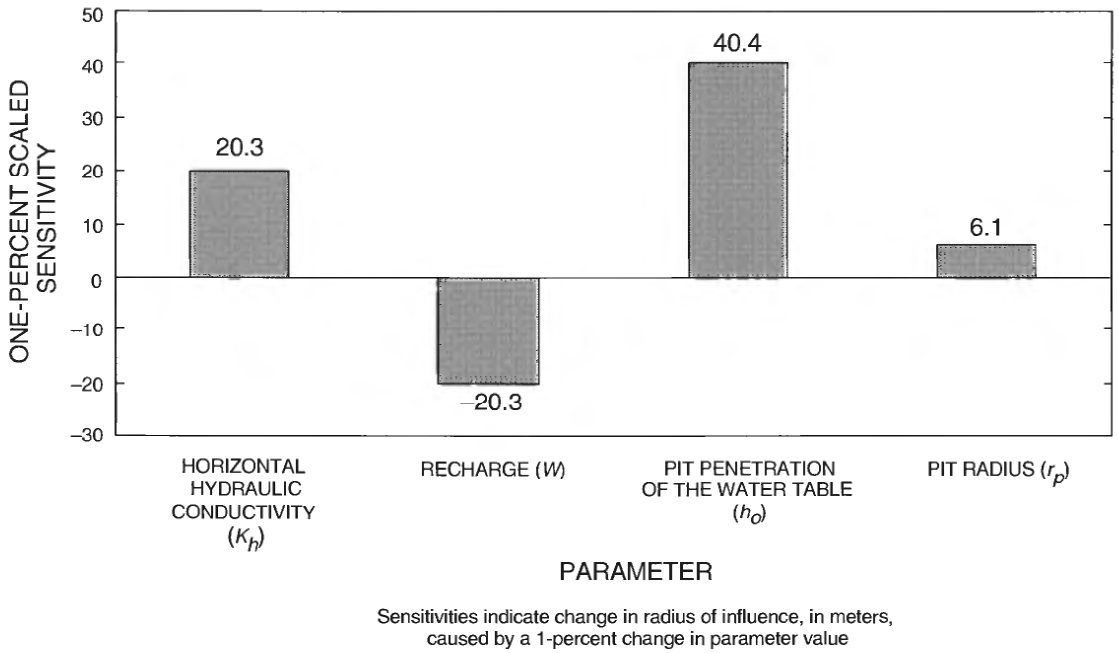

Figure 8. One-percent scaled sensitivities for parameters in the analytical solution of Marinelli and Niccoli (2000), calculated for a pit in a sand-and-gravel aquifer under intermediate conditions (K_h = 100 m/d, W = 0.00005 m/d, h_o = 6 m, r_p = 100 m).

simulation results because they are inversely correlated in the analytical solution. Radius of influence increased as horizontal hydraulic conductivity increased and as recharge decreased.

Numerical Simulations

MODFLOW–2000 (Harbaugh and others, 2000) was used to compute (1) hydraulic heads in a hypothetical sand-and-gravel aquifer under steady-state, premining conditions, (2) steady-state drawdown caused by a dewatered pit in the sand-and-gravel aquifer under different hydrogeologic conditions, and (3) inflow to the pit under different hydrogeologic conditions. In addition, the observation and sensitivity capabilities (Hill and others, 2000) of MODFLOW–2000 were used to compute sensitivities for simulation input parameters. Because simulations are of hypothetical aquifers, model calibration was not necessary. However, generalized aquifer data from real sites were used to guide development of simulated premining conditions. Six numerical simulations of the hydrologic effects of mining aggregate in hypothetical sand-and-gravel aquifers are presented as follows:

Simulation 1–The hydrologic effects of a dewatered pit in a medium-sized (about 2,500-m wide) alluvial valley under homogeneous and isotropic conditions are simulated. Comparison of simulation 1 to analytical simulation results shows the effects of boundary conditions.

Simulation 2–The hydrologic effects of a dewatered pit in a medium-sized alluvial valley under homogeneous but anisotropic conditions are simulated. Comparison of simulation 2 to simulation 1 shows the effects of vertical anisotropy.

Simulation 3–The hydrologic effects of a dewatered pit in a large (about 5,000-m wide) alluvial valley under homogeneous and isotropic conditions are simulated. Comparison of simulation 3 to simulation 1 shows the effects of increasing aquifer size and changing boundary conditions.

Simulation 4–The hydrologic effects of a dewatered pit in a small (about 1,200-m wide) alluvial valley under homogeneous and isotropic conditions are simulated. Comparison of simulation 4 to simulation 1 shows the effects of decreasing aquifer size and changing boundary conditions.

Simulation 5–The hydrologic effects of five closely spaced pits lined with slurry walls in a medium-sized homogeneous, isotropic sand-and-gravel aquifer are simulated.

Simulation 6–The hydrologic effects of five closely spaced, water-filled pits undergoing evaporative losses in a medium-sized homogeneous, isotropic sand-and-gravel aquifer are simulated.

Simulation 1–Pit in a medium-sized, homogeneous, isotropic aquifer

Simulation 1 shows the potential hydrologic effects of dewatering a pit in a medium-sized alluvial valley. The simulation uses the intermediate values of horizontal hydraulic conductivity, recharge, and pit width from the analytical simulations, but a shallow pit is simulated so that water-table penetration is constant among all numerical simulations, including simulation 4 (pit in a small sand-and-gravel aquifer), which is too shallow for the intermediate penetration depth.

Model design

A sand-and-gravel aquifer is represented using two layers in the numerical model (fig. 9). Layer 1 (top layer) is 6 m thick with about 2 to 5 m of saturated thickness. Layer 2 (bottom layer) is 2 m thick and is fully saturated. Both layers are simulated as convertible, which allows hydraulic head to be computed for either confined or unconfined conditions. Total premining saturated thickness near the pit is about 6 m. The model grid has 35 rows and 80 columns (fig. 10) with a cell size of 50 m × 50 m near the pit and 100 m × 100 m at a distance 600 m from the pit. The alluvial valley represented by the model is 7,000 m long and about 2,500 m wide, which is representative of medium-sized alluvial valleys in the Front Range area. Hydraulic gradient is about 0.005 along the length of the valley. Horizontal hydraulic conductivity in both layers is 100 m/d, and vertical hydraulic conductivity is equal to horizontal hydraulic conductivity.

Boundary conditions

The upgradient and downgradient ends of the valley are simulated as constant-head boundaries. The sides of the valley are simulated as general-head boundaries to simulate inflow to the model from a thin part of the alluvial aquifer beyond the boundaries of the valley. General-head boundaries are defined to simulate flow through a saturated thickness of 2.5 m under a gradient about twice that of the downvalley gradient. General-head boundaries also are defined using a hydraulic conductivity value of 10 m/d to simulate finer grained and somewhat less permeable material at the valley edges. The aquifer base is simulated as a no-flow boundary at the bedrock surface. A specified-flux boundary with a value of 0.00005 m/d is used to simulate areal recharge from precipitation.

Water flow between the river and the aquifer is simulated by using the River package of MODFLOW–2000. Definition of riverbed conductance is based on a river 10 m wide with a stage 4 m above the base of the aquifer and a riverbed 1 m thick with a hydraulic conductivity value of 1 m/d. The pit is simulated in layer 1 as a 200-m wide square with a water-table penetration of 4 m by using the Flow and Head Boundary package (Leake and Lilly, 1997) of MODFLOW–2000. Initial heads in the pit cells are set to match those of the steady-state conditions of the premining aquifer, and final heads for the pit cells are set 4 m below the water table to simulate drawdown in the dewatered pit. Horizontal and vertical hydraulic conductivity of pit cells is increased by a factor of 1,000 to represent the open area of the pit where sand and gravel were removed.

Results and comparison to analytical simulation

The simulated steady-state premining distribution of hydraulic head in the aquifer is shown in figure 11*a*, and steady-state drawdown near a dewatered pit in the aquifer is shown in figure 11*b*. Steady-state drawdown computed using the analytical solution of Marinelli and Niccoli (2000) for a dewatered pit in a homogeneous, isotropic sand-and-gravel aquifer of infinite extent is shown in figure 11*c*. Results of the analytical simulation were computed using the same input values of horizontal hydraulic conductivity, recharge, pit penetration of the water table, and pit radius as the numerical simulation.

Lines of equal drawdown computed by the analytical simulation are concentric circles centered around the pit, and area of influence computed by the analytical simulation (defined by the limit of 0.1 m drawdown) has a radius of 3,187 m, measured from the pit center. Lines of equal drawdown computed by the numerical simulation are asymmetrical because of boundary effects, and area of influence computed by the numerical simulation (also defined by the limit of 0.1 m drawdown) has a maximum extent of about 3,200 m, measured from the pit center. Area of influence in the numerical simulation is smaller in general than in the analytical simulation because ground-water flow to the pit in the numerical simulation is contributed by many sources, including precipitation, river leakage, and inflow from constant-head and general-head boundaries, whereas ground-water flow to the pit

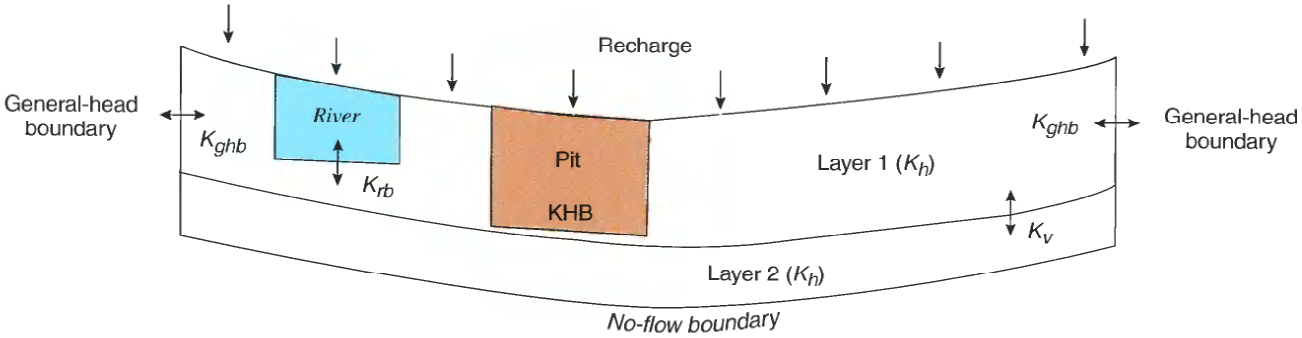

EXPLANATION

K_h = Horizontal hydraulic conductivity of layers 1 and 2
K_v = Vertical hydraulic conductivity of layers 1 and 2
K_{ghb} = Hydraulic conductance controlling flow between external source and aquifer
K_{rb} = Hydraulic conductance controlling flow between river and aquifer
KHB = Flow-and-head boundary

Figure 9. Conceptual diagram for numerical simulation 1 (pit in a hypothetical, medium-sized sand-and-gravel aquifer under homogeneous and isotropic conditions.

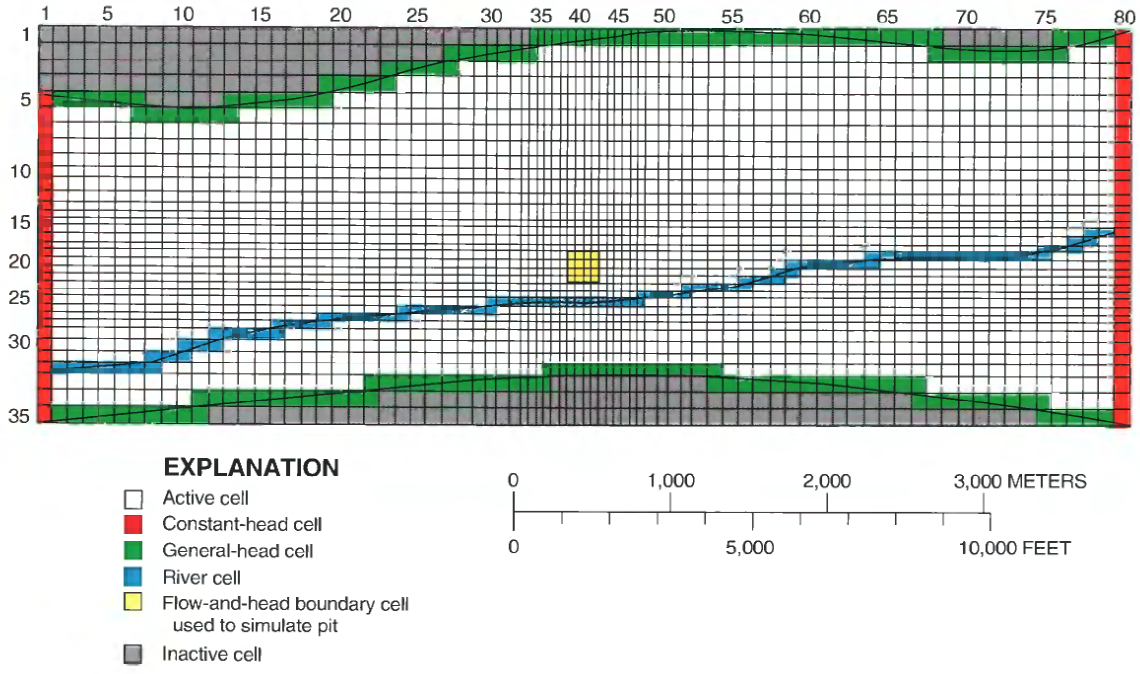

Figure 10. Finite-difference grid and boundary conditions for numerical simulation 1 (pit in a hypothetical, medium-sized sand-and-gravel aquifer under homogeneous and isotropic conditions).

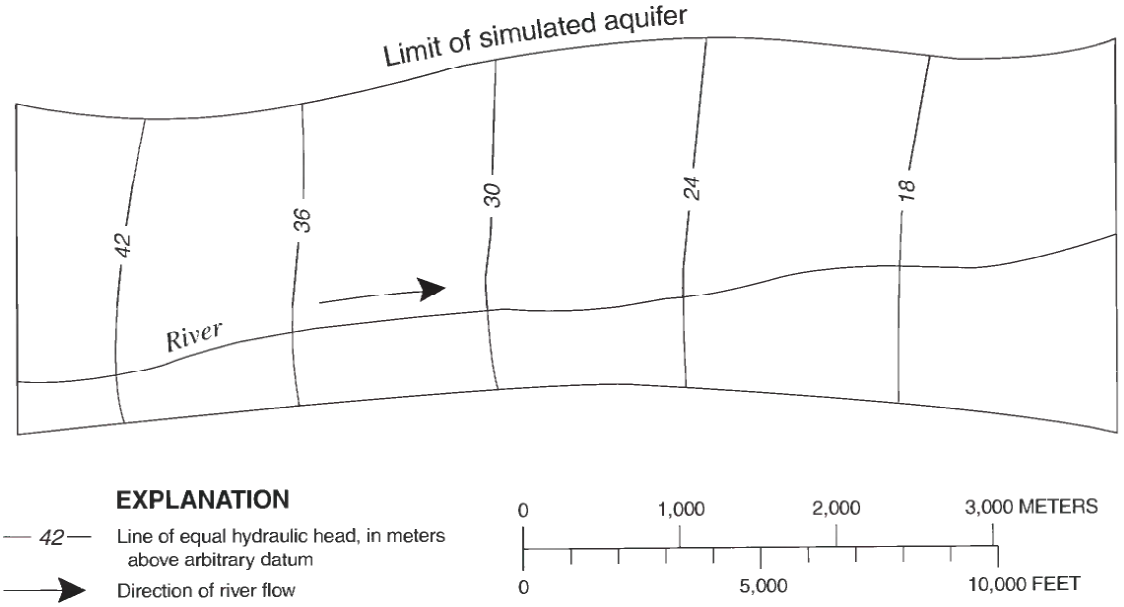

Figure 11*a*. Numerical simulation 1– Steady-state premining distribution of hydraulic head in a hypothetical, medium-sized sand-and-gravel aquifer under homogeneous and isotropic conditions.

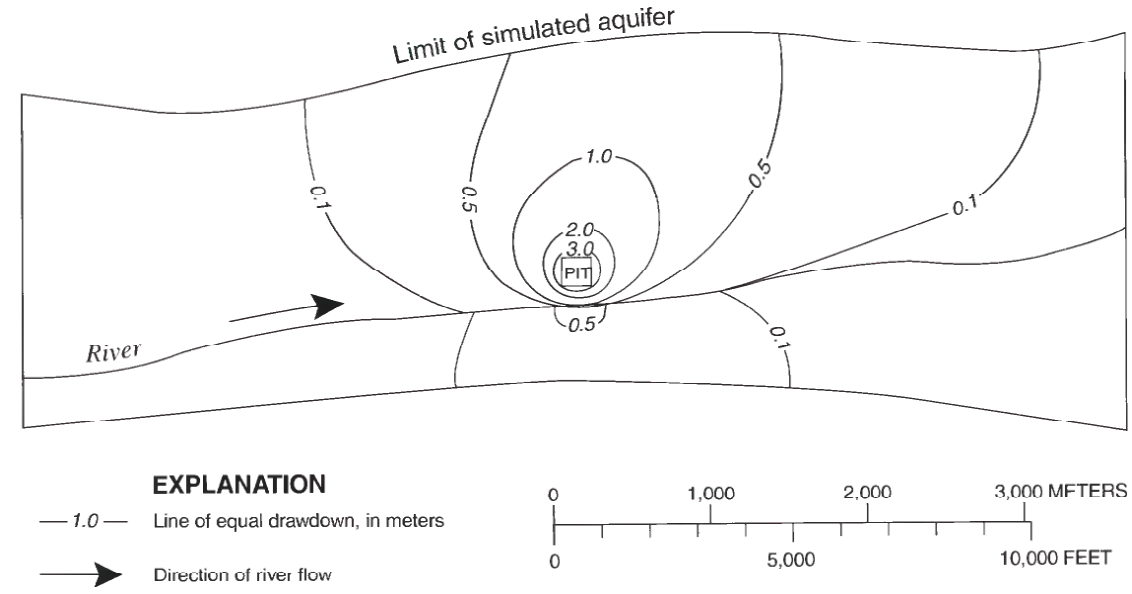

Figure 11*b*. Numerical simulation 1–Steady-state drawdown caused by a dewatered pit in a hypothetical, medium-sized sand-and-gravel aquifer under homogeneous and isotropic conditions.

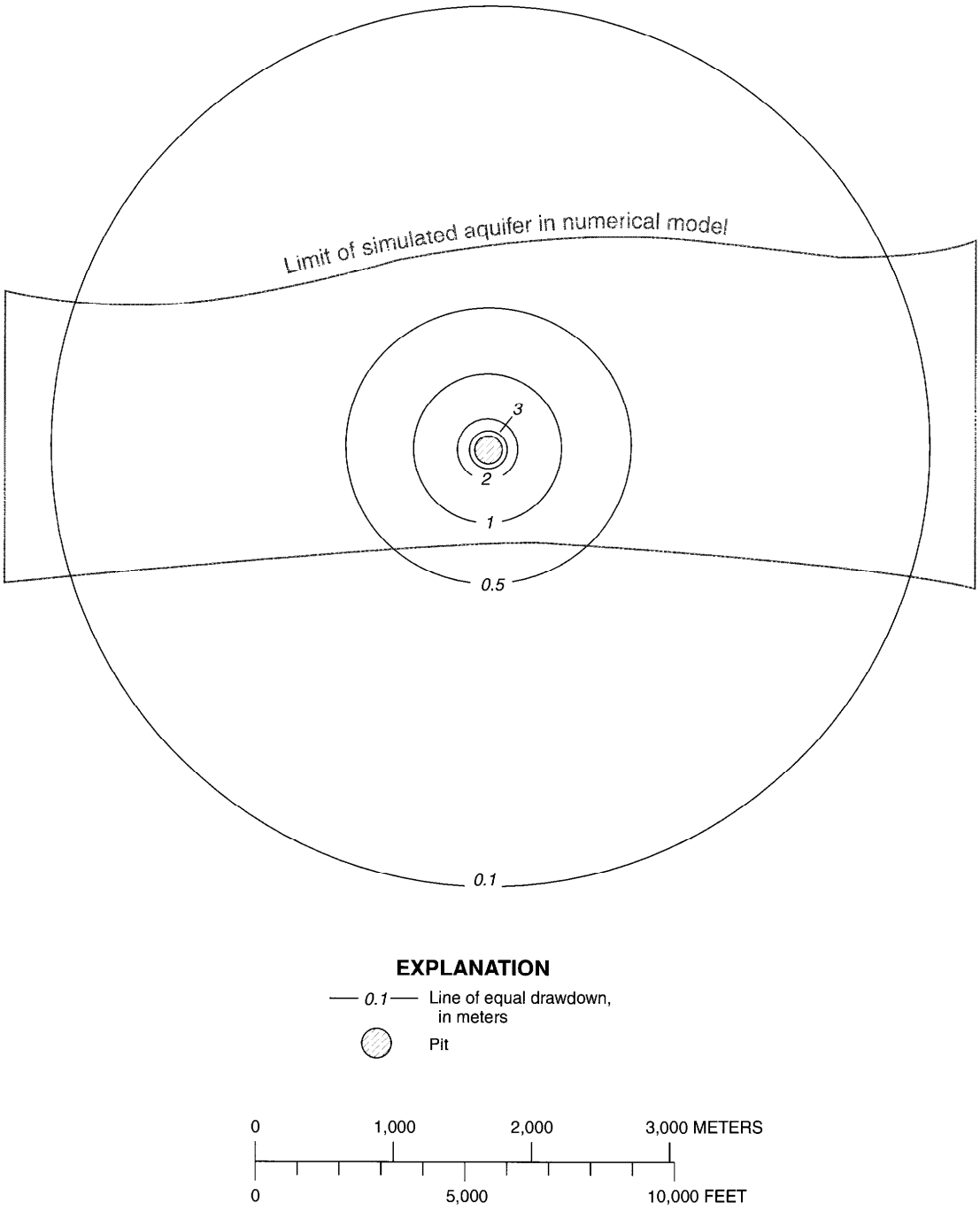

Figure 11*c*. Steady-state drawdown caused by a dewatered pit in a homogeneous, isotropic sand-and-gravel aquifer of infinite extent, simulated by use of the Marinelli and Niccoli (2000) analytical solution.

in the analytical simulation is contributed only by distributed recharge from precipitation.

Drawdown in the area between the pit and the river in the numerical simulation is less than drawdown in the analytical simulation because the river in the numerical simulation acts as a recharge boundary and maintains hydraulic head in the aquifer near premining levels at the river. Although the river contributes flow to the pit and acts as a recharge boundary in the numerical simulation, some drawdown (0.1 m) does occur across the river because ground water flows to the pit through the underlying aquifer in layer 2. Drawdown away from the river in the numerical simulation is greater than drawdown in the analytical simulation because the area of influence in the numerical simulation contacts the boundary of the aquifer, which limits flow to the area of influence and causes hydraulic head to drop more substantially.

Under premining conditions, the largest component of recharge is from inflow at the upgradient end of the aquifer, and the second largest component of recharge is from inflow along the sides of the aquifer. Precipitation is a relatively small component of recharge, and river leakage to the aquifer is the smallest component. Discharge at the downgradient end of the aquifer under premining conditions is similar in magnitude to discharge to the river. The complete ground-water budget for premining conditions in simulation 1 is shown in table 1, and the complete ground-water budget for the effects of the dewatered pit in simulation 1 is shown in table 2. The ground-water budgets give an accounting of recharge to the aquifer and discharge from the aquifer. Values given in the tables indicate total volumetric fluxes for each category. Recharge to the aquifer includes (1) ground-water inflow from the constant-head boundary at the upgradient end of the aquifer, (2) ground-water inflow from general-head boundaries along the sides of the aquifer, (3) river leakage to the aquifer, and (4) distributed recharge from precipitation. Discharge from the aquifer includes (1) ground-water outflow to the constant-head boundary at the downgradient end of the aquifer, (2) ground-water discharge to the river,

Table 1. Steady-state ground-water budget for six numerical simulations of premining conditions in hypothetical sand-and-gravel aquifers

[All values are in cubic meters per day; totals reflect sum of all rounded individual components; --, not computed]

Budget component	Simulation 1	Simulation 2	Simulation 3	Simulation 4	Simulation 5	Simulation 6
Recharge to aquifer						
Ground-water inflow from constant-head boundary at upgradient end of aquifer	6,928	6,928	24,748	2,019	6,929	6,929
Ground-water inflow from general-head boundaries along sides of aquifer	3,966	3,966	7,551	--	3,966	3,966
River leakage to aquifer	271	270	1,067	705	271	271
Precipitation recharge	749	749	1,599	404	749	749
Total	11,914	11,913	34,965	3,128	11,915	11,915
Discharge from aquifer						
Ground-water outflow to constant-head boundary at downgradient end of aquifer	6,650	6,650	28,374	2,352	6,649	6,649
Ground-water discharge to river	5,264	5,263	6,577	777	5,265	5,265
Total	11,914	11,913	34,951	3,129	11,914	11,914
Recharge – Discharge	0	0	14	–1	1	1

Model simulations:

1. Medium-sized, homogeneous, isotropic aquifer.
2. Medium-sized, homogeneous, vertically anisotropic aquifer.
3. Large, homogeneous, isotropic aquifer.
4. Small, homogeneous, isotropic aquifer.
5. Medium-sized, homogeneous, isotropic aquifer.
6. Medium-sized, homogeneous, isotropic aquifer.

Table 2. Steady-state ground-water budget for six numerical simulations of the effects of mining aggregate in hypothetical sand-and-gravel aquifers

[All values are in cubic meters per day; totals reflect sum of all rounded individual components; --, not computed]

Budget component	Simulation 1	Simulation 2	Simulation 3	Simulation 4	Simulation 5	Simulation 6
Recharge to aquifer						
Ground-water inflow from constant-head boundary at upgradient end of aquifer	6,937	6,937	25,532	2,019	6,921	6,933
Ground-water inflow from general-head boundaries along sides of aquifer	4,043	4,043	7,684	--	3,956	3,975
River leakage to aquifer	4,652	4,639	18,541	3,608	328	587
Precipitation recharge	747	747	1,597	402	739	749
Total	16,379	16,366	53,354	6,029	11,944	12,244
Discharge from aquifer						
Ground-water outflow to constant-head boundary at downgradient end of aquifer	6,505	6,504	27,253	2,338	6,653	6,662
Ground-water discharge to river	3,135	3,132	1,634	432	5,292	5,403
Ground-water discharge to actively dewatered pit	6,740	6,730	24,500	3,260	--	--
Cumulative evaporative losses at pits	--	--	--	--	--	680
Total	16,380	16,366	53,387	6,030	11,945	12,745
Recharge – Discharge	–1	0	–33	–1	–1	–501

Model simulations:

1. Pit in medium-sized, homogeneous, isotropic aquifer.
2. Pit in medium-sized, homogeneous, vertically anisotropic aquifer.
3. Pit in large, homogeneous, isotropic aquifer.
4. Pit in small, homogeneous, isotropic aquifer.
5. Five pits lined with slurry walls in medium-sized, homogeneous, isotropic aquifer.
6. Five water-filled pits undergoing evaporative losses in medium-sized, homogeneous, isotropic aquifer.

and (3) ground-water discharge to the pit under conditions of active mining.

Under conditions of active mining, when the pit is dewatered, inflow from the upgradient end and the sides of the aquifer is slightly greater than under premining conditions because drawdown caused by the pit increases the hydraulic gradient in the area between the pit and the upgradient end and sides of the aquifer. Recharge from precipitation is nearly unchanged between premining and active mining conditions. The slight difference in precipitation recharge between the two simulations likely is due to cells going dry during the rewetting process for unconfined conditions in the active mining simulation. River leakage to the aquifer is much greater under active mining conditions than under premining conditions because drawdown caused by the pit reverses the hydraulic gradient in the area between the pit and the river, which causes water to flow from the river to the aquifer. The largest component of discharge under active mining conditions is ground-water discharge to the pit. Outflow to the downgradient end of the aquifer under active mining conditions is somewhat less than under premining conditions because drawdown caused by the pit decreases the hydraulic gradient in the area between the pit and the down-gradient end of the aquifer. Ground-water discharge to the river under active mining conditions is less than under premining conditions because drawdown caused by the pit intercepts ground water that, under premining conditions, flows to the river.

Simulation 2–Pit in a medium-sized, homogeneous aquifer with vertical anisotropy

Simulation 2 shows the effect vertical anisotropy may have on steady-state drawdown near a dewatered pit in a medium-sized (about 2,500 m wide) alluvial valley. Simulation 2 is identical to simulation 1 except vertical hydraulic conductivity is uniformly set to a value equal to one-tenth the horizontal hydraulic conductivity. Simulation 2 represents a system in which lithologic stratification of the sand-and-gravel aquifer has produced vertical anisotropy.

The simulated steady-state premining distribution of hydraulic head in the anisotropic aquifer (fig. 12*a*) and steady-state drawdown near a dewatered pit in the anisotropic aquifer (fig. 12*b*) are nearly identical to those in the isotropic aquifer of simulation 1. The premining ground-water budget (table 1) for simulation 2 also is nearly identical to that of simulation 1. The active mining ground-water budget (table 2) for simulation 2 differs only slightly from that of simulation 1. River leakage to the aquifer, ground-water discharge to the river, and ground-water discharge to the pit under active mining conditions are slightly less in simulation 2 than in simulation 1 because the lower vertical hydraulic conductivity of simulation 2 reduces flow between the layers and, therefore, reduces exchange of water with the river and inflow to the pit bottom.

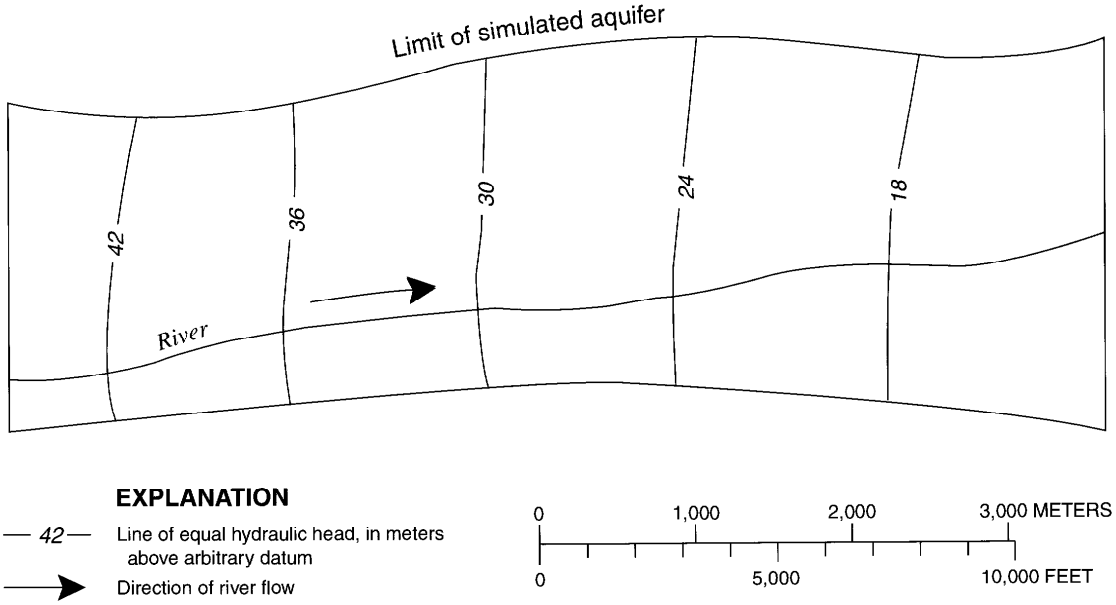

Figure 12*a*. Numerical simulation 2–Steady-state premining distribution of hydraulic head in a hypothetical, medium-sized sand-and-gravel aquifer under homogeneous and vertically anisotropic conditions.

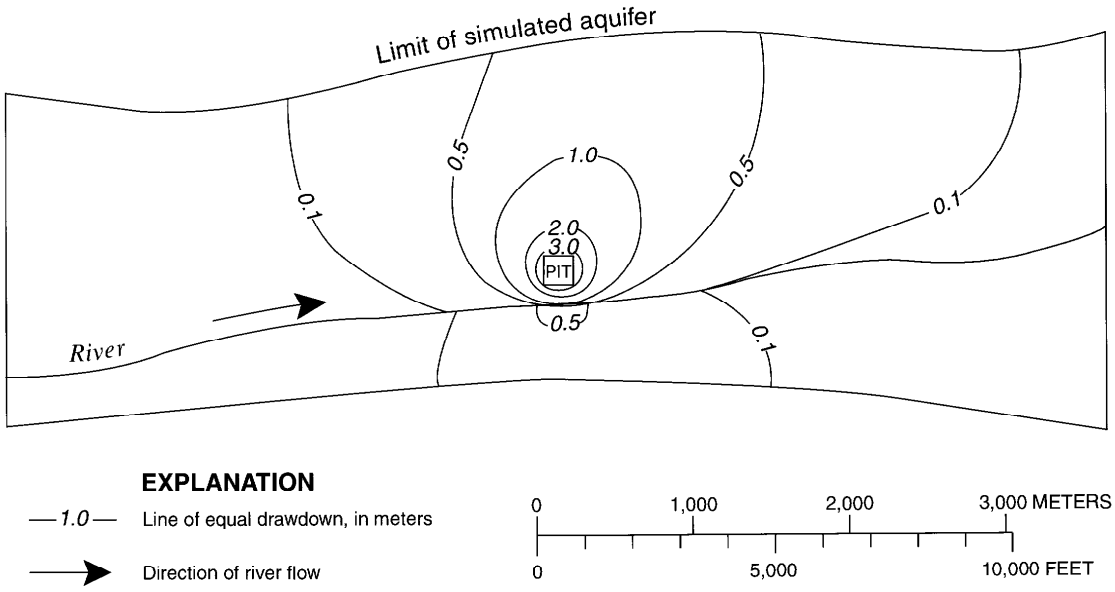

Figure 12*b*. Numerical simulation 2–Steady-state drawdown caused by a dewatered pit in a hypothetical, medium-sized sand-and-gravel aquifer under homogeneous and vertically anisotropic conditions.

Simulation 3–Pit in a large, homogeneous, isotropic aquifer

Simulation 3 shows the potential hydrologic effects of dewatering a pit in a large alluvial valley. Simulation 3 is similar to simulation 1 except the alluvial valley in which mining occurs is deeper and wider, and the hydraulic conductance of the general-head boundaries and river are larger. The simulation represents a valley 7,000 m long and about 5,000 m wide. Layer 1 is 6 m thick with about 3 to 5 m of saturated thickness. Layer 2 is 16 m thick and is fully saturated. Total premining saturated thickness near the pit is about 20 m. The premining steady-state hydraulic gradient is about 0.003, which is typical of gradients in larger alluvial valleys in the Front Range area. Grid spacing and number of columns in the model are the same as in simulation 1, but 25 rows were added to accommodate the greater valley width.

To simulate a greater amount of inflow to the larger valley, the hydraulic conductance of general-head boundaries along the valley sides in simulation 3 is approximately double that of simulation 1. Similarly, the hydraulic conductance of the riverbed is doubled to simulate a larger river with a greater capacity to exchange flow with the aquifer.

The simulated steady-state premining distribution of hydraulic head in the large aquifer is shown in figure 13*a*, and steady-state drawdown near a dewatered pit in the large aquifer is shown in figure 13*b*. Area of influence in simulation 3 has a maximum extent (measured from pit center) of about 4,350 m. Area of influence in simulation 3 is larger and more symmetrical than in simulation 1. Area of influence is larger in simulation 3 because the greater aquifer thickness and riverbed conductance allow more ground water to flow to the pit, which must then be removed to maintain drawdown at the pit. As more

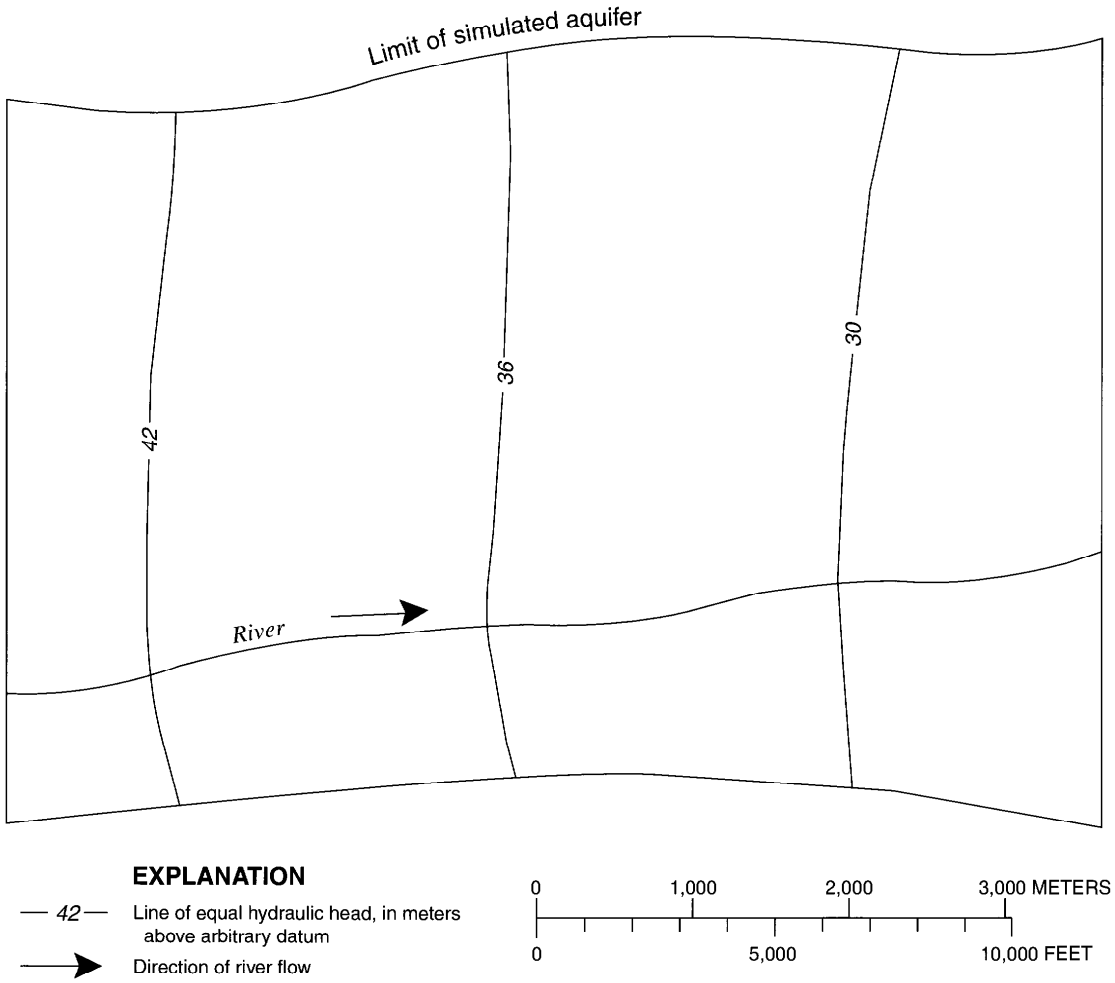

Figure 13*a*. Numerical simulation 3–Steady-state premining distribution of hydraulic head in a hypothetical, large sand-and-gravel aquifer under homogeneous and isotropic conditions.

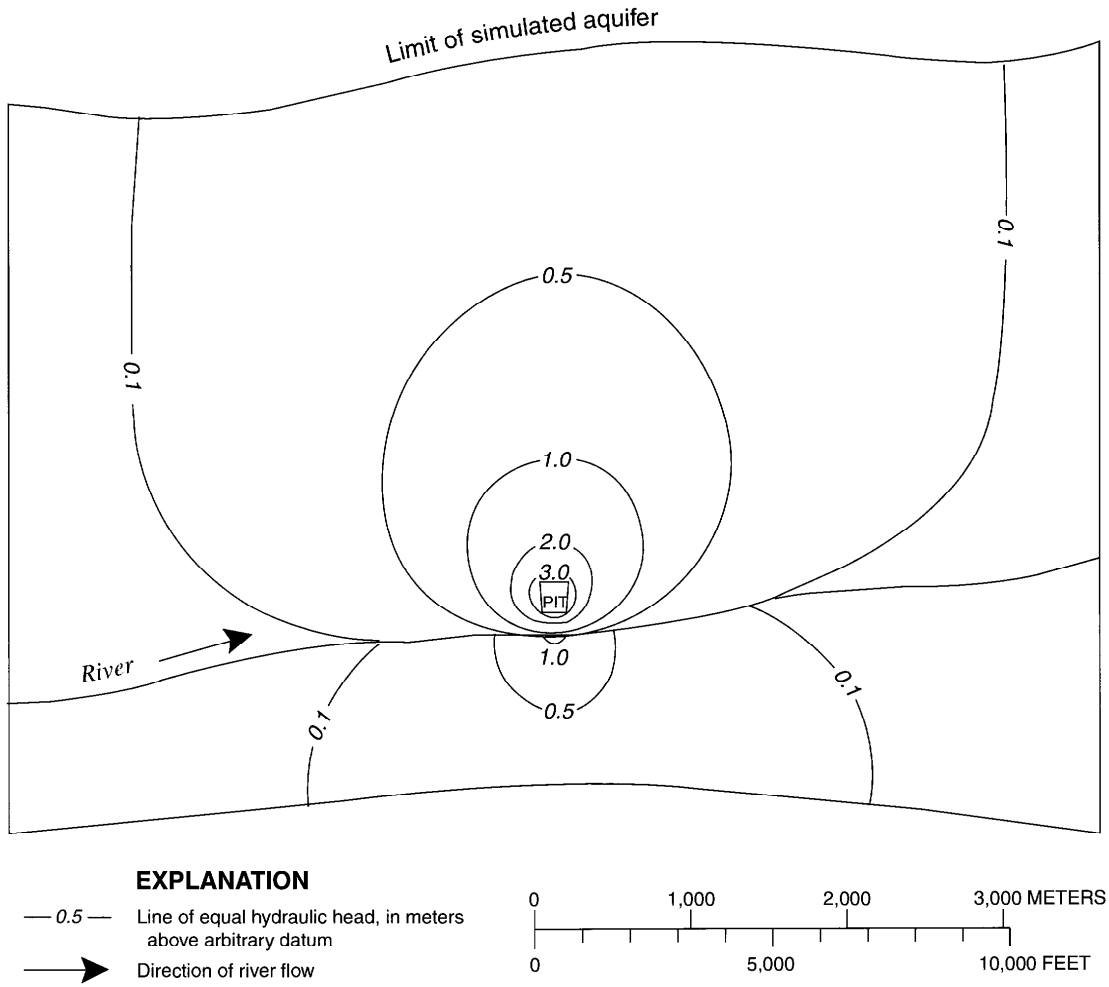

Figure 13*b*. Numerical simulation 3–Steady-state drawdown caused by a dewatered pit in a hypothetical, large sand-and-gravel aquifer under homogeneous and isotropic conditions.

water is removed, the effects of drawdown at the pit occur farther away. Area of influence in simulation 3 is more symmetrical than that in simulation 1 because aquifer boundaries are farther from the pit and, therefore, have less effect on the shape of the area of influence. The shape of the area of influence in simulation 3 is more like that of the infinite aquifer simulated using the analytical solution. Drawdown across the river in simulation 3 is greater than in simulation 1 because flow to the pit is greater and the bottom layer of the aquifer in simulation 3 is thicker, which allows the pit to draw more ground water from across the river.

With the exception of ground-water discharge to the river under active mining conditions (table 2), flow for all ground-water budget components under pre-mining and active mining conditions (tables 1 and 2) in simulation 3 is larger than in simulation 1 because the aquifer in simulation 3 is larger and has higher conductances for the general-head boundaries and riverbed. Ground-water discharge to the river under active mining conditions is less than that in simulation 1 because the larger area of influence in simulation 3 reduces the area where ground water can flow to the river.

Simulation 4–Pit in a small, homogeneous, isotropic aquifer

Simulation 4 shows the potential hydrologic effects of dewatering a pit in a small alluvial valley. Simulation 4 is similar to simulation 1 except the width of the alluvial valley in which mining occurs is smaller, no-flow boundaries are used along the sides of the valley, and the conductance term of the riverbed is smaller. The simulation represents a valley 7,000 m long and about 1,200 m wide. Layer 1 is 4 m thick

with about 1 to 3 m of saturated thickness. Layer 2 is 2 m thick and is fully saturated. Total premining saturated thickness near the pit is about 4 m. Because the aquifer in simulation 4 is shallow, the base of the pit occurs in model layer 2 rather than layer 1. The steady-state premining hydraulic gradient is similar to that of simulation 1. Grid spacing and number of columns in the model are the same as in simulation 1, but only 24 rows are needed to represent the smaller valley width. No-flow boundaries are used along the sides of the model to simulate an alluvial valley incised into bedrock with no ground-water inflow to the sides of the valley. Riverbed conductance is decreased by a factor of 2 to simulate a smaller capacity river flowing in the valley.

The simulated steady-state premining distribution of hydraulic head in the small aquifer is shown in figure 14*a*, and steady-state drawdown near a dewatered pit in the small aquifer is shown in figure 14*b*.

Area of influence in simulation 4 has a maximum extent (measured from pit center) of about 2,050 m. Area of influence in simulation 4 is smaller than that in simulation 1, but drawdown generally is greater because the sides of the aquifer are closer to the pit, and the no-flow boundaries do not contribute ground-water inflow to the aquifer as do the general-head boundaries in simulation 1. Drawdown across the river in simulation 4 is similar to that in simulation 1.

Flow for all ground-water budget components in simulation 4 (tables 1 and 2), except river leakage to the aquifer under premining conditions (table 1), is smaller than in simulation 1 because the aquifer in simulation 4 is smaller and the riverbed has smaller hydraulic conductance than in simulation 1. River leakage to the aquifer under premining conditions in simulation 4 is larger than in simulation 1 because the no-flow boundaries along the sides of the aquifer in simulation 4 do not contribute flow to the aquifer,

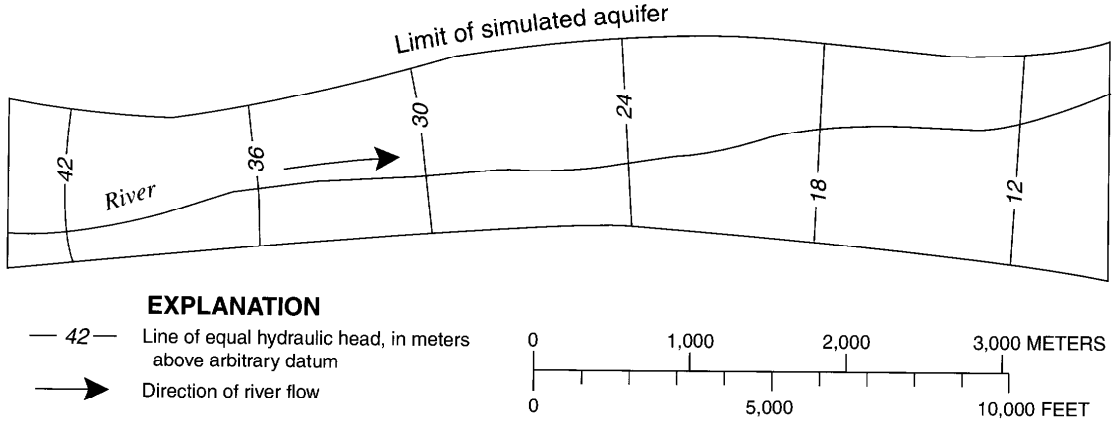

Figure 14*a*. Numerical simulation 4 –Steady-state premining distribution of hydraulic head in a hypothetical, small sand-and-gravel aquifer under homogeneous and isotropic conditions.

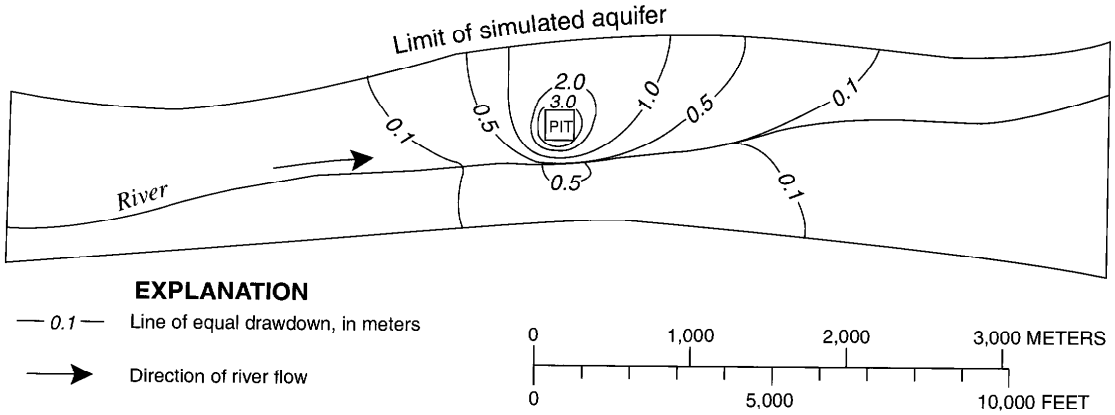

Figure 14*b*. Numerical simulation 4 –Steady-state drawdown caused by a dewatered pit in a hypothetical, small sand-and-gravel aquifer under homogeneous and isotropic conditions.

which causes the ground-water gradient between the sides of the aquifer and the river to be flatter and the water table to be lower than the river in places.

Simulation 5–Five pits lined with slurry walls in a medium-sized, homogeneous, isotropic aquifer

A slurry wall sometimes is installed around a pit to isolate it from ground water while mining continues or after mining ceases. Simulation 5 shows the potential cumulative effect of five closely spaced pits lined with slurry walls in a medium-sized (about 2,500 m wide) alluvial valley. Simulation 5 is similar to simulation 1 except five medium-sized pits are simulated simultaneously, and the area of grid refinement near the pits was enlarged to encompass five pits rather than one. The revised model grid has 35 rows and 90 columns with a cell size of 50 m × 50 m near the pits and a cell size of 100 m × 100 m at a distance of 500 m to 650 m from the pits. The five pits in simulation 5 are placed 100 m apart. Pits lined with slurry walls are simulated by using inactive cells at pit locations, thereby simulating no-flow barriers at the edges of the pits where slurry walls would be present. Simulating the slurry walls as no-flow barriers maximizes the hydrologic effects of the pit on the aquifer.

The simulated steady-state premining distribution of hydraulic head in the aquifer in simulation 5 is the same as in simulation 1 (fig. 11*a*), and steady-state drawdown near the pits in simulation 5 is shown in figure 15. Drawdown near the pits is complex and ranges from about –0.5 m to 0.3 m. Drawdown is negative upgradient from the pits, which indicates ground water is mounding against the impermeable slurry walls. Drawdown is positive downgradient from the pits, which indicates the pits have a shadow effect on ground-water flow. The extent of upgradient mounding (defined by the limit of –0.1-m drawdown) is about 2,200 m wide, and the extent of downgradient drawdown (defined by the limit of 0.1-m drawdown) is about 400 m wide. Ground-water levels across the river are not significantly affected by the pits in simulation 5.

The premining ground-water budget (table 1) of simulation 5 is nearly identical to that of simulation 1. Slight differences between the two simulations likely are due to the larger area of grid refinement in simulation 5. Recharge to the aquifer from precipitation (table 2) under active mining conditions is slightly less than in simulation 1 because inactive cells used to simulate lined pits do not contribute flow to the aquifer. Recharge from all other ground-water budget components and discharge to all ground-water budget components are greater than in simulation 1 because active pit dewatering is not simulated.

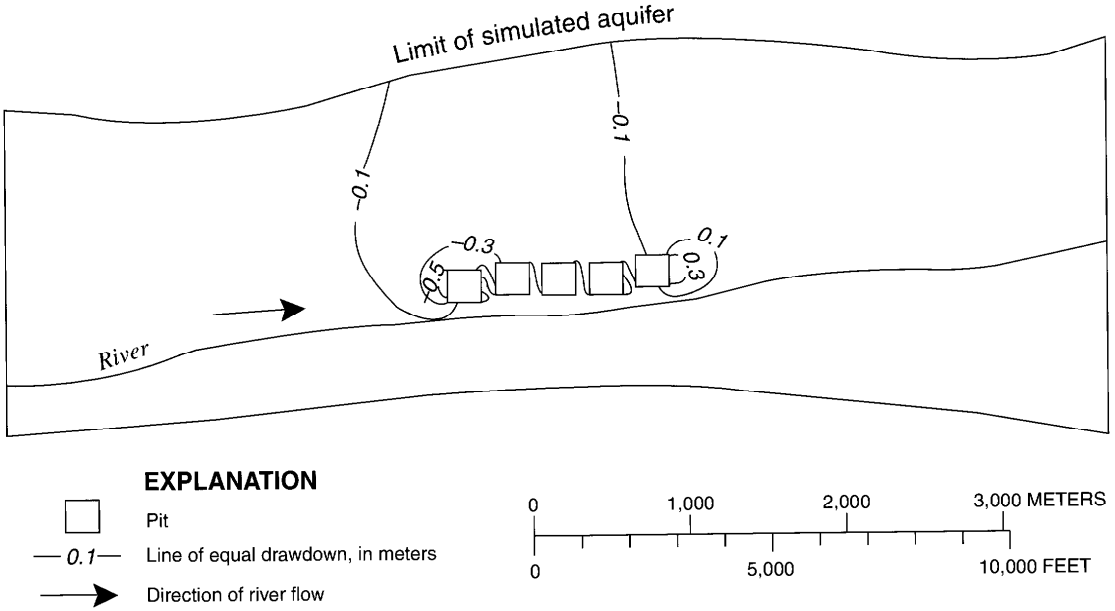

Figure 15. Numerical simulation 5–Steady-state drawdown caused by five closely spaced pits lined with slurry walls in a hypothetical, medium-sized sand-and-gravel aquifer under homogeneous and isotropic conditions.

Simulation 6–Five pits undergoing evaporative losses in a medium-sized, homogeneous, isotropic aquifer

Once mining is completed, aggregate pits may be refilled with water and used as water-storage reservoirs or for environmental or recreational purposes. Simulation 6 shows the potential cumulative effect of evaporative losses from five pits after refilling with water in a medium-sized (about 2,500 m wide) alluvial valley. Simulation 6 is the same as simulation 5 except cells at the pit locations are active (no slurry walls) and have horizontal and vertical hydraulic conductivity values 1,000 times greater than the surrounding aquifer material to simulate the open area of the pits. Using the MODFLOW–2000 Well package, evaporative losses are simulated as constant discharge from pit cells at a rate of 0.0034 m/d, which is approximately equal to average annual pan evaporation minus average annual precipitation for the Colorado Piedmont part of the Front Range area (see "Hydrogeologic Settings").

The simulated steady-state premining distribution of hydraulic head in the aquifer is the same as that of simulation 1 (fig. 11*a*), and steady-state drawdown caused by evaporation from the pits is shown in figure 16. To separate the effects of pit evaporation from the hydraulic effects of open pits in the aquifer, drawdown is calculated relative to initial steady-state post-mining conditions, rather than premining conditions. Drawdown near the pits is less than 0.1 m at all locations in simulation 6. For illustrative purposes, the limit of 0.05-m drawdown is shown in figure 16, but this area of influence is not comparable to other simulations, which have areas of influence defined by the limit of 0.1-m drawdown.

The premining ground-water budget (table 1) of simulation 6 is nearly identical to that of simulation 1. Slight differences between the two simulations likely are due to the larger area of grid refinement in simulation 6. Total evaporative loss from the pits is 680 m^3/d (table 2). The hydrologic effects of pits in simulation 6 are small because evaporative discharge from refilled pits is small compared to the overall ground-water budget for the aquifer.

Numerical Sensitivity Analysis

Composite scaled sensitivities were calculated for each simulation input parameter by using the Parameter Sensitivity with Observations mode (Hill and others, 2000) of MODFLOW–2000. Composite scaled sensitivities are dimensionless quantities that provide information about the importance of each input parameter to calculations of simulated equivalents (head or flow) at specific locations (observations) and indicate the amount of information that observations contain for the estimation of a parameter (Hill, 1998). The actual value of sensitivity for each

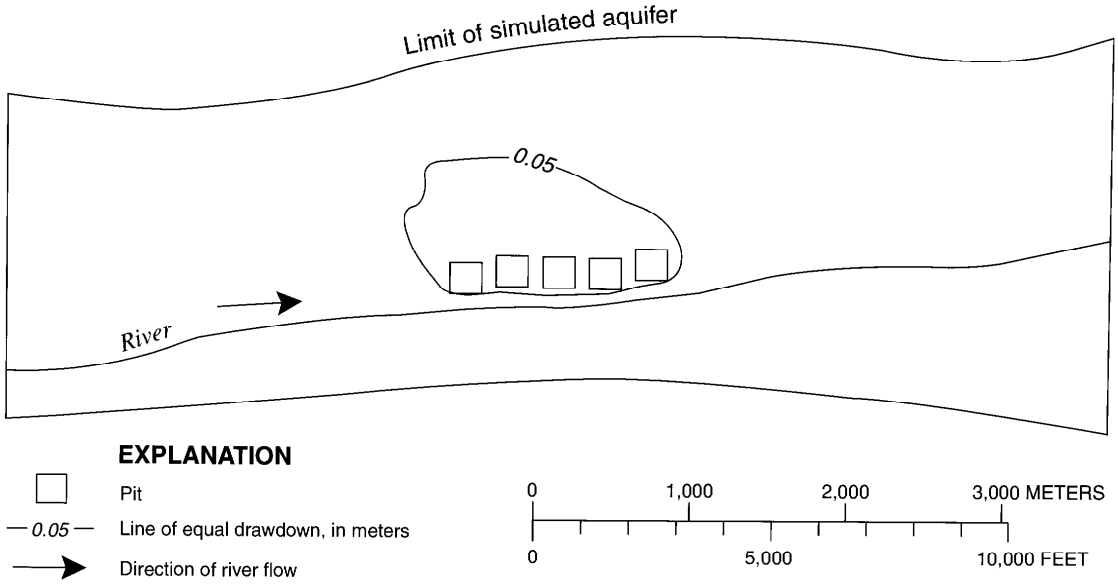

Figure 16. Numerical simulation 6–Steady-state drawdown caused by five closely spaced, water-filled pits undergoing evaporative losses in a hypothetical, medium-sized sand-and-gravel aquifer under homogeneous and isotropic conditions.

parameter is less meaningful than the relative magnitude of the value compared to the sensitivities for other parameters. Parameters with high sensitivities affect simulated equivalents more than parameters with low sensitivities, and high sensitivities indicate that available observations provide much information on which parameters can be estimated. In this report, composite scaled sensitivities indicate the sensitivity of simulated head to variations in parameter values. The sensitivity of simulated flow to variations in parameter values was not calculated because changes in head (drawdown and area of influence) are the primary quantities of interest in the study.

Sensitivities of simulated head were calculated for each parameter by using hypothetical observations distributed evenly throughout the numerical model domain. Twenty-six observations were used to calculate sensitivities in simulations 1, 2, 5, and 6 (medium-sized alluvial valley); 52 observations were used to calculate sensitivities in simulation 3 (large alluvial valley); and 20 observations were used to calculate sensitivities in simulation 4 (small alluvial valley). Observation locations are shown in figure 17. The use of hypothetical head observations does not affect simulation results, but the observations are necessary to generate composite scaled sensitivities using MODFLOW–2000.

Composite scaled sensitivities depend on model construction and observation locations and are, therefore, unique to each model. However, because observations are distributed evenly throughout the hypothetical aquifers, composite scaled sensitivities describe the approximate overall sensitivity of simulated head to each parameter and may indicate which parameters are most critical to define at real sites having conditions similar to those of the hypothetical aquifers. Parameters with high sensitivities may be more important to accurately define for predictions of mining effects than parameters with low sensitivities. Results of sensitivity analysis for simulation 1 are shown in figure 18. Results of sensitivity analyses for all sand-and-gravel aquifer simulations are shown in table 3.

Results of the sensitivity analyses indicate simulated head was most sensitive to variations in horizontal hydraulic conductivity in every simulation except simulation 6 (five pits undergoing evaporative losses), in which simulated head was most sensitive to variations in the hydraulic conductance term of the

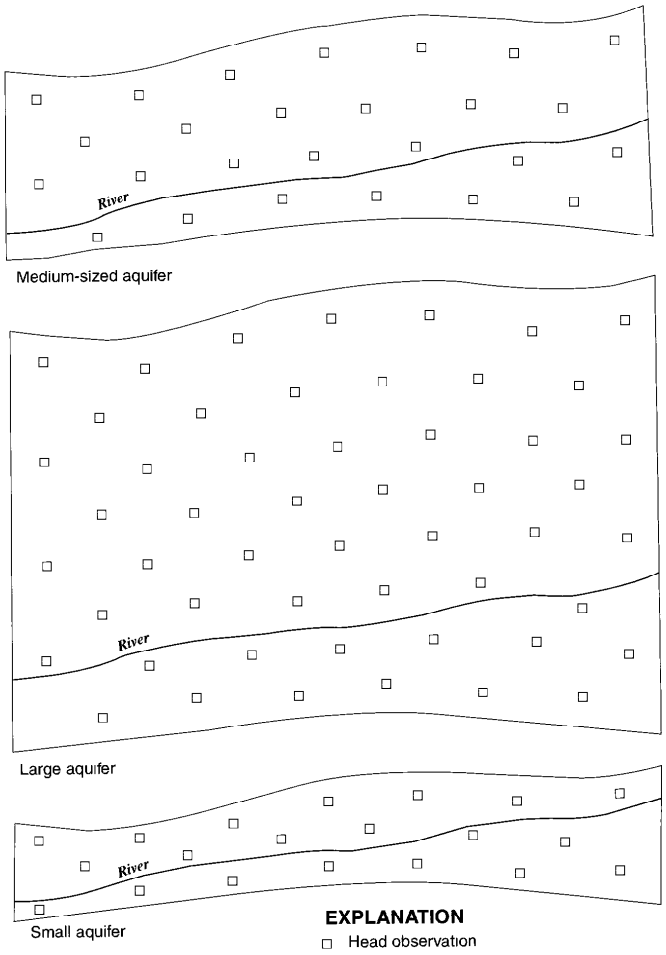

Figure 17. Location of hypothetical head observations used to calculate composite scaled sensitivities for numerical simulations of the hydrologic effects of mining aggregate in sand-and-gravel aquifers.

general-head boundaries. In all simulations except simulation 6 and simulation 4 (no general-head boundaries present), the sensitivity for general-head boundary conductance was second only to that for horizontal hydraulic conductivity and was similar in magnitude to that of horizontal hydraulic conductivity. Similarly, the sensitivities for riverbed conductance and recharge were similar in magnitude to each other in all simulations except simulations 3 and 4, but the sensitivities were relatively small compared to those for horizontal hydraulic conductivity and general-head boundary conductance. Simulated head was relatively insensitive to vertical hydraulic conductivity in all simulations.

For simulations of a real gravel pit or quarry, it would be important to include hydrologic observations of both hydraulic head and flow data for simulation

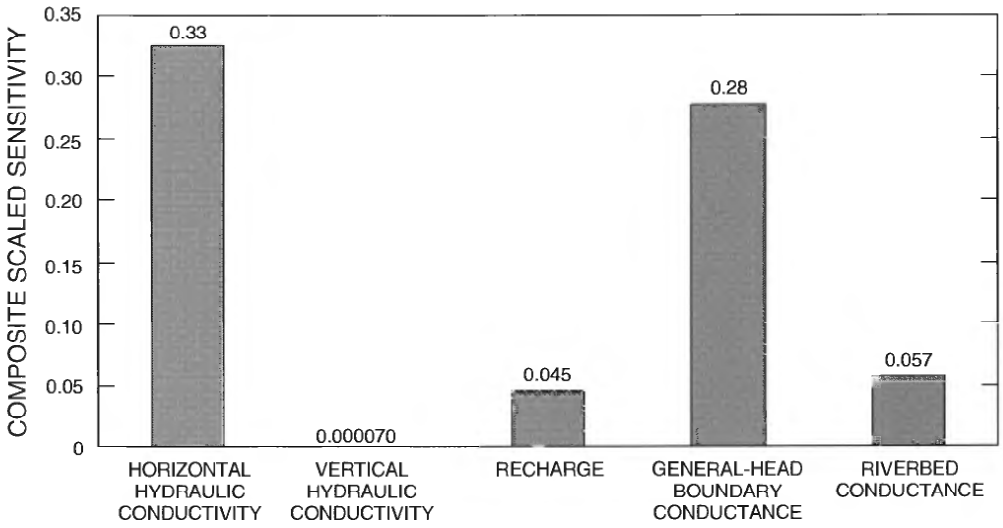

Figure 18. Composite scaled sensitivities for parameters in numerical simulation 1 (pit in a hypothetical, medium-sized sand-and-gravel aquifer under homogeneous and isotropic conditions.

Table 3. Composite scaled sensitivities for parameters used in six numerical simulations of the effects of mining aggregate in hypothetical sand-and-gravel aquifers

[--, not applicable]

Simulation	Parameter				
	Horizontal hydraulic conductivity	Vertical hydraulic conductivity	Recharge	General-head boundary conductance	Riverbed conductance
1	0.33	0.000070	0.045	0.28	0.057
2	0.33	0.00069	0.045	0.28	0.057
3	0.33	0.0034	0.044	0.23	0.10
4	0.12	0.000056	0.024	--	0.10
5	0.29	0.000042	0.051	0.29	0.069
6	0.25	0.000077	0.043	0.26	0.064

Model simulations:

1. Pit in medium-sized, homogeneous, isotropic aquifer.
2. Pit in medium-sized, homogeneous, vertically anisotropic aquifer.
3. Pit in large, homogeneous, isotropic aquifer.
4. Pit in small, homogeneous, isotropic aquifer.
5. Five pits lined with slurry walls in medium-sized, homogeneous, isotropic aquifer.
6. Five water-filled pits undergoing evaporative losses in medium-sized, homogeneous, isotropic aquifer.

calibration (Hill, 1998). Hydraulic head data alone often do not provide enough information to break the inverse correlation between the hydraulic conductivity and recharge parameters and therefore obtain a unique solution to the ground-water flow equation (Hill, 1998). Streamflow or pit-discharge measurements provide a measure of ground-water discharge from an aquifer, and such flow measurements would be important to include when simulating actual gravel pits or quarries. Anderman and others (1996) present a detailed analysis of different types of hydrologic observations and their importance in ground-water flow simulations.

Simulation of Quarries in Fractured Crystalline-Rock Aquifers

Definitions of input parameters for simulations of aggregate mining in fractured crystalline-rock aquifers were based on data reported in the literature (see "Hydrogeologic Settings"). Definitions of mining extents (area and depth) were based on mine permit information, site data, and quarry footprints shown on U.S. Geological Survey 1:50,000 County Maps. Intermediate parameter values and boundary conditions were used in the simulations to represent average hydrogeologic conditions and mining extents. Parameter values and boundary conditions were then varied over a range of values and conditions typical for quarries in fractured crystalline-rock aquifers to determine the potential effects of mining over a wide range of conditions. Intermediate hydraulic conductivity was defined in the simulations as 0.01 m/d, and intermediate recharge was defined as 0.0001 m/d, which is about 7 percent of average annual precipitation for the Rocky Mountain part of the Colorado Front Range area. Intermediate quarry penetration of the water table was defined as 50 m, and intermediate quarry radius was defined as 200 m.

Analytical Simulations and Sensitivities

Two analytical solutions were used to simulate the effects of mining aggregate in a fractured crystalline-rock aquifer. The analytical solution of Marinelli and Niccoli (2000) was used to solve for the radius of influence (r_i) and saturated thickness (h) above the base of a dewatered circular quarry in a homogeneous, isotropic, fractured crystalline-rock aquifer of infinite extent. Equation 7 was used to solve for the distance of influence (x_i) and saturated thickness (h) above the base of a dewatered linear quarry in a homogeneous, isotropic, fractured crystalline-rock aquifer of infinite extent. Horizontal hydraulic conductivity (K_h), recharge (W), initial saturated thickness above the quarry base ($h = h_o$), and quarry radius (r_p, circular quarry only) were varied independently over a range of values typical for quarries in fractured crystalline-rock aquifers in the Front Range area. By varying the parameters independently, the effects of each parameter on simulation results were evaluated, and sensitivities for parameters were calculated. Because initial saturated thickness is measured relative to the quarry base, h_o also is equal to the depth to which the quarry penetrates the water table. The water level in the quarry was defined at the base of the quarry.

Figures 19–22 show drawdown ($h_o - h$) and radius of influence measured from the quarry wall ($r_i - r_p$) caused by a dewatered circular quarry in a fractured crystalline-rock aquifer for different values of K_h (0.0001, 0.01, and 1 m/d), W (0.000025, 0.0001, and 0.0004 m/d), h_o (20, 50, and 80 m), and r_p (100, 200, and 400 m). Figures 23–25 show drawdown and distance of influence (x_i) caused by a dewatered linear quarry in a fractured crystalline-rock aquifer for the same values of K_h, W, and h_o. Results indicate radius of influence from the wall of a dewatered circular quarry in a homogeneous, isotropic fractured crystalline-rock aquifer of infinite extent was 411 m under intermediate conditions ($K_h = 0.01$ m/d, $W = 0.0001$ m/d, $h_o = 50$ m, $r_p = 200$ m). Distance of influence from the wall of a dewatered linear quarry under the same conditions was 500 m. Radius (or distance) of influence increased as K_h, h_o, and r_p (circular quarry only) increased and as W decreased.

Equation 9 was used to calculate 1-percent scaled sensitivities (see "Analytical Simulations and Sensitivities" under "Simulation of Pits in Sand-and-Gravel Aquifers") for each parameter used in the analytical solutions of Marinelli and Niccoli (2000) and equation 7 to determine the effect of each parameter on simulation results under intermediate conditions. Resulting sensitivities have units of meters and are the change in radius or distance of influence caused by a 1-percent change in the parameter value.

Results of analytical sensitivity analysis under intermediate conditions ($K_h = 0.01$ m/d, $W = 0.0001$ m/d, $h_o = 50$ m, $r_p = 200$ m) are shown in figure 26 for a circular quarry and in figure 27 for a linear quarry.

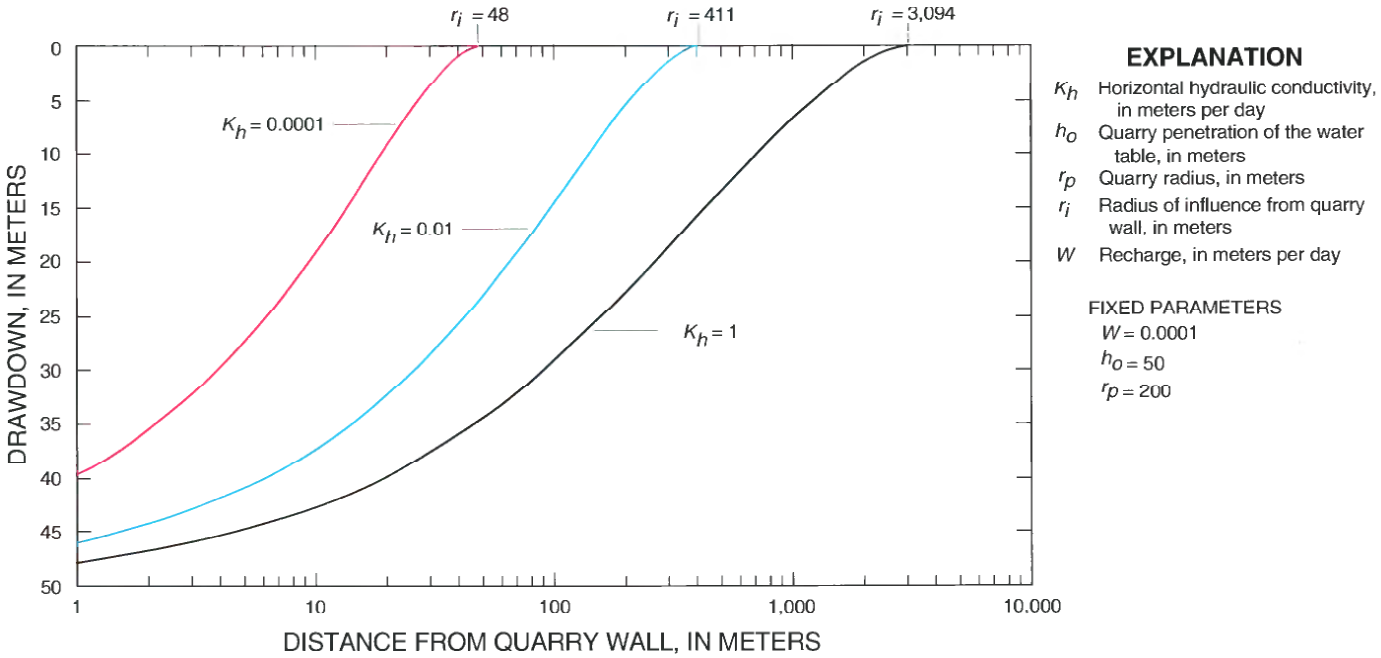

Figure 19. Drawdown relative to distance from a dewatered circular quarry in a fractured crystalline-rock aquifer for three values of horizontal hydraulic conductivity, simulated by use of the Marinelli and Niccoli (2000) analytical solution.

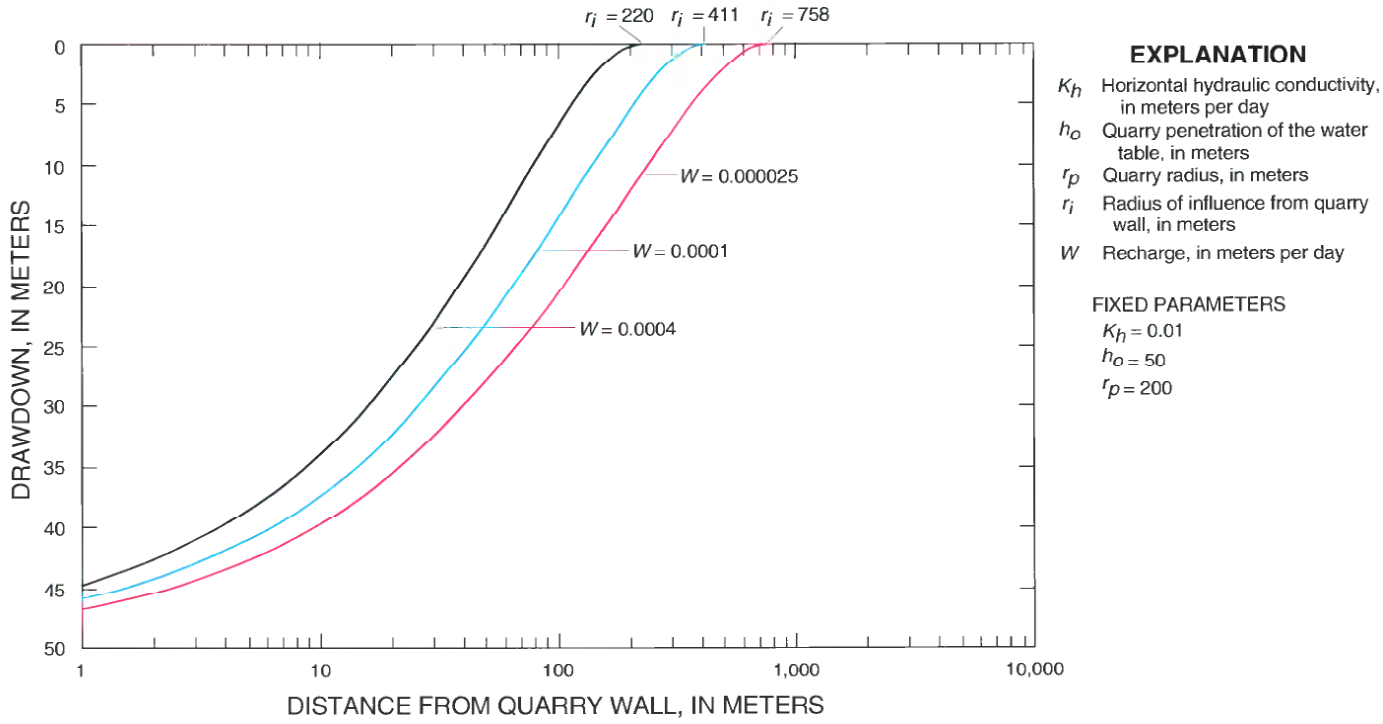

Figure 20. Drawdown relative to distance from a dewatered circular quarry in a fractured crystalline-rock aquifer for three values of recharge, simulated by use of the Marinelli and Niccoli (2000) analytical solution.

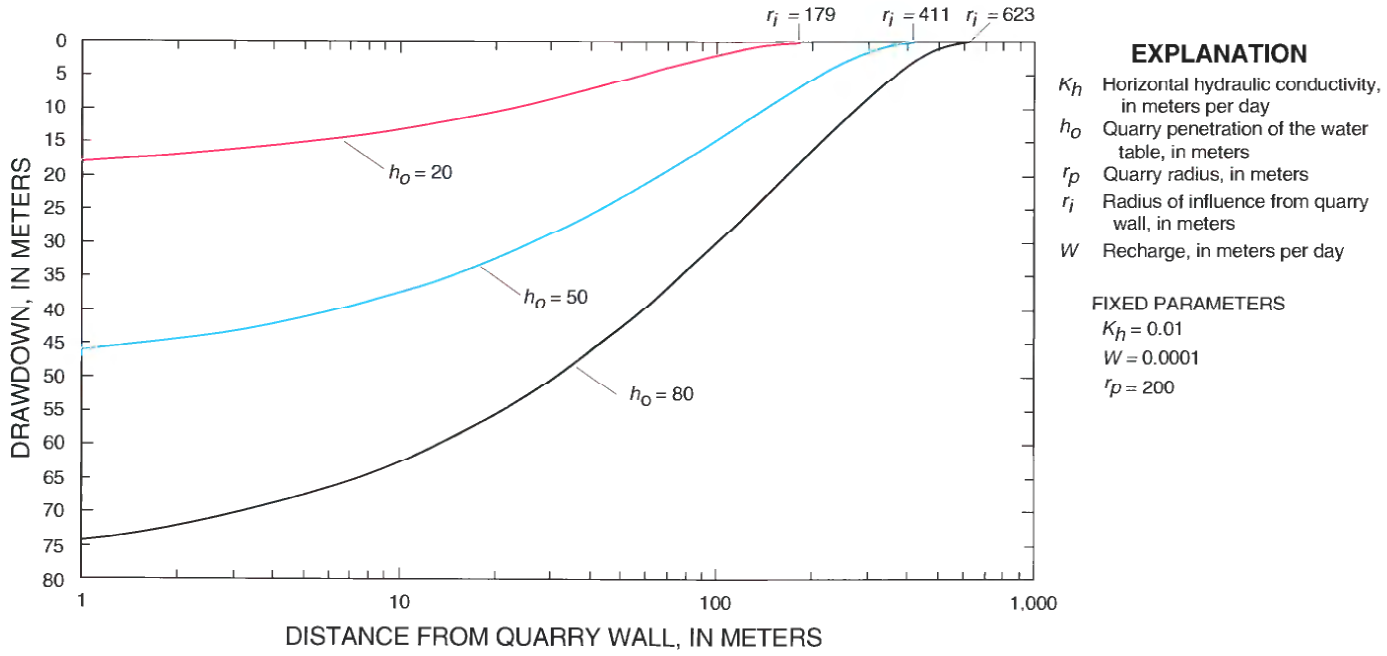

Figure 21. Drawdown relative to distance from a dewatered circular quarry in a fractured crystalline-rock aquifer for three values of quarry penetration of the water table, simulated by use of the Marinelli and Niccoli (2000) analytical solution.

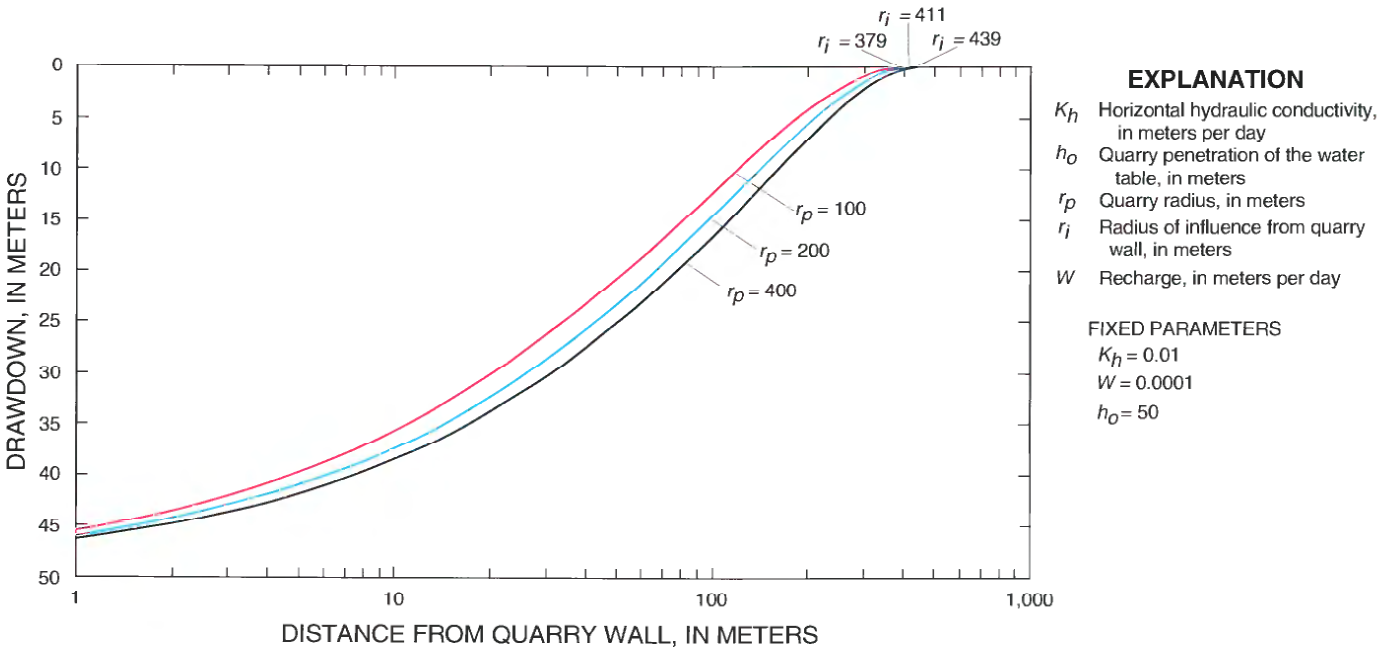

Figure 22. Drawdown relative to distance from a dewatered circular quarry in a fractured crystalline-rock aquifer for three values of quarry radius, simulated by use of the Marinelli and Niccoli (2000) analytical solution.

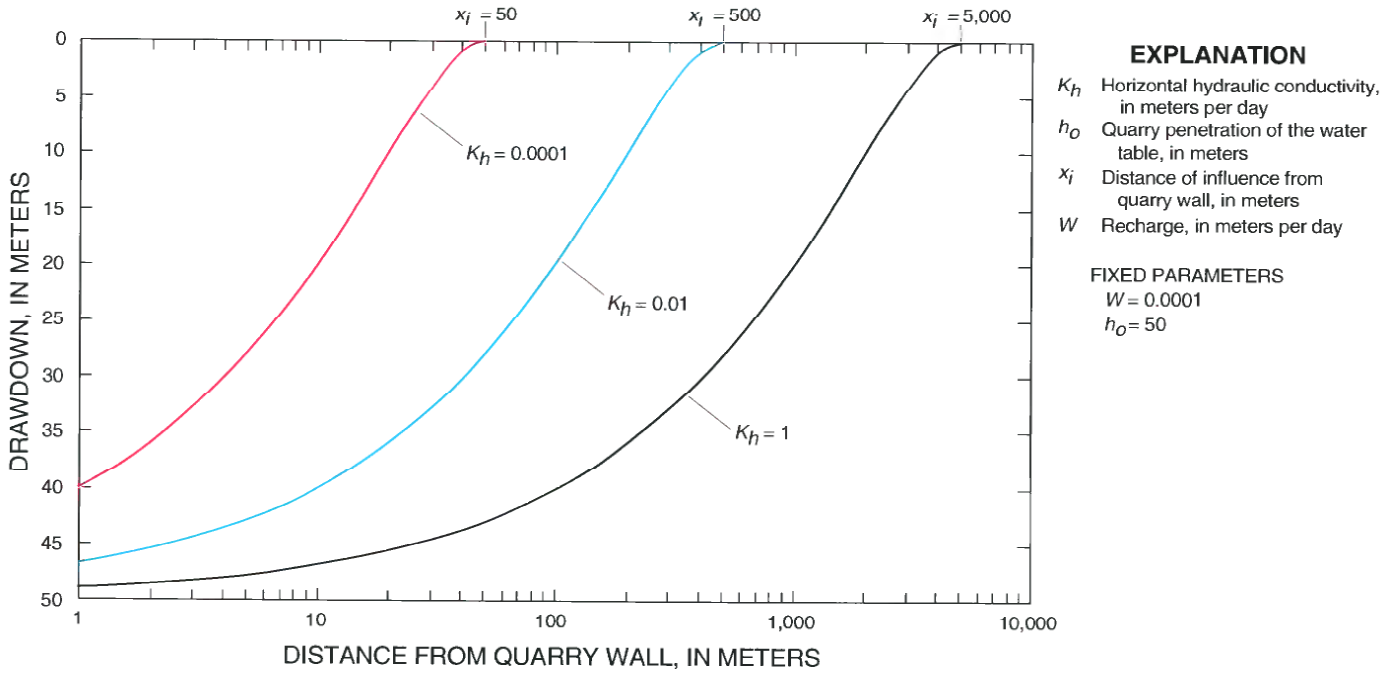

Figure 23. Drawdown relative to distance from a dewatered linear quarry in a fractured crystalline-rock aquifer for three values of quarry penetration of the water table, simulated by use of equation 7.

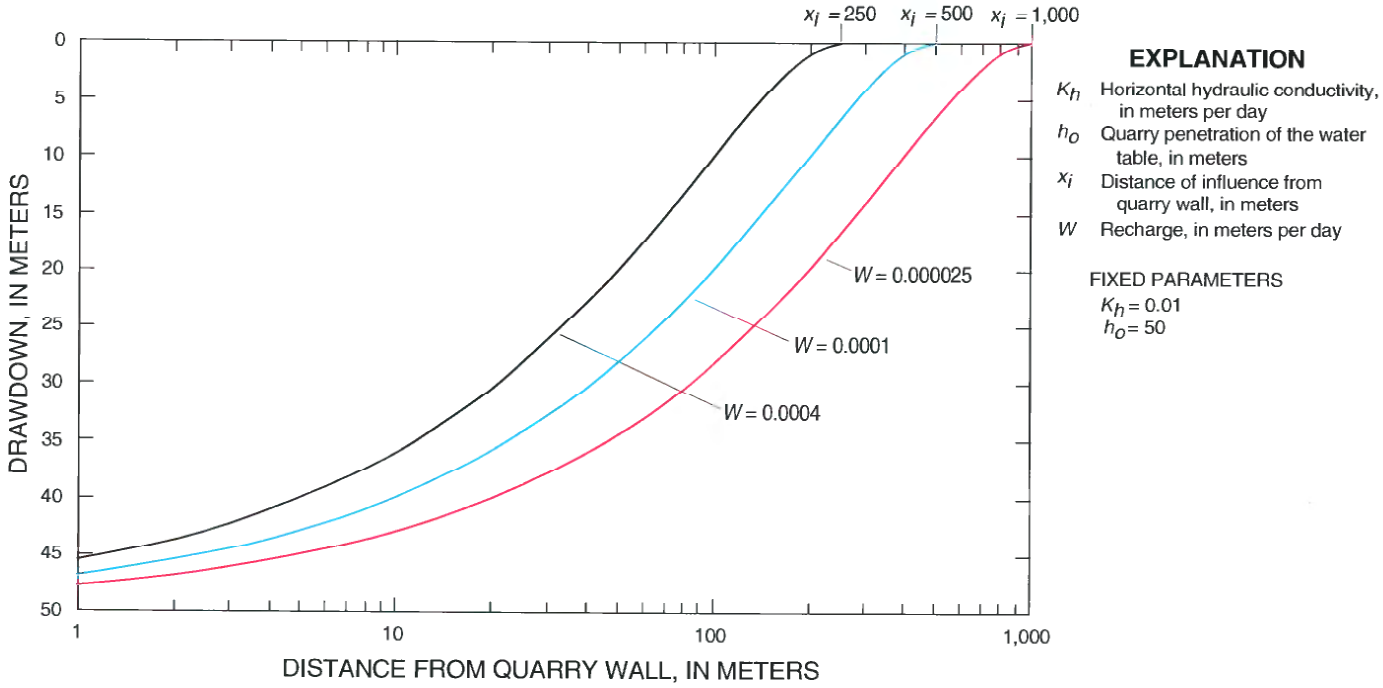

Figure 24. Drawdown relative to distance from a dewatered linear quarry in a fractured crystalline-rock aquifer for three values of recharge, simulated by use of equation 7.

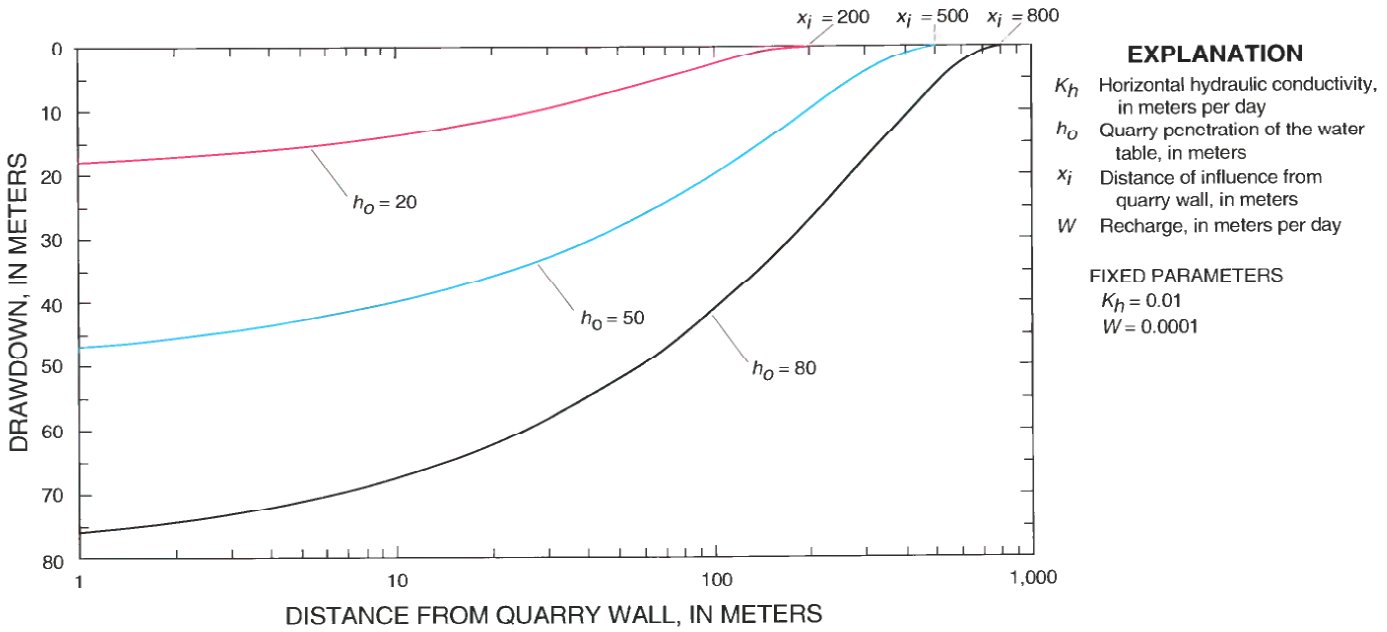

Figure 25. Drawdown relative to distance from a dewatered linear quarry in a fractured crystalline-rock aquifer for three values of quarry penetration of the water table, simulated by use of equation 7.

Results indicate that radius or distance of influence was most sensitive to changes in quarry penetration of the water table and least sensitive to changes in quarry radius (circular quarry only). Radius of influence was equally sensitive to changes in horizontal hydraulic conductivity and recharge. However, the parameters had opposite effects on simulation results because they are inversely correlated in the analytical solution. Radius (or distance) of influence increased as horizontal hydraulic conductivity increased and as recharge decreased.

Numerical Simulations

MODFLOW–2000 (Harbaugh and others, 2000) was used to compute (1) hydraulic heads in a hypothetical fractured crystalline-rock aquifer under steady-state, premining conditions, (2) steady-state drawdown caused by a dewatered quarry in the fractured crystalline-rock aquifer under different hydrogeologic conditions, and (3) inflow to the quarry under different hydrogeologic conditions. In addition, the observation and sensitivity capabilities (Hill and others, 2000) of MODFLOW–2000 were used to compute sensitivities for simulation input parameters. Although MODFLOW–2000 is designed to simulate ground-water flow in a porous medium, such as a sand-and-gravel aquifer, the code also was used in this study to simulate the effects of mining in a fractured crystalline-rock aquifer because it is well documented, well supported, and has been successfully applied to other fractured-rock settings (Tiedeman and others, 1997; Daniel and others, 1997; Long and others, 1982). Because simulations are of hypothetical aquifers, model calibration was not necessary. However, generalized aquifer data from real sites were used to guide development of simulated premining conditions. Six numerical simulations of the hydrologic effects of mining aggregate in hypothetical fractured crystalline-rock aquifers are presented as follows:

Simulation 7–The hydrologic effects of a dewatered quarry in a homogeneous and isotropic fractured crystalline-rock aquifer are simulated. Comparison of simulation 7 to analytical simulation results shows the effects of boundary conditions.

Simulation 8–The hydrologic effects of a dewatered quarry in a homogeneous but horizontally anisotropic, fractured crystalline-rock aquifer are simulated.

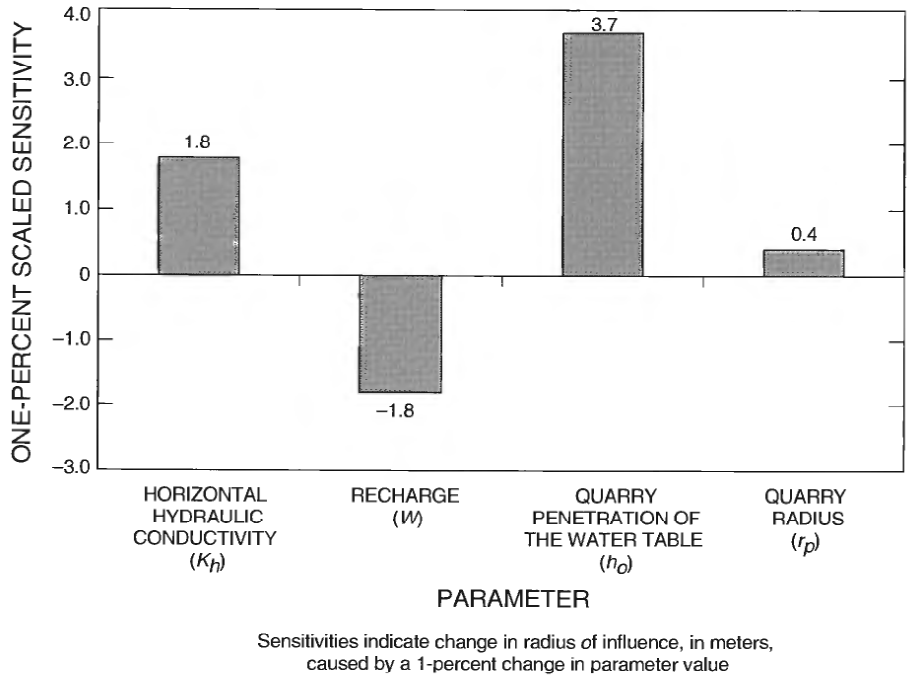

Figure 26. One-percent scaled sensitivities for parameters in the analytical solution of Marinelli and Niccoli (2000), calculated for a circular quarry in a fractured crystalline-rock aquifer under intermediate conditions (K_h = 0.01 m/d, W = 0.0001 m/d, h_o = 50 m, r_p = 200 m).

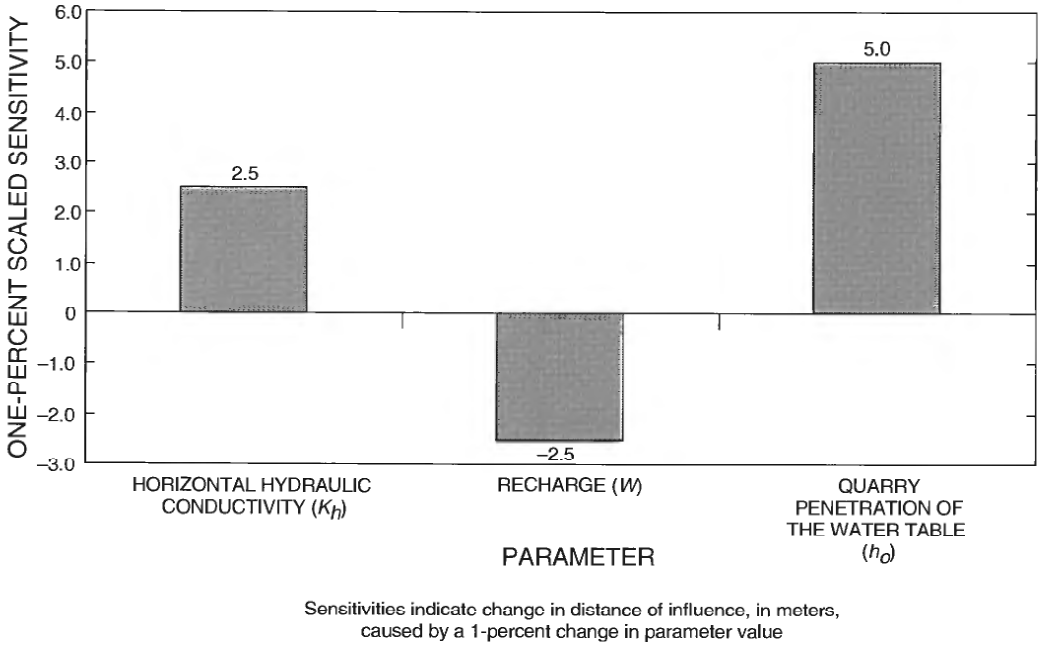

Figure 27. One-percent scaled sensitivities for parameters in equation 7, calculated for a linear quarry in a fractured crystalline-rock aquifer under intermediate conditions (K_h = 0.01 m/d, W = 0.0001 m/d, h_o = 50 m).

Comparison of simulation 8 to simulation 7 shows the effects of horizontal anisotropy.

Simulation 9–The hydrologic effects of a dewatered quarry in a fractured crystalline-rock aquifer with three hydraulic conductivity zones are simulated. Comparison of simulation 9 to simulation 7 shows the effects of lateral variations of hydraulic conductivity.

Simulation 10–The hydrologic effects of a dewatered quarry in a fractured crystalline-rock aquifer with ground-water flow in deep, low-permeability fractures are simulated. Comparison of simulation 10 to simulation 7 shows the effects of adding a layer of low hydraulic conductivity to the bottom of the model.

Simulation 11–The hydrologic effects of a dewatered quarry intersected by a hydraulically conductive fault zone in a homogeneous and isotropic fractured crystalline-rock aquifer are simulated. Comparison of simulation 11 to simulation 7 shows the effects of a fault zone that provides a conduit for ground-water flow.

Simulation 12–The hydrologic effects of a dewatered quarry intersected by a low-conductivity fault zone in a homogeneous and isotropic fractured crystalline-rock aquifer are simulated. Comparison of simulation 12 to simulation 7 shows the effects of a fault zone that forms a barrier to ground-water flow.

Simulation 7–Quarry in a homogeneous, isotropic aquifer

Simulation 7 shows the potential hydrologic effects of a dewatered quarry in a homogeneous and isotropic fractured crystalline-rock aquifer. The simulation uses the intermediate values of horizontal hydraulic conductivity, recharge, quarry depth, and quarry width from the analytical simulations to facilitate comparison between the simulations.

Model design

A fractured crystalline-rock aquifer is represented using one layer with a thickness of 100 m and a horizontal hydraulic conductivity of 0.01 m/d (fig. 28). Vertical hydraulic conductivity is not considered because the model has only one layer. Saturated thickness in the vicinity of the quarry ranges from about 75 to 100 m. The aquifer is simulated as convertible, which allows hydraulic head to be computed for either confined or unconfined conditions. The model grid has 34 rows and 31 columns with a cell size of 100 m × 100 m near the pit and 200 m × 200 m at a distance 1,000 m from the quarry (fig. 29). The model domain is 4,800 m by 5,200 m. The hydraulic gradient is about 0.1 in the vicinity of the quarry.

Boundary conditions

The left side of the aquifer (fig. 29) is simulated as a no-flow boundary to represent a ground-water divide coincident with hilltops along a major topographic high. The top and bottom edges of the aquifer (map-view) also are simulated as no-flow boundaries and are assumed far enough from the quarry that their influence on simulation results was negligible. The right side of the aquifer is simulated as a constant-head boundary to represent a large stream flowing along the bottom of a prominent valley. The aquifer base is simulated as a no-flow boundary at a depth 100 m below land surface to represent the depth below which fracture permeability is assumed negligible. A specified-flux boundary with a value of 0.0001 m/d is used to simulate areal recharge from precipitation.

Valleys in the model domain are simulated as drains by using the Drain package of MODFLOW-2000. The hydraulic conductance of drains is defined based on a valley 30-m wide with a 3-m thick layer of valley-bottom sediments having a hydraulic conductivity of 1 m/d. The use of drains in the mountain valleys was important to obtaining a realistic steady-state distribution of hydraulic head in the aquifer under premining conditions. The quarry is simulated as a 400 m wide square with truncated corners at the upgradient wall and a maximum water-table penetration of 50 m. The quarry also is simulated as a drain by using the Drain package of MODFLOW–2000 because ground-water inflow to quarries in fractured crystalline-rock aquifers commonly is slow enough that active dewatering measures are not needed (Knepper, 2002) and because the quarries commonly are cut into steep hillsides where the water table may not be penetrated by all parts of the quarry.

Results and comparison to analytical simulation

The simulated steady-state premining distribution of hydraulic head in the aquifer is shown in figure 30*a*, and steady-state drawdown near a dewatered quarry in the aquifer is shown in figure 30*b*. Steady-state drawdown computed using the analytical solution of Marinelli and Niccoli (2000) for a dewatered quarry in a homogeneous, isotropic fractured

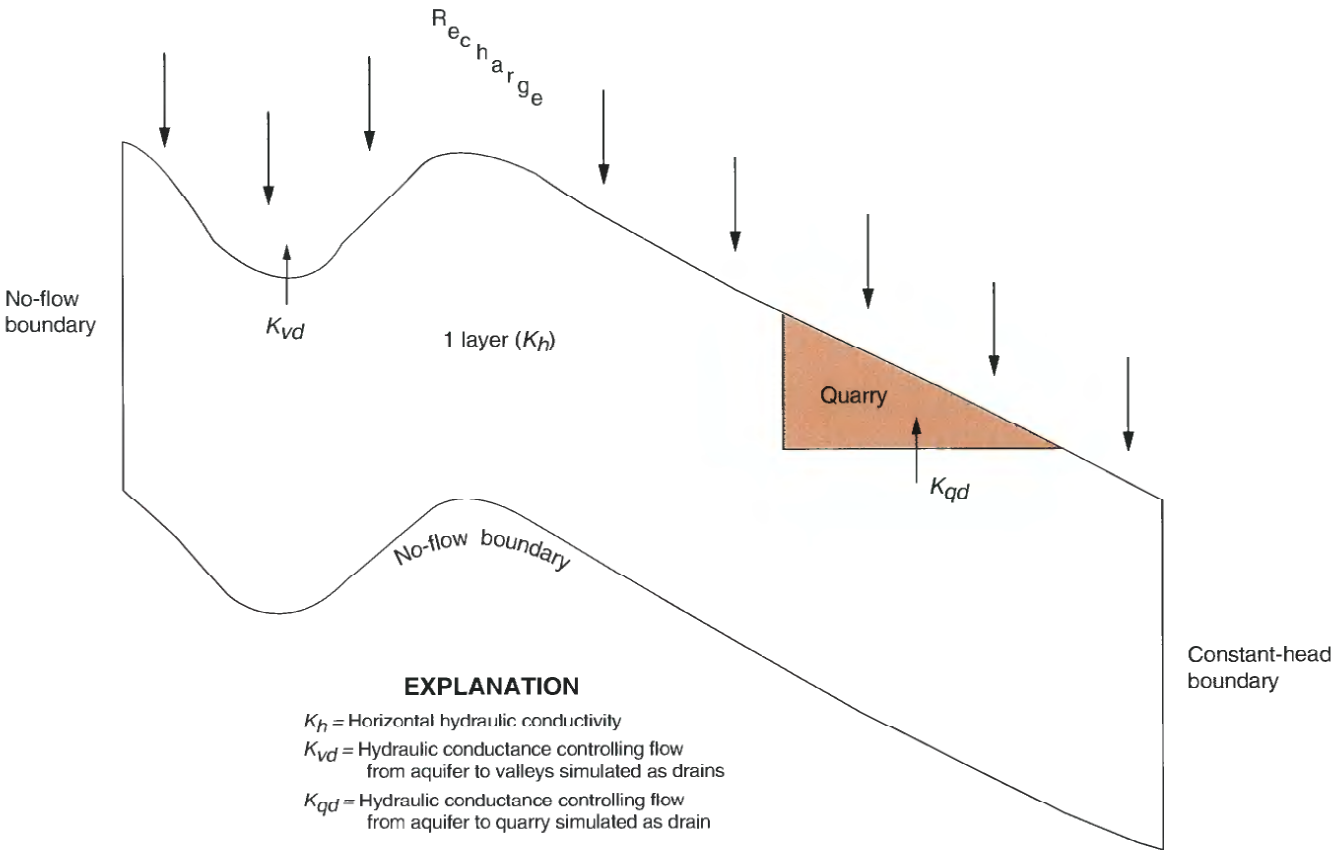

Figure 28. Conceptual diagram for numerical simulation 7 (quarry in a hypothetical fractured crystalline-rock aquifer under homogeneous and isotropic conditions).

crystalline-rock aquifer of infinite extent is shown in figure 30*c*. Results of the analytical simulation were computed using the same values of horizontal hydraulic conductivity, recharge, pit penetration of the water table, and pit radius as the numerical simulation.

Lines of equal drawdown computed by the analytical simulation occur as concentric circles centered around the quarry, and area of influence computed by the analytical simulation (defined by limit of 1-m drawdown) has a radius of 513 m, measured from the quarry center. Lines of equal drawdown computed by the numerical simulation are asymmetrical because of boundary effects. Area of influence (defined by limit of 1-m drawdown) computed by the numerical simulation has a maximum extent of about 1,300 m, measured from the quarry center. Area of influence in the numerical simulation is larger than in the analytical simulation because saturated thickness near the quarry in the numerical simulation is greater, which increases aquifer transmissivity. Area of influence increases as aquifer transmissivity increases. Drawdown in the numerical simulation is centered around the upgradient wall of the quarry because the quarry is excavated into a water table with a steep gradient. Because the base of the simulated quarry is level, the upgradient wall of the quarry penetrates the water table to a greater degree than the downgradient wall. Valleys simulated as drains in the numerical simulation affect the shape of area of influence, but area of influence extends across the valley nearest the quarry.

The complete ground-water budget for premining conditions in simulation 7 is shown in table 4, and the complete ground-water budget for the effects of the dewatered quarry in simulation 7 is shown in table 5. The ground-water budgets give an accounting of recharge to the aquifer and discharge from the aquifer. Values given in the tables indicate total volumetric fluxes for all cells of a given type. Recharge to the aquifer includes ground-water inflow from the

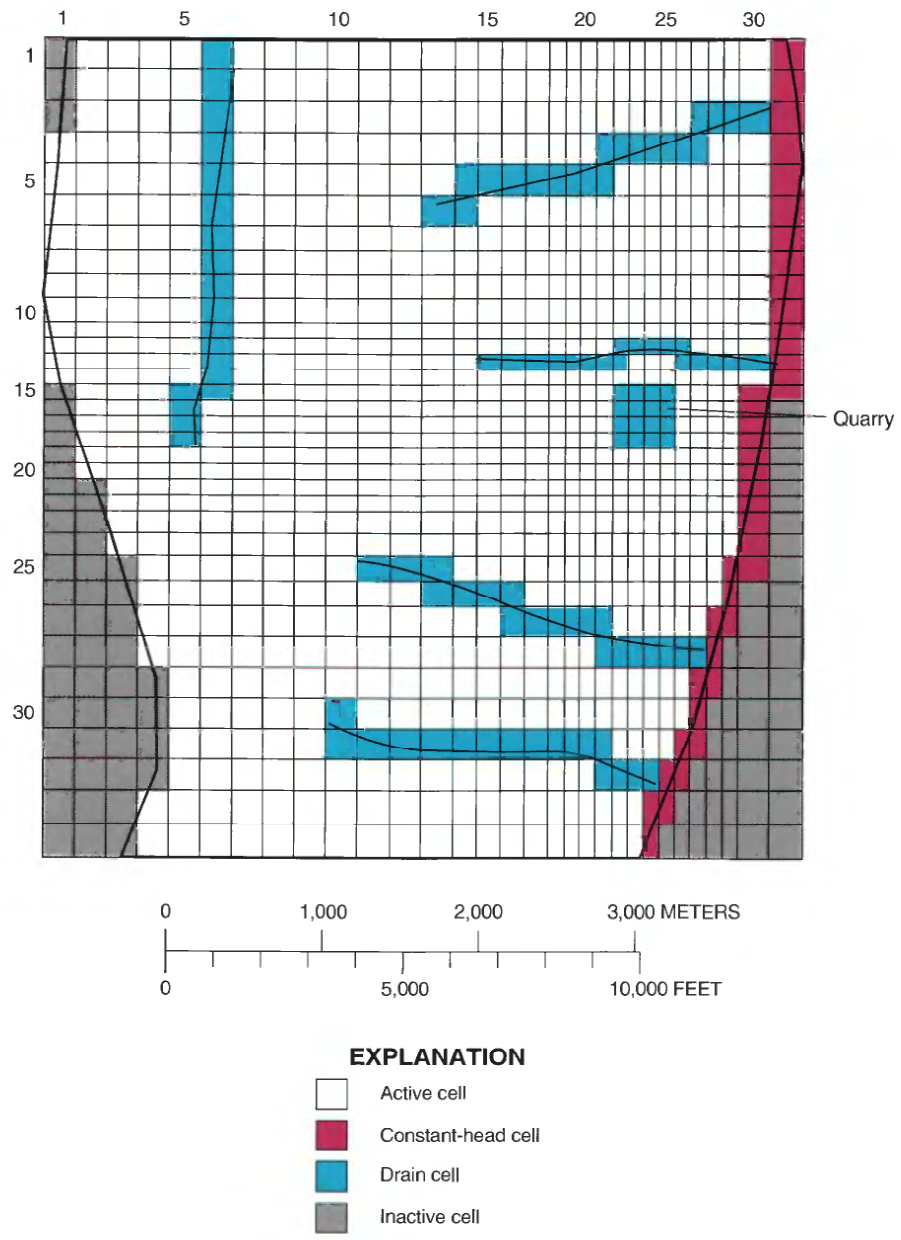

Figure 29. Finite-difference grid and boundary conditions for numerical simulation 7 (quarry in a hypothetical fractured crystalline-rock aquifer under homogeneous and isotropic conditions).

constant-head boundary and distributed recharge from precipitation. Discharge from the aquifer includes (1) ground-water outflow to the constant-head boundary, (2) ground-water discharge to valleys simulated as drains, and (3) ground-water discharge to the quarry under conditions of active mining.

Under premining conditions, nearly all recharge is from precipitation. Very little recharge is contributed by the constant-head boundary because the boundary occurs along the downgradient edge of the model. Most discharge from the aquifer under premining conditions occurs to valleys simulated as drains, but discharge to the constant-head boundary also is significant. Under conditions of active mining, when the quarry is dewatered, recharge is nearly identical to premining conditions, but discharge to valleys and the constant-head boundary is less because the quarry intercepts ground water that, under premining conditions, flows to the valleys and the constant-head boundary. Discharge to the quarry in simulation 7 is much less than discharge to the pit in simulation 1 because the hydraulic conductivity of the fractured crystalline-rock aquifer is much less than that of the sand-and-gravel aquifer.

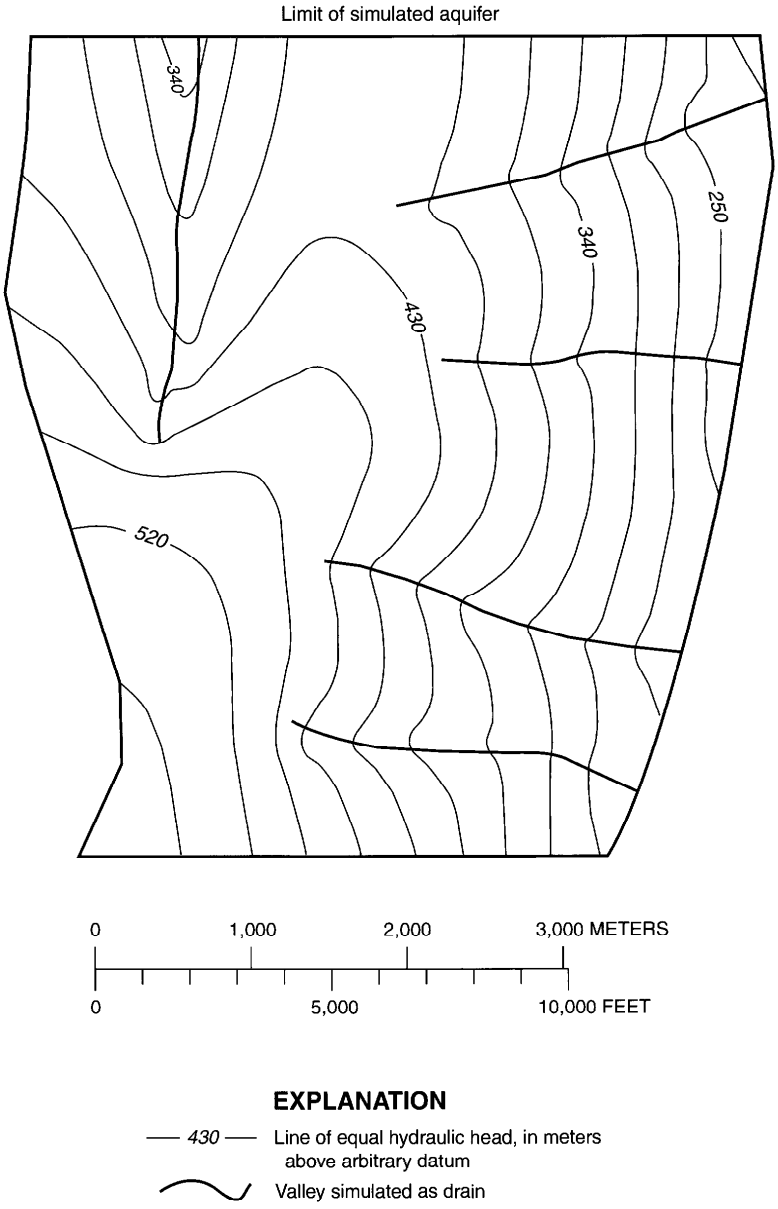

Figure 30*a*. Numerical simulation 7–Steady-state premining distribution of hydraulic head in a hypothetical fractured crystalline-rock aquifer under homogeneous and isotropic conditions.

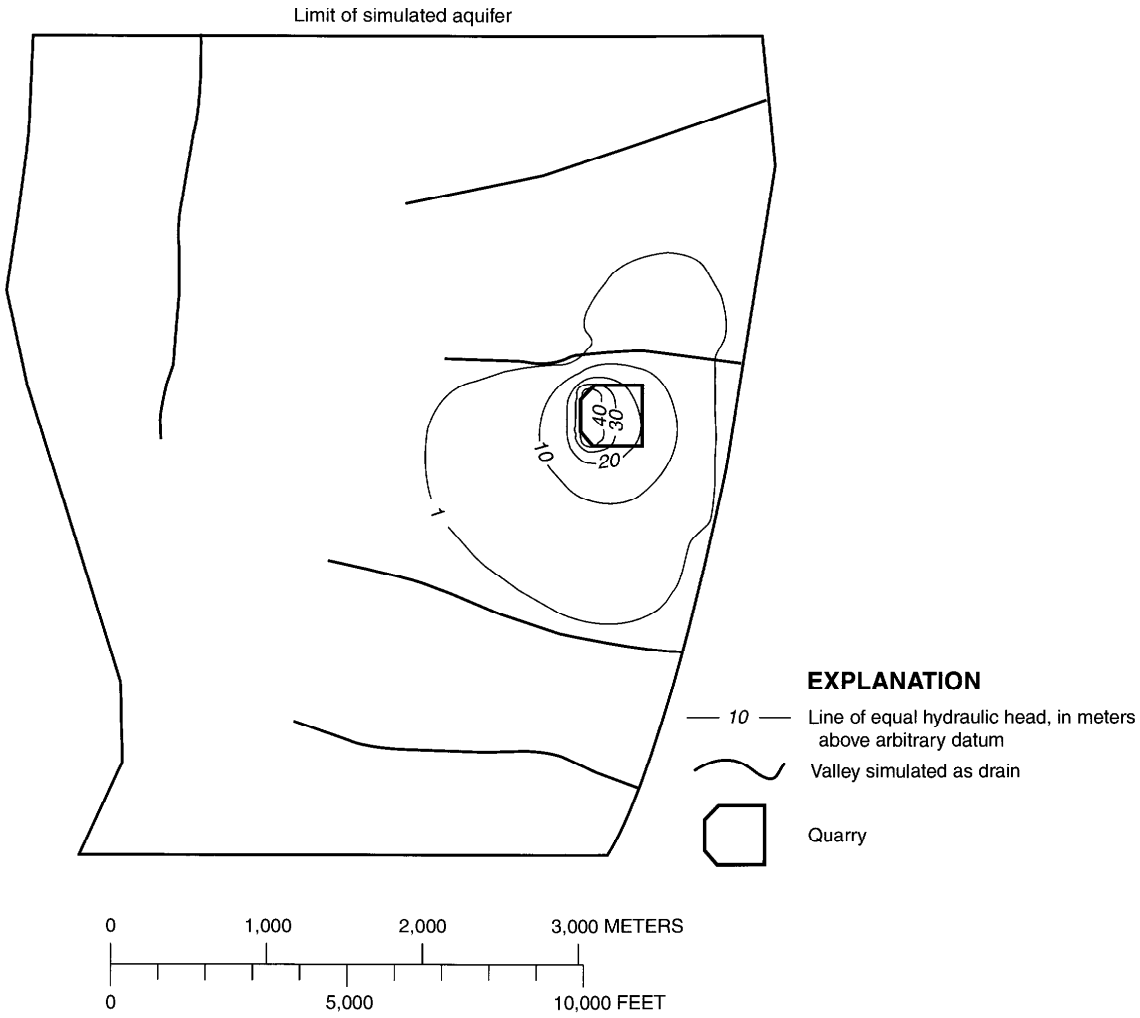

Figure 30*b*. Numerical simulation 7–Steady-state drawdown caused by a dewatered quarry in a hypothetical fractured crystalline-rock aquifer under homogeneous and isotropic conditions.

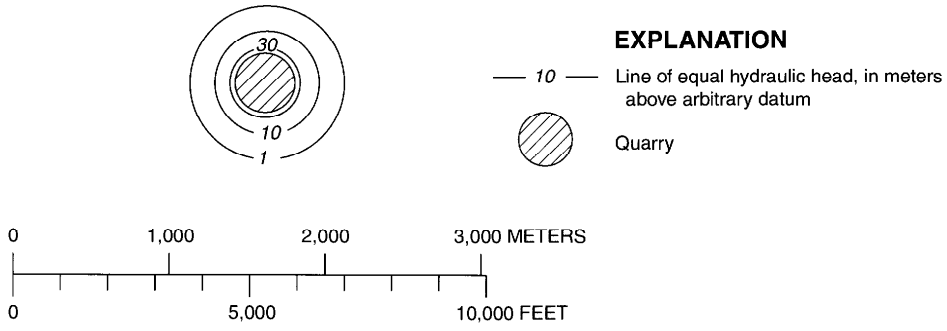

Figure 30*c*. Steady-state drawdown caused by a dewatered quarry in a homogeneous, isotropic, fractured crystalline-rock aquifer of infinite extent, simulated by use of the Marinelli and Niccoli (2000) analytical solution.

Simulation 8–Quarry in a homogeneous aquifer with horizontal anisotropy

Simulation 8 shows the effects horizontal anisotropy may have on steady-state drawdown near a quarry. Simulation 8 is identical to simulation 7 except hydraulic conductivity along columns in the model is assigned a value three times greater than the hydraulic conductivity along rows. Hydraulic conductivity along rows is 0.01 m/d as in simulation 7. Simulation 8 represents a system in which fracture permeability in one horizontal coordinate direction is greater than that in another coordinate direction.

The simulated steady-state premining distribution of hydraulic head in the aquifer is shown in figure 31*a*, and steady-state drawdown near a dewatered quarry in the anisotropic aquifer is shown in figure 31*b*. Premining hydraulic head in simulation 8 generally is slightly lower than in simulation 7 because the increased hydraulic conductivity along columns in simulation 8 increases discharge to valleys, which lowers the water table. The water table of simulation 8

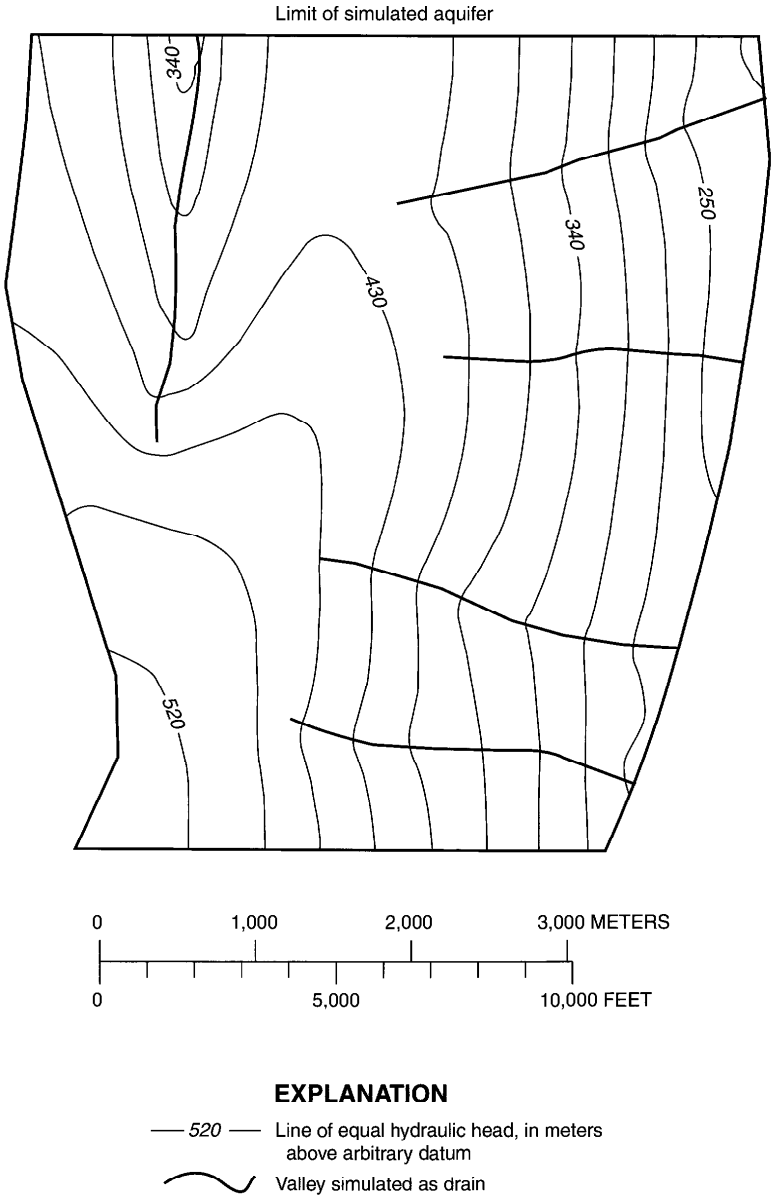

Figure 31*a*. Numerical simulation 8–Steady-state premining distribution of hydraulic head in a hypothetical fractured crystalline-rock aquifer under homogeneous and horizontally anisotropic conditions.

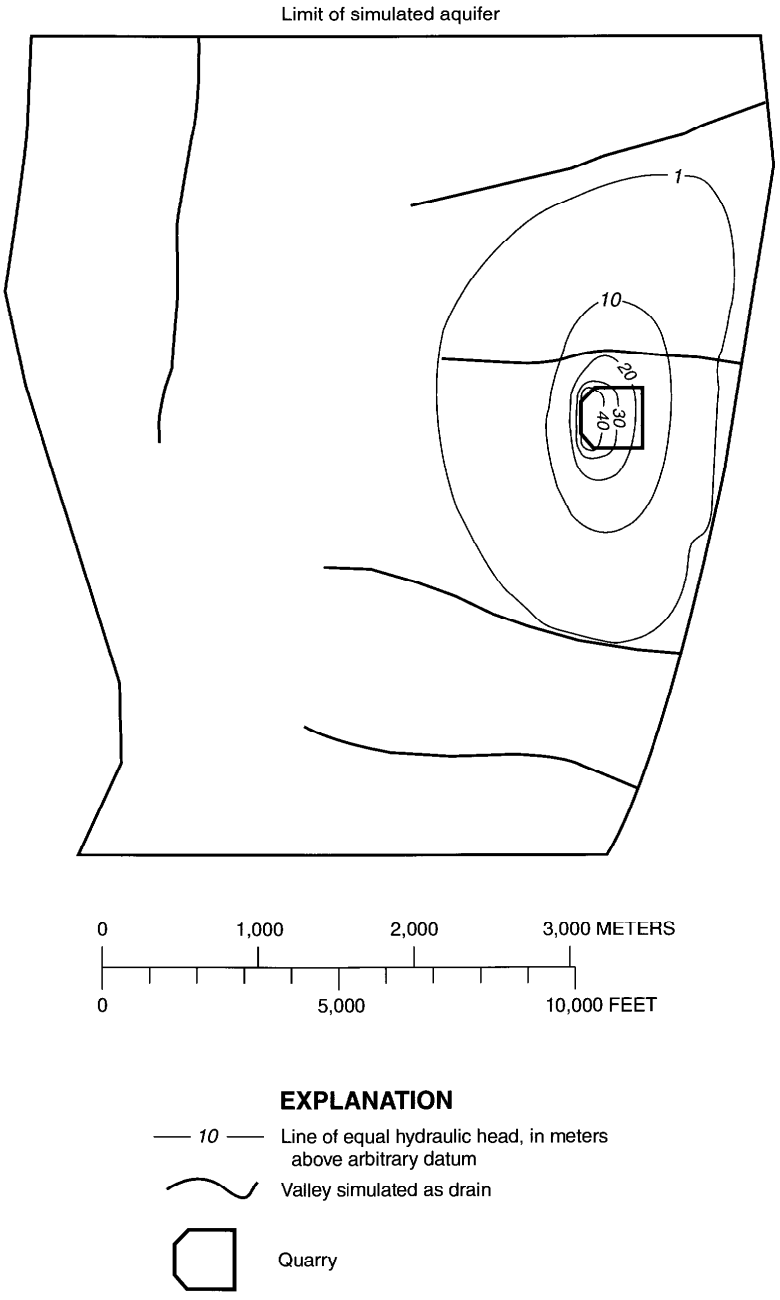

Figure 31*b*. Numerical simulation 8–Steady-state drawdown caused by a dewatered quarry in a hypothetical fractured crystalline-rock aquifer under homogeneous and horizontally anisotropic conditions.

is mostly below the elevation of the valley nearest the quarry; consequently, the valley has less effect on the quarry area of influence than in simulation 7. Area of influence in simulation 8 has a maximum extent (measured from the quarry center) of about 1,600 m and is elongated in the direction of greater hydraulic conductivity along columns because area of influence increases with increasing hydraulic conductivity. Area of influence along rows is similar to that of simulation 7 because hydraulic conductivity along rows is the same for both simulations.

Ground-water inflow from the constant-head boundary is larger and outflow to the constant-head boundary is smaller under premining conditions (table 4) in simulation 8 than in simulation 7 because the lower water table of simulation 8 causes the

hydraulic gradient between the aquifer and boundary to be less. Discharge to valleys simulated as drains under premining conditions in simulation 8 is larger than in simulation 7 because the greater hydraulic conductivity along columns increases ground-water flow to the valleys. The ground-water budget for simulation 8 under active mining conditions (table 5) is similar to that for premining conditions except the quarry intercepts some ground water that, under premining conditions, flows to valleys. Ground-water discharge to the quarry is greater in simulation 8 than in simulation 7 because the greater hydraulic conductivity along columns increases ground-water flow to the quarry.

Simulation 9–Quarry in an aquifer with lateral variations of hydraulic conductivity

Simulation 9 shows the effects lateral variations of hydraulic conductivity may have on steady-state drawdown near a dewatered quarry. Simulation 9 is the same as simulation 7 except the model domain is divided into three zones with each having a different horizontal hydraulic conductivity (fig. 32*a*). Hilltops are assigned a horizontal hydraulic conductivity value of 0.005 m/d to represent relatively unweathered crystalline rock with fewer fractures at the core of mountains. Major valleys are assigned a horizontal hydraulic conductivity value of 0.05 m/d to represent areas where streams have incised into more highly fractured rock. The area between hilltops and major valleys is assigned a horizontal hydraulic conductivity value of 0.01 m/d as in simulation 7. Hydraulic conductivity is homogeneous and isotropic within each zone.

The simulated steady-state premining distribution of hydraulic head in the aquifer is shown in figure 32*a*, and steady-state drawdown near a dewatered quarry in the aquifer is shown in figure 32*b*. The lower horizontal hydraulic conductivity of hilltops in simulation 9 causes hydraulic head to be higher and the water table to be steeper beneath hilltops than in simulation 7. Similarly, higher horizontal hydraulic conductivity along major valleys in simulation 9 causes hydraulic head to be lower and the water table to be flatter beneath major valleys than in simulation 7. Area of influence in simulation 9 has a maximum

Table 4. Steady-state ground-water budget for six numerical simulations of premining conditions in hypothetical fractured crystalline-rock aquifers

[All values are in cubic meters per day; totals reflect sum of all rounded individual components]

Budget component	Simulation 7	Simulation 8	Simulation 9	Simulation 10	Simulation 11	Simulation 12
			Recharge to aquifer			
Ground-water inflow from constant-head boundary	4	14	39	4	4	4
Precipitation recharge	2,151	2,151	2,151	2,151	2,151	2,151
Total	2,155	2,165	2,190	2,155	2,155	2,155
			Discharge from aquifer			
Ground-water outflow to constant-head boundary	580	438	890	600	620	551
Ground-water discharge to valleys simulated as drains	1,575	1,726	1,299	1,555	1,534	1,603
Total	2,155	2,164	2,189	2,155	2,154	2,154
Recharge – Discharge	0	1	1	0	1	1

Model simulations:

7. Homogeneous, isotropic aquifer.
8. Homogeneous, horizontally anisotropic aquifer.
9. Aquifer with lateral variations of hydraulic conductivity.
10. Aquifer with ground-water flow in deep, low-permeability fractures.
11. Aquifer with a fault zone that acts as a conduit for ground-water flow.
12. Aquifer with a fault zone that acts as a barrier to ground-water flow.

Table 5. Steady-state ground-water budget for six numerical simulations of the effects of mining aggregate in hypothetical fractured crystalline-rock aquifers

[All values are in cubic meters per day; totals reflect sum of all rounded individual components]

Budget component	Simulation 7	Simulation 8	Simulation 9	Simulation 10	Simulation 11	Simulation 12
Recharge to aquifer						
Ground-water inflow from constant-head boundary	4	14	40	4	4	4
Precipitation recharge	2,151	2,151	2,151	2,151	2,151	2,151
Total	2,155	2,165	2,191	2,155	2,155	2,155
Discharge from aquifer						
Ground-water outflow to constant-head boundary	540	438	842	558	550	529
Ground-water discharge to valleys simulated as drains	1,504	1,587	1,258	1,483	1,456	1,531
Ground-water discharge to quarry	109	139	91	115	149	94
Total	2,153	2,164	2,191	2,156	2,155	2,154
Recharge –Discharge	2	1	0	–1	0	1

Model simulations:

7. Quarry in a homogeneous, isotropic aquifer.
8. Quarry in a homogeneous, horizontally anisotropic aquifer.
9. Quarry in an aquifer with lateral variations of hydraulic conductivity.
10. Quarry in an aquifer with ground-water flow in deep, low-permeability fractures.
11. Quarry intersected by a fault zone that acts as a conduit for flow.
12. Quarry intersected by a fault zone that acts as a barrier to ground-water flow.

extent (measured from quarry center) of about 1,100 m. Area of influence in simulation 9 is smaller than in simulation 7 because the lower horizontal hydraulic conductivity of hilltops reduces the area of influence upgradient from the quarry, and the higher horizontal hydraulic conductivity of the major valley along the right side of the model domain increases the effects of the constant-head boundary, thereby reducing area of influence downgradient from the quarry.

Ground-water inflow from the constant-head boundary and outflow to the constant-head boundary under premining conditions (table 4) in simulation 9 is greater than in simulation 7 because the higher horizontal hydraulic conductivity of the major valley along the constant-head boundary facilitates ground-water flow between the boundary and the aquifer. Discharge to valleys under premining conditions in simulation 9 is less than in simulation 7 because the water table in the vicinity of valleys simulated as drains in simulation 9 is lower than in simulation 7. The ground-water budget for simulation 9 under active mining conditions (table 5) is similar to that for premining conditions except the quarry intercepts some ground water that, under premining conditions, flows to valleys and the constant-head boundary. Ground-water discharge to the quarry in simulation 9 is less than in simulation 7 because saturated thickness near the quarry in simulation 9 is less and aquifer transmissivity is smaller.

Simulation 10–Quarry in an aquifer with ground-water flow in deep, low-permeability fractures

Simulation 10 shows the effects adding a model layer to simulate ground-water flow in deep, low-permeability fractures may have on steady-state drawdown near a dewatered quarry. Simulation 10 is similar to simulation 7 except a second layer is added. As in simulation 7, the top layer (layer 1) is 100 m thick with a horizontal hydraulic conductivity of 0.01 m/d. The new layer (layer 2) underlies layer 1 and is 50 m thick with a horizontal hydraulic conduc-

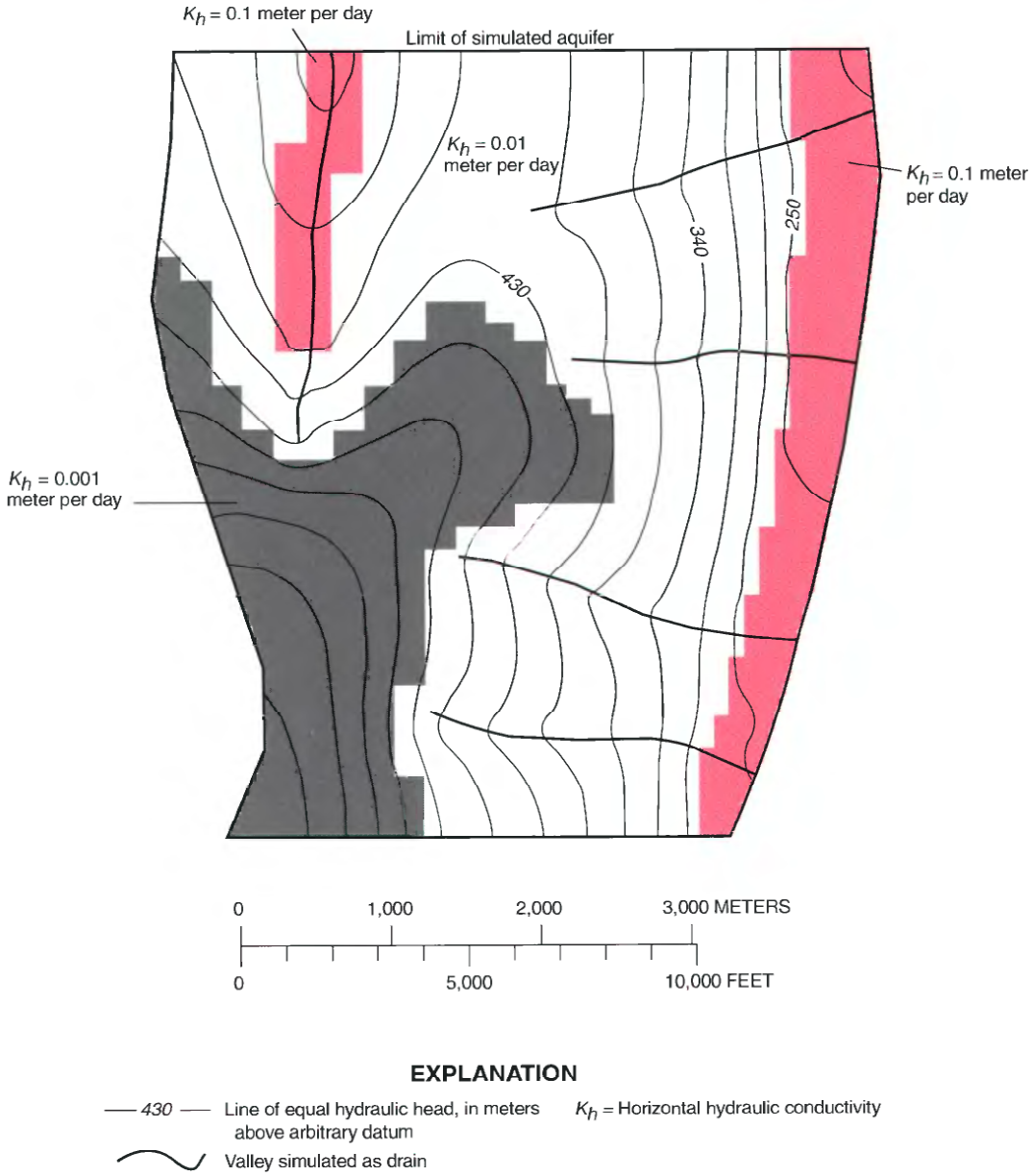

Figure 32*a*. Numerical simulation 9–Steady-state premining distribution of hydraulic head in a hypothetical fractured crystalline-rock aquifer with lateral variations of hydraulic conductivity.

tivity of 0.001 m/d. Vertical hydraulic conductivity is set equal to horizontal hydraulic conductivity in each layer.

The simulated steady-state premining distribution of hydraulic head in the aquifer is shown in figure 33*a*, and steady-state drawdown near a dewatered quarry in the aquifer is shown in figure 33*b*. Area of influence in simulation 10 has a maximum extent (measured from quarry center) of about 1,300 m, which is the same as in simulation 7. However, area of influence across the valley nearest the quarry is larger in simulation 10 than in simulation 7 because the aquifer represented by two layers in simulation 10 is thicker and has higher transmissivity. Because horizontal and vertical hydraulic conductivity in layer 2 are an order of magnitude lower than in layer 1, the additional thickness created by adding layer 2 has only a small effect on transmissivity and, consequently, on area of influence.

Recharge to the aquifer under premining conditions (table 4) in simulation 10 is identical to that in

simulation 7. Discharge to the constant-head boundary is slightly larger under premining conditions in simulation 10 than in simulation 7 because saturated thickness adjacent to the constant-head boundary is greater in simulation 10. Discharge to valleys under premining conditions in simulation 10 is smaller than in simulation 7 because the water table is slightly lower in simulation 10. The ground-water budget for simulation 10 under active mining conditions (table 5) is similar to that for premining conditions except the quarry intercepts some ground water that, under premining conditions, flows to valleys and the constant-head boundary. Ground-water discharge to the quarry in simulation 10 is greater than in simulation 7 because the saturated thickness near the quarry in simulation 10 is greater, which causes aquifer transmissivity to be larger.

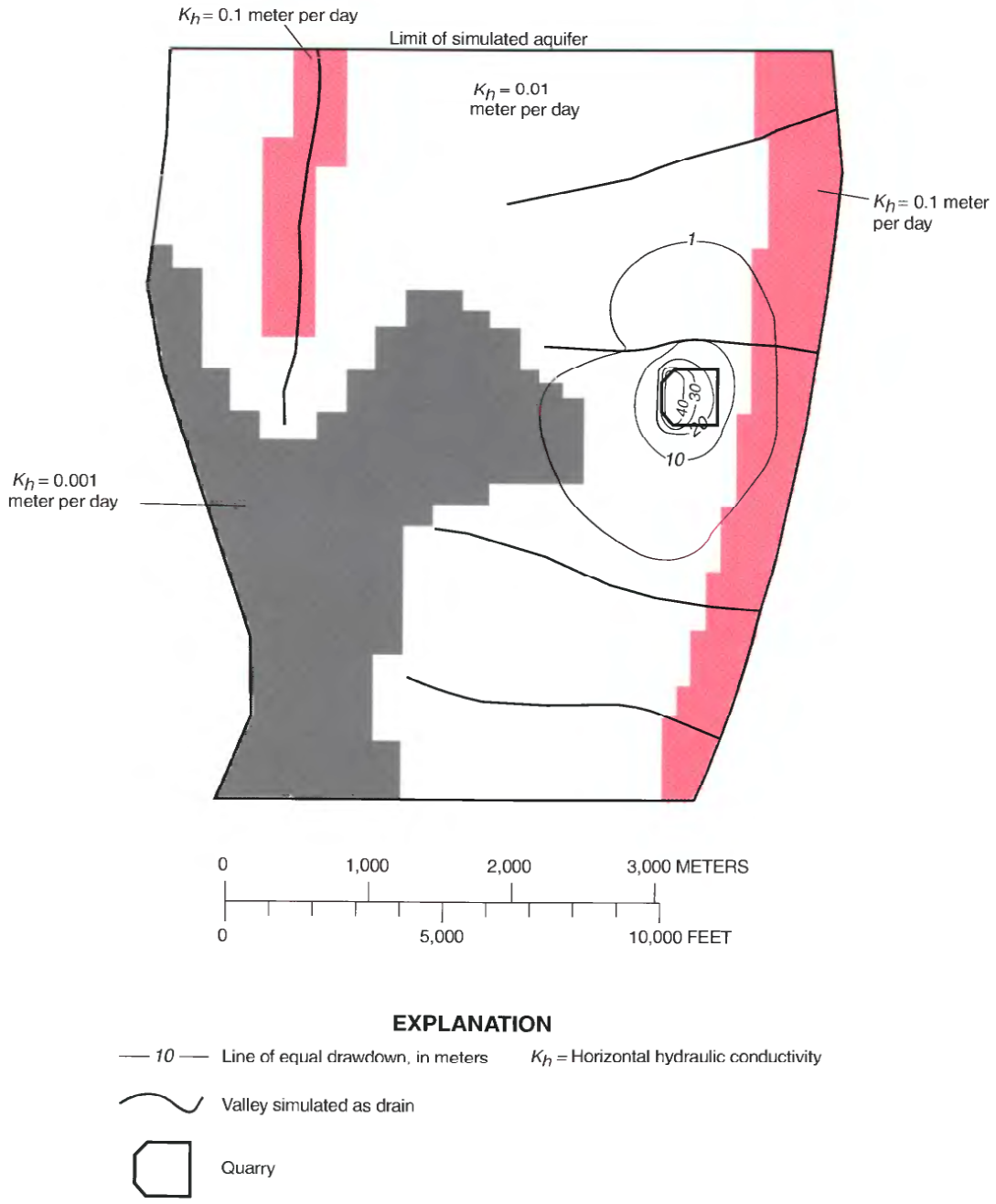

Figure 32*b*. Numerical simulation 9–Steady-state drawdown caused by a dewatered quarry in a hypothetical fractured crystalline-rock aquifer with lateral variations of hydraulic conductivity.

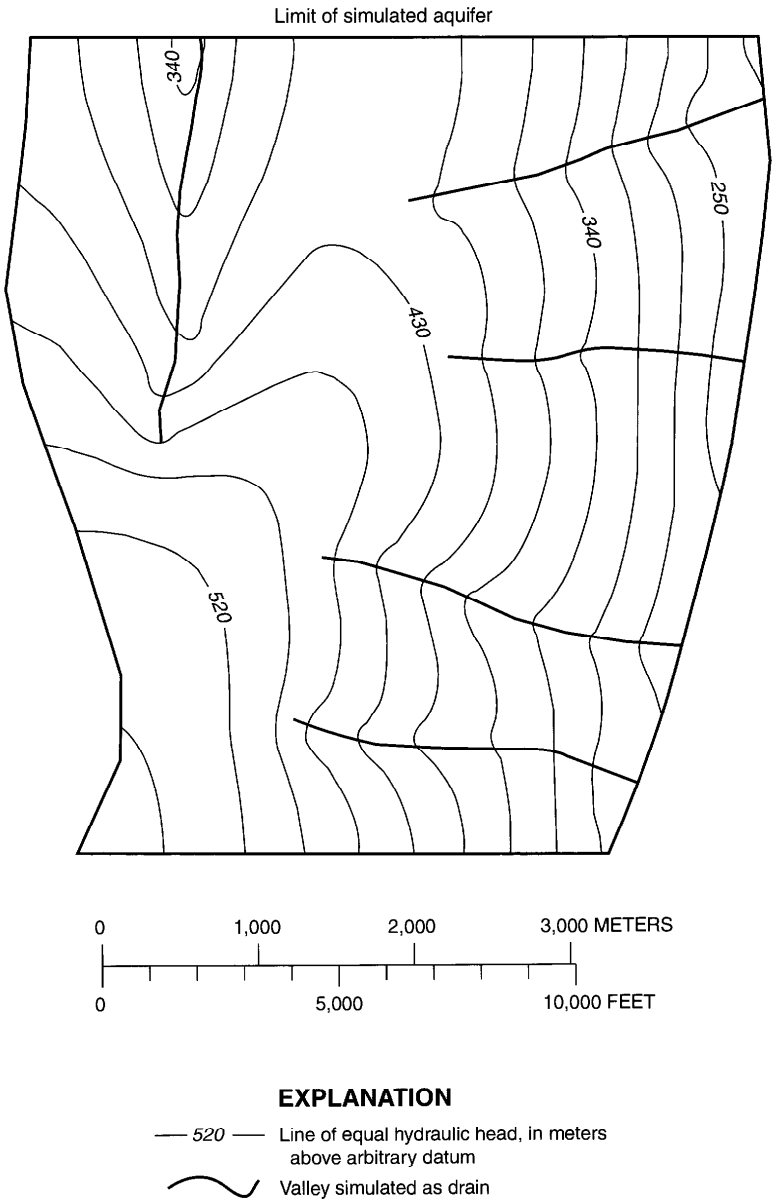

Figure 33*a*. Numerical simulation 10–Steady-state premining distribution of hydraulic head in a hypothetical fractured crystalline-rock aquifer with ground-water flow in deep, low-permeability fractures.

Simulation 11–Quarry intersected by a hydraulically conductive fault zone

Simulation 11 shows the effects a hydraulically conductive fault or fault zone may have on steady-state drawdown around a dewatered quarry. Simulation 11 is similar to simulation 7 except a fault zone having a horizontal hydraulic conductivity of 0.1 m/d intersects the quarry.

Recharge to the aquifer under premining conditions (table 4) in simulation 11 is identical to that in simulation 7. Discharge to the constant-head boundary is slightly larger under premining conditions in simulation 11 than in simulation 7 because the hydraulically conductive fault zone increases ground-water flow to the boundary. Discharge to valleys under premining conditions in simulation 11 is smaller than in simulation 7 because the water table is slightly lower beneath the valley nearest the fault zone in simulation 11. The ground-water budget for simulation 11 under active mining conditions (table 5) is similar

to that for premining conditions except the quarry intercepts some ground water that, under premining conditions, flows to valleys and the constant-head boundary. Ground-water discharge to the quarry in simulation 11 is greater than in simulation 7 because the hydraulically conductive fault zone increases ground-water flow to the quarry. The simulated steady-state premining distribution of hydraulic head in the aquifer is shown in figure 34*a*, and steady-state drawdown near a dewatered quarry intersected by a hydraulically conductive fault zone is shown in figure 34*b*. Premining hydraulic head in simulation 11 is slightly lower along and upgradient of the fault zone compared to simulation 7 because the fault zone facilitates ground-water flow along the fault. Area of influence in simulation 11 extends along the fault zone and has a maximum extent (measured from quarry center) of about 1,600 m. Area of influence in simulation 11 is larger than in simulation 7 because area of influence increases as hydraulic conductivity increases.

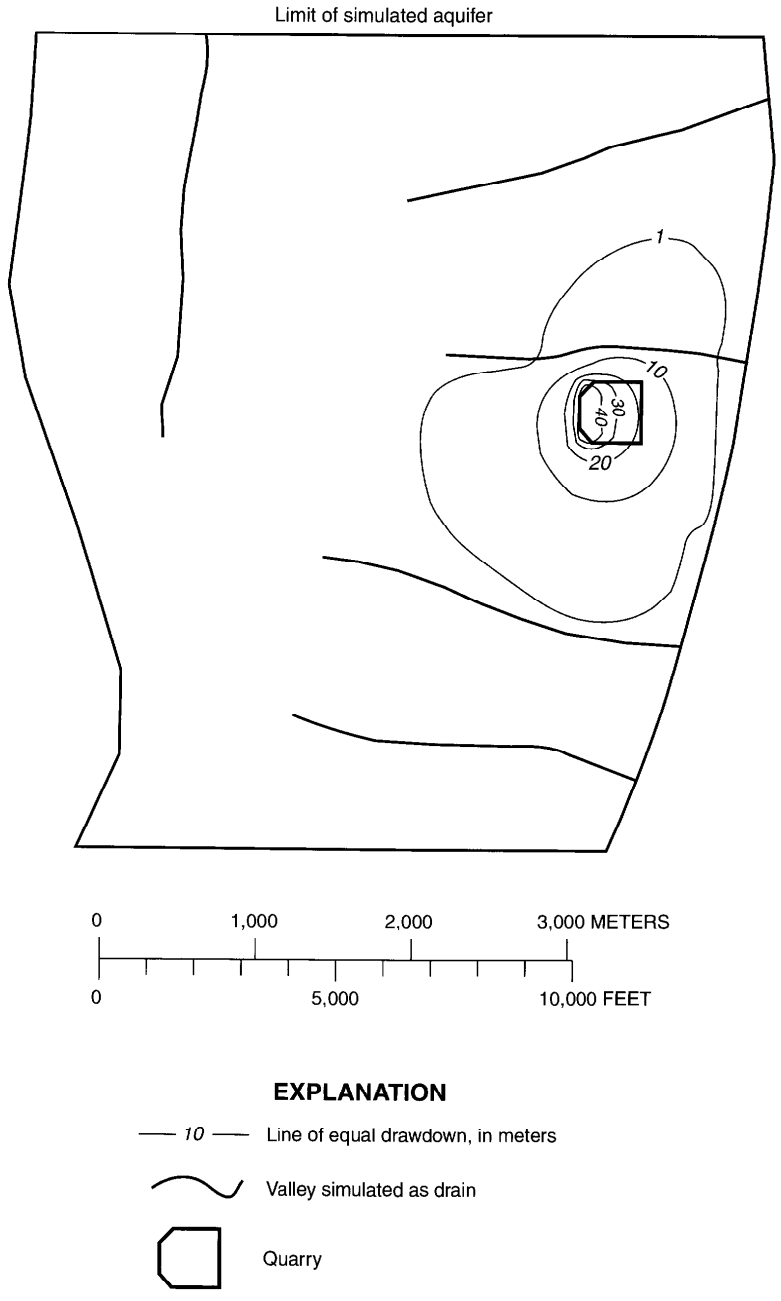

Figure 33*b*. Numerical simulation 10–Steady-state drawdown caused by a dewatered quarry in a hypothetical fractured crystalline-rock aquifer with ground-water flow in deep, low-permeability fractures.

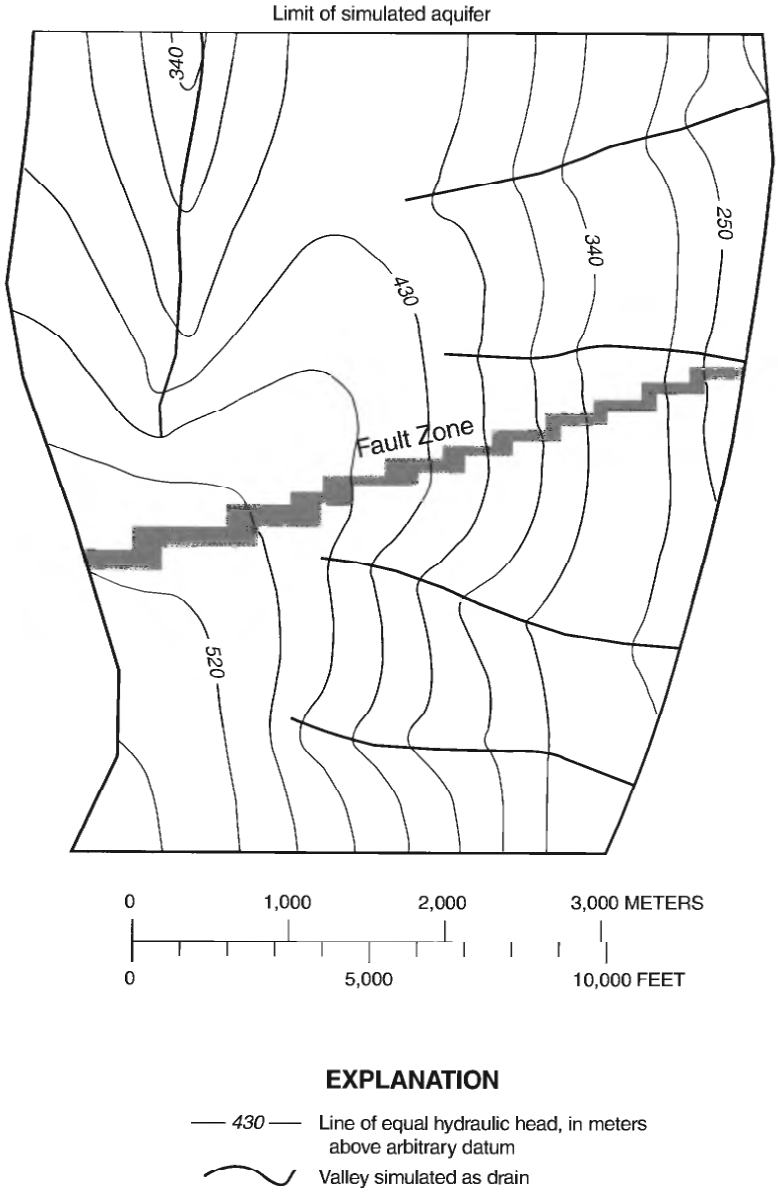

Figure 34*a*. Numerical simulation 11–Steady-state premining distribution of hydraulic head in a hypothetical fractured crystalline-rock aquifer with a hydraulically conductive fault zone.

Simulation 12–Quarry intersected by a low-conductivity fault zone

Simulation 12 shows the effects a low-conductivity fault or fault zone may have on steady-state drawdown around a quarry. Simulation 12 is identical to simulation 11 except the fault zone has a horizontal hydraulic conductivity of 0.001 m/d.

The simulated steady-state premining distribution of hydraulic head in the aquifer is shown in figure 35*a*, and steady-state drawdown near a dewatered quarry intersected by a low-conductivity fault zone is shown in figure 35*b*. Premining hydraulic head in simulation 12 is slightly higher along and upgradient of the fault zone compared to simulation 7 because the fault zone impedes ground-water flow from upgradient areas to downgradient areas. Area of influence in simulation 12 has a maximum extent (measured from quarry center) of about 1,300 m, and area of influence in simulation 12 is smaller than in simulation 7 because the fault zone decreases ground-water flow to the quarry.

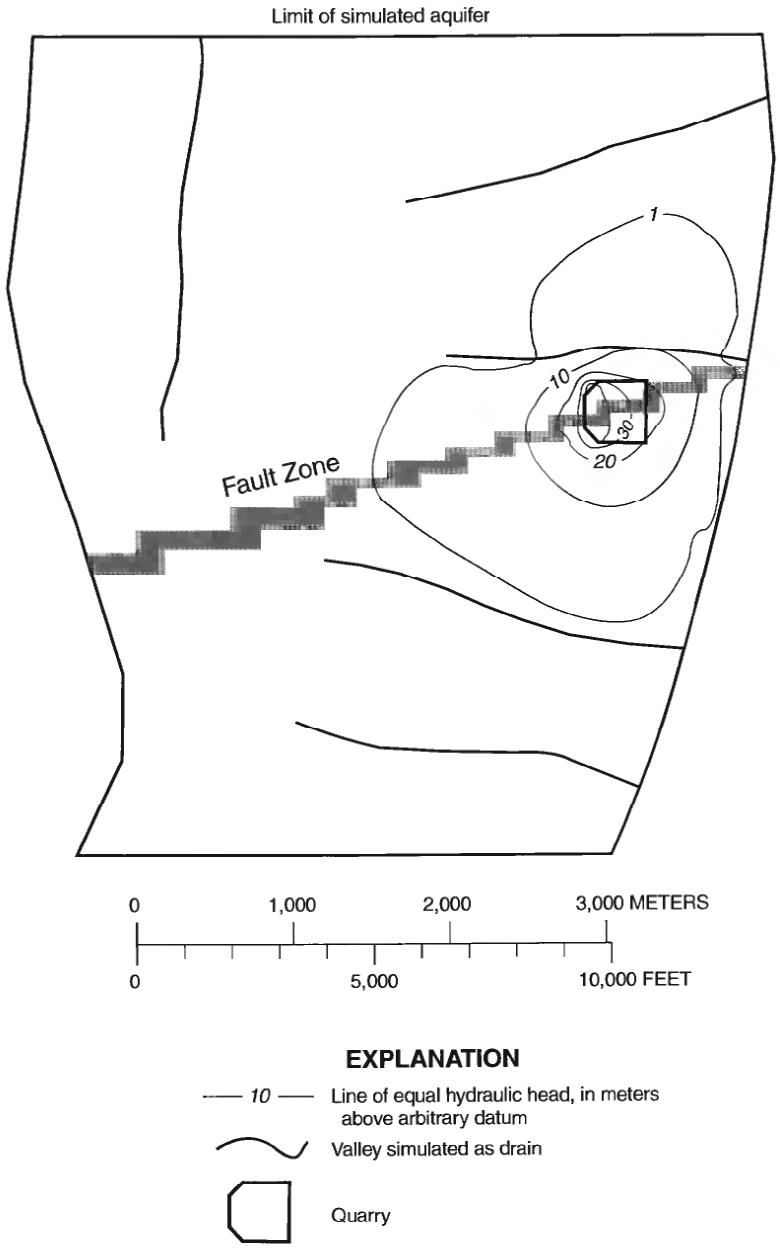

Figure 34*b*. Numerical simulation 11–Steady-state drawdown caused by a dewatered quarry intersected by a hydraulically conductive fault zone in a hypothetical fractured crystalline-rock aquifer.

Recharge to the aquifer under premining conditions (table 4) in simulation 12 is identical to that in simulation 7. Discharge to the constant-head boundary is slightly smaller under premining conditions in simulation 12 than in simulation 7 because the low-conductivity fault zone decreases ground-water flow to the boundary. Discharge to valleys under premining conditions in simulation 12 is larger than in simulation 7 because the water table is higher beneath the valley nearest the fault zone in simulation 12. The ground-water budget for simulation 12 under active mining conditions (table 5) is similar to that for premining conditions except the quarry intercepts some ground water that, under premining conditions, flows to valleys and the constant-head boundary. Ground-water discharge to the quarry in simulation 12 is less than in simulation 7 because the low-conductivity fault zone decreases ground-water flow to the quarry.

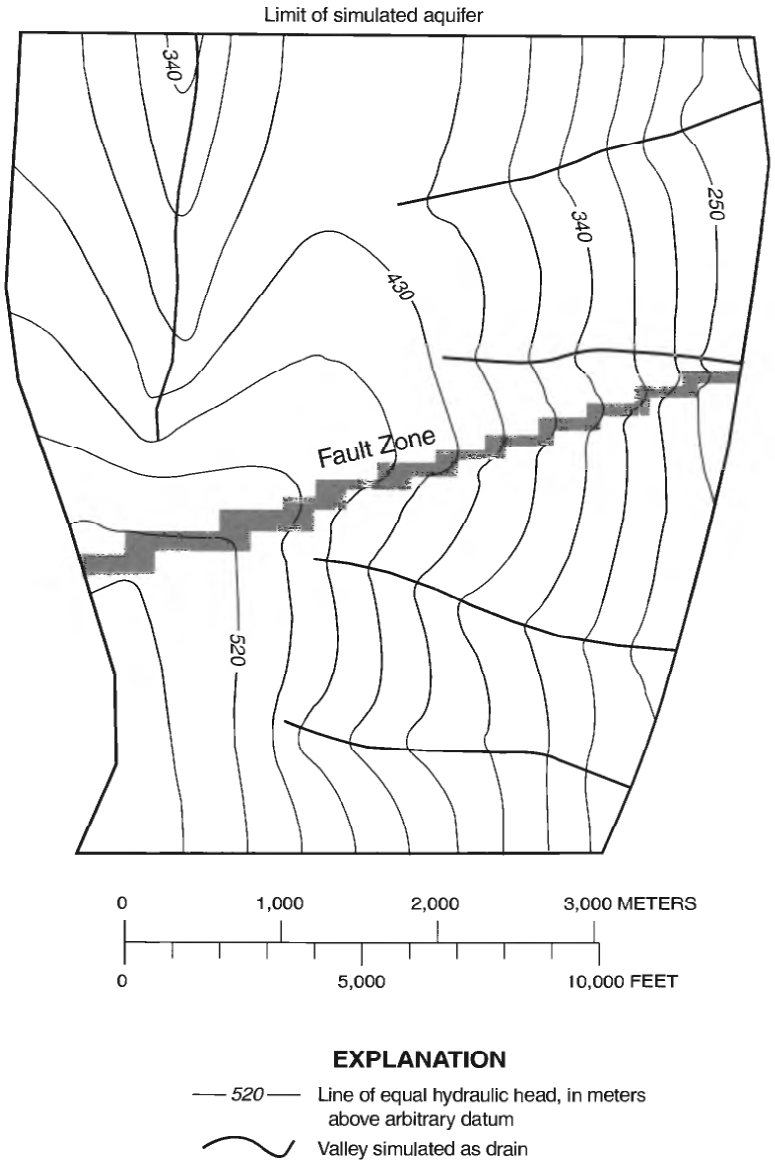

Figure 35a. Numerical simulation 12–Steady-state premining distribution of hydraulic head in a hypothetical fractured crystalline-rock aquifer with a low-conductivity fault zone.

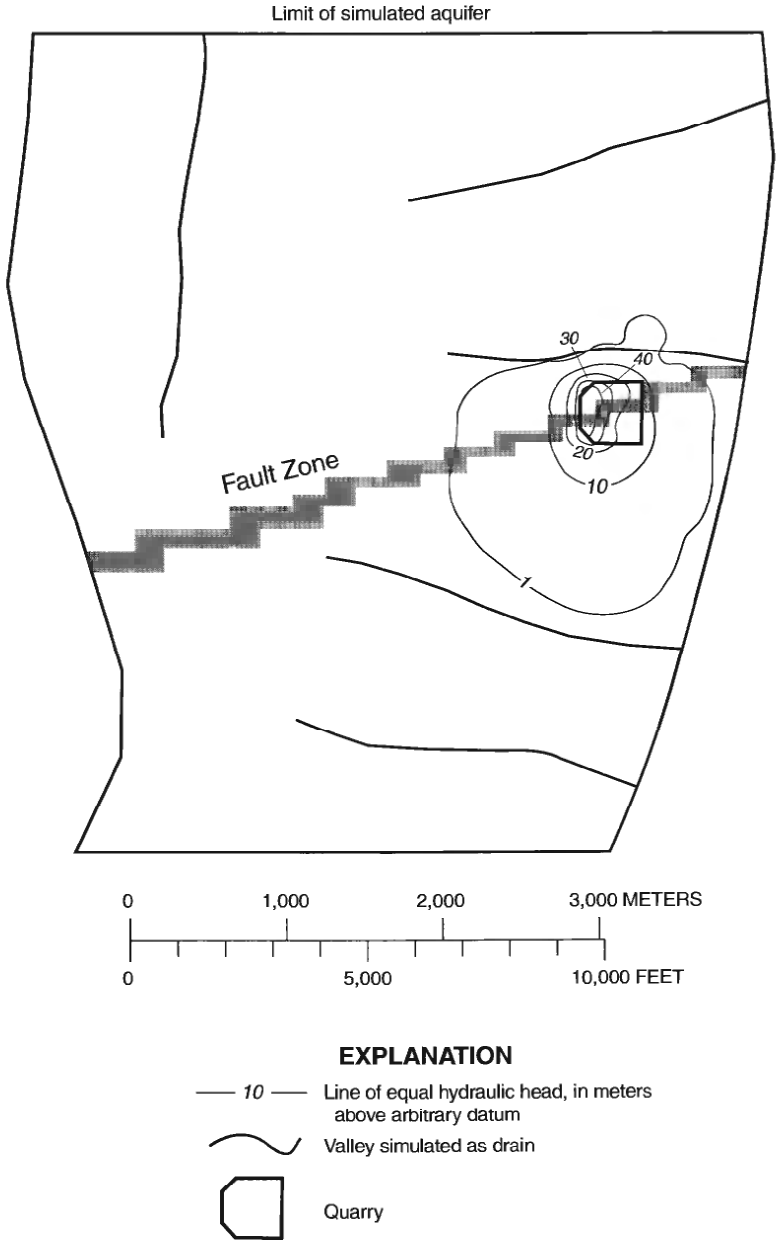

Figure 35b. Numerical simulation 12–Steady-state drawdown caused by a dewatered quarry intersected by a low-conductivity fault zone in a hypothetical fractured crystalline-rock aquifer.

Numerical Sensitivity Analysis

Composite scaled sensitivities (see "Numerical Sensitivity Analysis" under "Simulation of Pits in Sand-and-Gravel Aquifers") were calculated for each model parameter by using the Parameter Sensitivity with Observations mode (Hill and others, 2000) of MODFLOW–2000. Sensitivities were calculated for each parameter by using 27 hypothetical head observations distributed evenly throughout the numerical model domain as shown in figure 36. Sensitivity analysis results for simulation 7 are shown in figure 37, and sensitivity analysis results for all simulations in fractured crystalline rock are shown in table 6.

Sensitivity analyses results indicate simulated hydraulic head was most sensitive to recharge and horizontal hydraulic conductivity in every simulation. In simulations 7 and 8, the sensitivities for recharge and horizontal hydraulic conductivity were almost equal. However, in simulations 9, 10, 11, and 12, more than one horizontal hydraulic-conductivity parameter was used, and the sensitivity for recharge was greater than that for any individual horizontal hydraulic-conductivity parameter. In simulation 9 (quarry in an aquifer with lateral variations of hydraulic conductivity), sensitivity for horizontal hydraulic conductivity was greatest for hilltops (low hydraulic conductivity) and least for valleys (high hydraulic conductivity). In simulation 10 (quarry in an aquifer represented by two model layers, one of which simulates ground-water flow in deep, low-permeability fractures), the sensitivity for horizontal hydraulic conductivity in layer 2 was much less than that in layer 1. In simulations 11 and 12 (quarry intersected

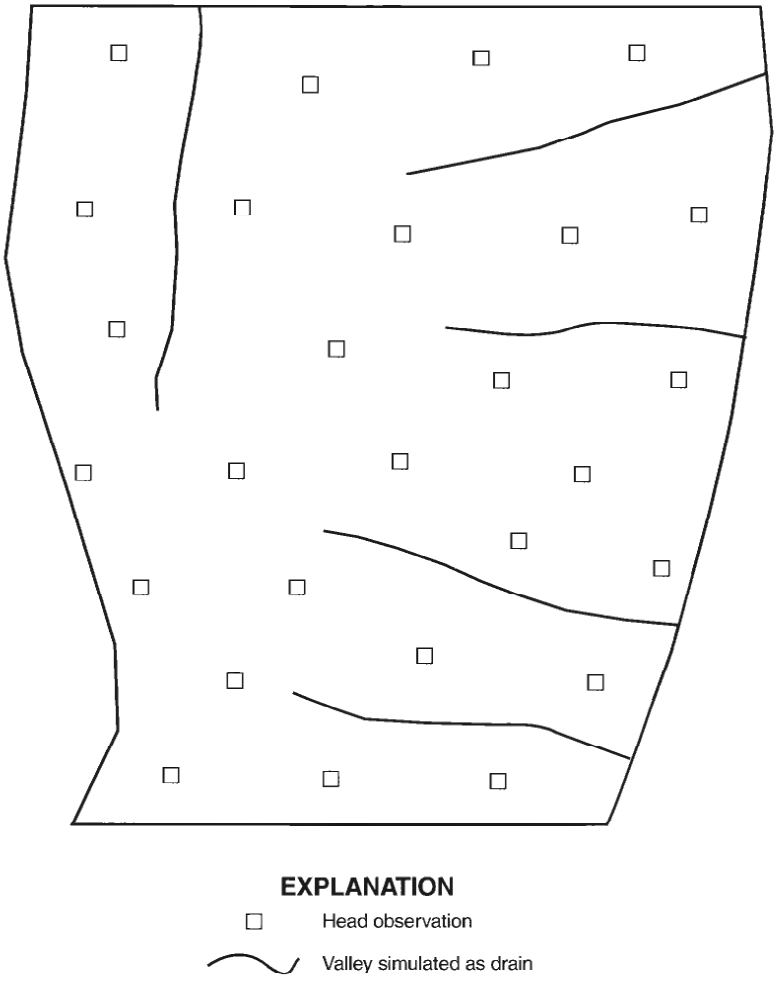

Figure 36. Location of hypothetical head observations used to calculate composite scaled sensitivities for numerical simulations of the hydrologic effects of mining aggregate in fractured crystalline-rock aquifers.

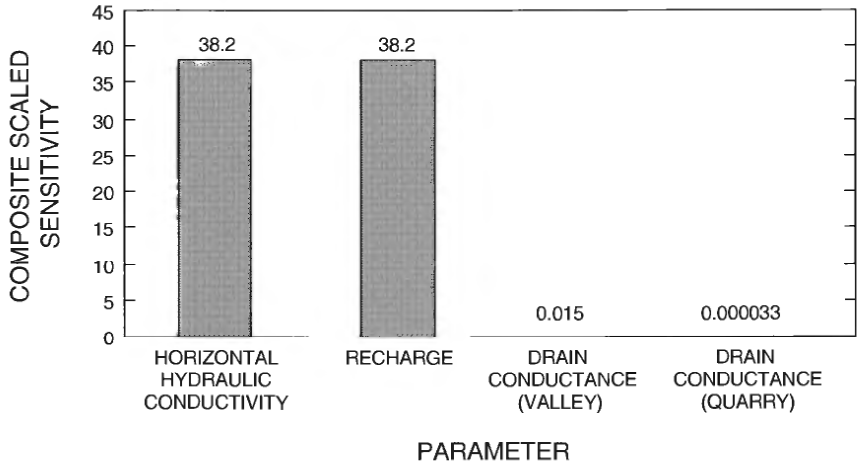

Figure 37. Composite scaled sensitivities for parameters in numerical simulation 7 (quarry in a fractured crystalline-rock aquifer under homogeneous and isotropic conditions).

Table 6. Composite scaled sensitivities for parameters used in six numerical simulations of the effects of mining aggregate in hypothetical fractured crystalline-rock aquifers

[--, not applicable]

Simulation	Parameter									
	Horizontal hydraulic conductivity (Layer 1)	Horizontal hydraulic conductivity (Layer 2)	Horizontal hydraulic conductivity (Hilltops)	Horizontal hydraulic conductivity (Valleys)	Horizontal hydraulic conductivity (Fault)	Vertical hydraulic conductivity (Layer 1)	Vertical hydraulic conductivity (Layer 2)	Recharge	Drain conductance (Valleys)	Drain conductance (Quarry)
7	38.2	--	--	--	--	--	--	38.2	0.015	0.000033
8	27.8	--	--	--	--	--	--	27.8	0.018	0.000031
9	24.6	--	32.6	3.5	--	--	--	52.0	0.015	0.000011
10	34.9	1.8	--	--	--	0.0055	0.032	36.7	0.014	0.000038
11	34.1	--	--	--	2.9	--	--	36.2	0.014	0.000143
12	38.6	--	--	--	1.2	----	--	39.3	0.015	0.000036

Model simulations:

7. Quarry in a homogeneous, isotropic aquifer.
8. Quarry in a homogeneous, horizontally anisotropic aquifer.
9. Quarry in an aquifer with lateral variations of hydraulic conductivity.
10. Quarry in an aquifer with ground-water flow in deep, low-permeability fractures.
11. Quarry intersected by a fault zone that acts as a conduit for ground-water flow.
12. Quarry intersected by a fault zone that acts as a barrier to ground-water flow.

by a fault zone), the sensitivity for horizontal hydraulic conductivity of the fault zone was small compared to the sensitivity for horizontal hydraulic conductivity of the surrounding rock. In all simulations, simulated head had little sensitivity to the hydraulic conductance of drain cells used to simulate valleys, and simulated head was relatively insensitive to the conductance of drain cells used to simulate the quarry. The sensitivity for vertical hydraulic conductivity could only be calculated for simulation 10, which had more than one model layer. Simulated head in simulation 10 had little sensitivity to vertical hydraulic conductivity in both layers.

SUMMARY AND CONCLUSIONS

Analytical solutions and numerical models were used to predict the extent of drawdown caused by mining aggregate below the water table in hypothetical sand-and-gravel and fractured crystalline-rock aquifers representative of hydrogeologic settings in the Front Range area of Colorado. A steady-state, two-dimensional analytical solution derived by Marinelli and Niccoli was used to predict the extent of drawdown caused by a circular pit or quarry in a homogeneous, isotropic sand-and-gravel or fractured crystalline-rock aquifer, respectively, of infinite extent. A similar, one-dimensional analytical solution derived during this study was used to predict the extent of drawdown caused by a linear quarry in a homogeneous, isotropic fractured crystalline-rock aquifer of infinite extent. Parameters used in the analytical solutions were varied independently over a range of values to simulate the effects of mining over a wide range of conditions. Results of analytical simulations indicate radius of influence was about 4,500 m for a circular pit in a sand-and-gravel aquifer under intermediate conditions. Radius of influence was about 400 m for a circular quarry in a fractured crystalline-rock aquifer under intermediate conditions, and distance of influence was 500 m for a linear quarry in a fractured crystalline-rock aquifer under the same conditions. Radius (or distance) of influence increased as horizontal hydraulic conductivity, mine penetration of the water table, and mine radius increased and as recharge decreased. One-percent sensitivities were calculated for each parameter in the analytical solutions to evaluate the influence of each parameter on simulation results. Results of analytical sensitivity analyses under intermediate conditions in sand-and-gravel and fractured crystalline-rock aquifers indicate radius of influence was most sensitive to mine penetration of the water table and least sensitive to mine radius. Radius of influence was equally sensitive to horizontal hydraulic conductivity and recharge, but the parameters had opposite effects on simulation because they are inversely correlated in the ground-water flow equation.

Numerical ground-water flow models were used to predict the extent of drawdown caused by a pit or quarry under conditions that consider heterogeneity, anisotropy, and boundaries and to simulate complex or unusual conditions that were not readily simulated by using analytical solutions. Six numerical simulations were presented for the effects of mining in sand-and-gravel aquifers, and six numerical simulations were presented for the effects of mining in fractured crystalline-rock aquifers.

Numerical simulations in sand-and-gravel aquifers predicted the hydrologic effects of mining in a homogeneous, vertically anisotropic aquifer of medium size and in homogeneous, isotropic aquifers of different sizes with different boundary conditions. Numerical simulations in sand-and-gravel aquifers also predicted the hydrologic effects of pits lined with slurry walls and the effects of pits that have been refilled with water and are undergoing evaporative losses. Drawdown caused by a pit in a medium-sized sand-and-gravel aquifer under homogeneous and isotropic conditions (simulation 1) was compared to drawdown simulated using an analytical solution. Area of influence in the numerical simulation was smaller than in the analytical simulation because of boundary effects and additional sources of recharge in the numerical simulation. Area of influence for a pit in a medium-sized sand-and-gravel aquifer under homogeneous but vertically anisotropic conditions (simulation 2) was nearly identical to that in simulation 1. Area of influence for a pit in a large sand-and-gravel aquifer under homogeneous and isotropic conditions (simulation 3) was larger and more symmetrical than that in simulation 1 because more water discharges to the pit and aquifer boundaries were farther away from the pit. Area of influence was smaller and drawdown was greater for a pit in a small, hydraulically isolated sand-and-gravel aquifer under homogeneous and isotropic conditions (simulation 4) because aquifer boundaries were closer to the pit and no recharge was contributed by general-head boundaries. Pits lined with imperme-

able slurry walls in a medium-sized sand-and-gravel aquifer under homogeneous and isotropic conditions (simulation 5) caused mounding to occur upgradient from the pits and drawdown to occur downgradient from the pits. Pits refilled with water after mining and undergoing evaporative losses in a medium-sized sand-and-gravel aquifer under homogeneous and isotropic conditions (simulation 6) had little hydrologic effect on the aquifer because discharge from the refilled pits was small compared to the overall groundwater budget.

Numerical simulations in fractured crystalline-rock aquifers predicted the hydrologic effects of mining in a homogeneous, isotropic aquifer and in heterogeneous, anisotropic aquifers. Drawdown caused by a quarry in a homogeneous, isotropic fractured crystalline-rock aquifer (simulation 7) was compared to drawdown simulated using analytical solutions. Area of influence in the numerical simulation was larger than in the analytical simulation because aquifer transmissivity in the numerical simulation was greater. Area of influence for a quarry in a homogeneous, horizontally anisotropic fractured crystalline-rock aquifer (simulation 8) was elongated in the direction of greater hydraulic conductivity. Area of influence for a quarry in a fractured crystalline-rock aquifer with lateral variations of hydraulic conductivity (simulation 9) was smaller than in simulation 7 because zones of low horizontal hydraulic conductivity beneath hilltops in simulation 9 limited expansion of the area of influence upgradient from the quarry, and zones of high horizontal hydraulic conductivity along the major valley represented as a constant-head boundary caused heads downgradient from the quarry to be maintained near premining levels. Area of influence for a quarry in a fractured crystalline-rock aquifer with ground-water flow in deep, low-permeability fractures (simulation 10) was larger than in simulation 7 because the thicker aquifer in simulation 10 increased aquifer transmissivity. Area of influence for a quarry intersected by a hydraulically conductive fault zone in a fractured crystalline-rock aquifer (simulation 11) was larger than in simulation 7 because the fault zone increased ground-water flow to the quarry. Area of influence for a quarry intersected by a low-conductivity fault zone in a fractured crystalline-rock aquifer (simulation 12) was smaller than in simulation 7 because the fault zone decreased ground-water flow to the quarry.

Composite scaled sensitivities were calculated for each parameter used in the numerical models to evaluate the influence of each parameter on simulated hydraulic head. Numerical sensitivity analysis results for sand-and-gravel aquifer simulations indicated simulated head was most sensitive to horizontal hydraulic conductivity and the hydraulic conductance of general-head boundaries. Simulated head in the sand-and-gravel aquifers was less sensitive to riverbed conductance and recharge, and simulated head was relatively insensitive to vertical hydraulic conductivity. Numerical sensitivity analysis results for fractured crystalline-rock aquifer simulations indicated simulated head was most sensitive to variations in recharge and horizontal hydraulic conductivity. Simulated head in the fractured crystalline-rock aquifers had little sensitivity to vertical hydraulic conductivity and the hydraulic conductance of drain cells used to simulate valleys. Simulated head was relatively insensitive to the hydraulic conductance of drain cells used to simulate quarries.

REFERENCES CITED

Anderman, E.R., Hill, M.C., and Poeter, E.P., 1996, Two-dimensional advective transport in ground-water flow parameter estimation: Ground Water, v. 34, no. 6., p. 1001–1009.

Anderson, M.P., and Woessner, W.W., 1992, Applied groundwater modeling: San Diego, Calif., Academic Press, Inc., 381 p.

Bolen, W.P., 2002, Sand and gravel (Construction): U.S. Geological Survey Mineral Commodity Summaries, p. 140–141.

Buckles, D.R., and Watts, K.R., 1988, Geohydrology, water quality, and preliminary simulations of ground-water flow of the alluvial aquifer in the upper Black Squirrel Creek basin, El Paso County, Colorado: U.S. Geological Survey Water-Resources Investigations Report 88–4017, 49 p.

Colton, R.B., 1978, Geological map of the Boulder-Fort Collins-Greeley area, Front Range Urban Corridor, Colorado: U.S. Geological Survey Miscellaneous Investigations Map I–855–G, scale 1:100,000.

Crosby, E.J., 1978, Landforms in the Boulder-Fort Collins-Greeley area, Front Range Urban Corridor, Colorado: U.S. Geological Survey Miscellaneous Investigations Series Map I–855–D, scale 1:100,000.

Daniel, C.C., III, Smith, D.G., and Eimers, J.L., 1997, Hydrogeology and simulation of ground-water flow in the thick regolith-fractured crystalline rock aquifer system of Indian Creek Basin, North Carolina: U.S. Geological Survey Water-Supply Paper 2341–C, 137 p.

Davis, S.N., and Turk, L.J., 1964, Optimum depth of wells in crystalline rocks: Groundwater, v. 2, no. 2, p. 6–11.

Domenico, P.A., and Schwartz, F.W., 1990, Physical and chemical hydrogeology: New York, John Wiley and Sons, 824 p.

Fenneman, N.M., 1946, Physical divisions of the United States: U.S. Geological Survey map, scale 1:7,000,000.

Fetter, C.W., 1994, Applied hydrogeology (3d ed.): New York, Macmillan College Publishing Company, 691 p.

Folger, P.F., 1995, A multidisciplinary study of the variability of dissolved Rn222 in ground water in a fractured crystalline rock aquifer and its impact on indoor air: Golden, Colorado School of Mines, unpublished Ph.D. dissertation, 181 p.

Freeze, R.A., and Cherry, J.A., 1979, Groundwater: Englewood Cliffs, N.J., Prentice-Hall, 588 p.

Goeke, J.W., 1970, The hydrogeology of Black Squirrel Creek basin, El Paso County, Colorado: Fort Collins, Colorado State University, Master's thesis, 79 p.

Harbaugh, A.W., Banta, E.R., Hill, M.C., and McDonald, M.G., 2000, MODFLOW–2000, the U.S. Geological Survey modular ground-water model—User guide to modularization concepts and the ground-water flow process: U.S. Geological Survey Open-File Report 00–92, 121 p.

Heath, R.C., 1983, Basic ground-water hydrology: U.S. Geological Survey Water-Supply Paper 2220, 84 p.

Hill, M.C., 1998, Methods and guidelines for effective model calibration: U.S. Geological Survey Water-Resources Investigations Report 98–4005, 90 p.

Hill, M.C., Banta, E.R., Harbaugh, A.W., and Anderman, E.R., 2000, MODFLOW–2000, the U.S. Geological Survey modular ground-water model —User guide to the observation, sensitivity, and parameter-estimation processes and three post-processing programs: U.S. Geological Survey Open-File Report 00–184, 209 p.

Hofstra, W.E., and Hall, D.C., 1975, Geologic control of supply and quality of water in the mountainous parts of Jefferson County, Colorado: Denver, Colorado Geological Survey Bulletin 36, 51 p.

Huyakorn, P.S., and Pinder, G.F., 1983, Computational methods in subsurface flow: Orlando, Fla., Academic Press, Inc., 473 p.

Knepper, D.H., Jr., ed., 2002, Planning for the conservation and development of infrastructure resources in urban areas–Colorado Front Range Urban Corridor: U.S. Geological Survey Circular 1219, 27 p.

Konikow, L.F., and Grove, D.B., 1977, Derivation of equations describing solute transport in ground water: U.S. Geological Survey Water-Resources Investigations Report 77–19 (revised 1984), 30 p.

Langer, W.H., 2001, Environmental impacts of mining natural aggregate, *in* Bon, R.L., Riordan, R.F., Tripp, B.T., and Krukowski, S.T., eds., Proceedings of the 35th Forum on the Geology of Industrial Minerals—The Intermountain West Forum: Utah Geological Survey Miscellaneous Publication 01–2, p. 127–138.

Lawrence, E., Poeter, E., and Wanty, R., 1991, Geohydrologic, geochemical, and geologic controls on the occurrence of radon in ground water near Conifer, Colorado, USA: Journal of Hydrology, v. 127, p. 367–386.

Leake, S.A., and Lilly, M.R., 1997, Documentation of a computer program (FHB1) for assignment of transient specified-flow and specified-head boundaries in applications of the modular finite-difference ground-water flow model (MODFLOW): U.S. Geological Survey Open-File Report 97–571, 50 p.

Lohman, S.W., 1979, Ground-water hydraulics: U.S. Geological Survey Professional Paper 708, 70 p.

Long, J.C.S., Remer, J.S., Wilson, C.R., and Witherspoon, P.A., 1982, Porous media equivalents for networks of discontinuous fractures: Water Resources Research, v. 18, no. 3, June 1982, p. 645–658.

Marinelli, Fred, and Niccoli, W.L., 2000, Simple analytical equations for estimating ground water inflow to a mine pit: Groundwater, v. 38, no. 2, p. 311–314.

McDonald, M.G., and Harbaugh, A.W., 1988, A modular three-dimensional finite-difference ground-water flow model: U.S. Geological Survey Techniques of Water Resources Investigations, book 6, chap. A1.

Mueller, D.K., 1979, The effect of subdivision development on soil moisture and ground-water recharge in the Colorado Front Range: Fort Collins, Colorado State University, Master's thesis, 85 p., plus appendixes.

Robson, S.G., 1989, Alluvial and bedrock aquifers of the Denver Basin—Eastern Colorado's dual ground-water resource: U.S. Geological Survey Water-Supply Paper 2302, 40 p.

Robson, S.G., 1996, Geohydrology of the shallow aquifers in the Denver metropolitan area, Colorado: U.S. Geological Survey Hydrologic Investigations Atlas HA–736, 5 sheets, scale 1:50,000.

Robson, S.G., Arnold, L.R., and Heiny, J.S., 2000a, Geohydrology of the shallow aquifers in the Fort Collins-Loveland area, Colorado: U.S. Geological Survey Hydrologic Investigations Atlas HA–746–B, 5 sheets, scale 1:50,000.

Robson, S.G., Arnold, L.R., and Heiny, J.S., 2000b, Geohydrology of the shallow aquifers in the Greeley-Nunn area, Colorado: U.S. Geological Survey Hydrologic Investigations Atlas HA–746–A, 5 sheets, scale 1:50,000.

Robson, S.G., and Banta, E.R., 1995, Ground water atlas of the United States, segment 2: U.S. Geological Survey Hydrologic Investigations Atlas HA 730–C, 32 p.

Robson, S.G., Heiny, J.S., and Arnold, L.R., 2000a, Geohydrology of the shallow aquifers in the Boulder-Longmont area, Colorado: U.S. Geological Survey Hydrologic Investigations Atlas HA–746–D, 5 sheets, scale 1:50,000.

Robson, S.G., Heiny, J.S., and Arnold, L.R., 2000b, Geohydrology of the shallow aquifers in the Fort Lupton-Gilcrest area, Colorado: U.S. Geological Survey Hydrologic Investigations Atlas HA–746–C, 5 sheets, scale 1:50,000.

Snow, D.T., 1968, Hydraulic character of fractured metamorphic rocks of the Front Range and implications to the Rocky Mountain Arsenal well: Golden, Colorado School of Mines Quarterly, v. 63, no. 1, 33 p.

Tepordei, V.V., 2002, Stone (Crushed): U.S. Geological Survey Mineral Commodity Summaries, p. 156–157.

Tiedeman, C.R., Goode, D.J., and Hsieh, P.A., 1997, Numerical simulation of ground-water flow through glacial deposits and crystalline bedrock in the Mirror Lake area, Grafton County, New Hampshire: U.S. Geological Survey Professional Paper 1572, 50 p.

Trimble, D.E., and Machette, M.N., 1979, Geological map of the greater Denver area, Front Range Urban Corridor, Colorado: U.S. Geological Survey Miscellaneous Investigations Map I–856–H, scale 1:100,000.

Western Regional Climate Center, 1997, Map plot of 1961–1990 average annual precipitation contours: Western Regional Climate Center data available on the World Wide Web, accessed May 9, 2001, at URL http://www.wrcc.dri.edu/pcpn/co.gif

Wilburn, D.R., and Langer, W.H., 2000, Preliminary report on aggregate use and permitting along the Colorado Front Range: U.S. Geological Survey Open-File Report 00–258, 22 p.

Wilson, W.W., 1965, Pumping tests in Colorado: Denver, Colorado Water Conservation Board Ground-Water Circular 11, 361 p.